Electrostatic fluctuation and double layer interactions between surfaces.

Phil Attard

A thesis submitted for the degree of
Doctor of Philosophy
at the Australian National University.

Canberra, May, 1988.

Preface

This dissertation is an account of research carried out at the Department of Applied Mathematics, Research School of Physical Sciences, Australian National University, between February 1985 and May 1988.

The material presented here is the result of a collaboration between my supervisor, John Mitchell, and myself. Stjepan Marčelja was also my supervisor and suggested many of the topics investigated. Roland Kjellander participated in the work of Part I, and he and Stjepan gave me their HNC programme to modify for calculations presented in §§2.3, 4.1, 4.2, and 6.3. Bo Jönsson provided some simulation data presented in §§2.3 and 4.1.

The work presented here is my own, unless explicitly stated to the contrary. None of the work reported here has been submitted to any other institution of learning for any degree.

P. Attard

Phil Attard

Publications

1. P. Attard and D.J. Mitchell, "The forces between surfaces of mobile, orientable dipoles. Asymptotic expressions", Chem. Phys. Lett. **133**, 347-352 (1987).

2. P. Attard and D.J. Mitchell, "The forces between surfaces of mobile, orientable dipoles. The method of reflection coefficients", J. Chem. Phys. **88**, 4391-4396 (1988).

3. P. Attard, D.J. Mitchell and B.W. Ninham, "The attractive forces between polar lipid bilayers", Biophys. J. **53**, 457-560 (1988).

4. Bo. Jönsson, P. Attard and D.J. Mitchell, " The interactions between dipolar surfaces in a dielectric continuum model", J. Phys. Chem. (in press).

5. P. Attard, R. Kjellander and D.J. Mitchell, "Interactions between electro-neutral surfaces bearing mobile charges", Chem. Phys. Lett. **139**, 219-224 (1987).

6. P. Attard, R. Kjellander, D.J. Mitchell and Bo. Jönsson, "Electrostatic fluctuation interactions between neutral surfaces adsorbed with mobile ions or dipoles", J. Chem. Phys., (in press).

7. P. Attard, "Lifshitz theory for anisotropic multilayers", J. Colloid Interface Sci., (in press).

8. P. Attard, D.J. Mitchell and B.W. Ninham, "Beyond Poisson-Boltzmann: images and correlations in the electric double layer. I. Counterions only", J. Chem. Phys., (in press).

9. P. Attard, D.J. Mitchell and B.W. Ninham, "Beyond Poisson-Boltzmann: images and correlations in the electric double layer. II. Symmetric Electrolyte", J. Chem. Phys., (submitted).

10. P. Attard and M.T. Batchelor, "A mechanism for the hydration force demonstrated in a model system", Chem. Phys. Lett., (submitted).

Acknowledgements

I thank my supervisors, John Mitchell and Stjepan Marčelja, for their contribution to my doctorate and to the half megabyte which comprises this thesis. John has patiently taught me physics over the past three years. The depth of his understanding, the rigor of his logic, and the elegance of his explanation are manifest in this work. Stjepan has been generous in every way. Many enjoyable and fruitful dicussions have resulted from his deep intuition, and many of the topics treated here have been inspired by him.

Roland Kjellander made the material in Part I rigorous. For this I thank him, as well as for his technical assistance and for his advice during various stages of my PhD. Barry Ninham offered fulsome encouragement throughout. More importantly, he founded and nurtured this unique department, and I (and many others) have greatly benefitted from the informal atmosphere and from the intellectual excellence by which it is internationally recognised.

I thank Steve Garth, Stan Miklavic, John Parker (fellow dungeon dwellers) and Murray Batchelor for their most distracting problems, for their wise counsel, and for their beer and the excuse to drink it. My experimental colleagues and other friends in the department have all contributed to what on the whole has been a very enjoyable time. Finally, the ANU rugby club has very generously allowed me to vent frustration and blood over the past few seasons, an important contribution to Australian-Swedish relations and to this PhD.

Electrostatic fluctuation and double layer interactions between surfaces.

Abstract

The electrostatic interactions between planar surfaces are analysed using classical statistical mechanics and including the effects of correlations and of dielectric images. Three particular problems are considered: interactions between electroneutral surfaces bearing mobile charges; interacting dipolar surfaces; and the electric double layer between charged surfaces.

The electrostatic fluctuation interactions between two neutral surfaces which carry charged, laterally mobile particles, are investigated using both formally exact theory and approximate methods. Each surface constitutes the boundary between two dielectric continua and has no net charge. The exact analysis demonstrates the interdependence of the van der Waals interaction between the dielectric media and the electrostatic image interactions of the particles. General asymptotic laws for the pressure between the surfaces, valid at large separations, are extracted from the exact equations. Even at relatively small separations, the asymptotic expressions give surprisingly good estimates of the actual interactions, as calculated using the Hypernetted Chain equation and Monte Carlo techniques. A simple mean field perturbation approximation is also investigated and is shown to give good results, provided accurate pair distributions are known for the corresponding isolated, single surface.

The interactions between surfaces bearing mobile, orientable dipoles are investigated using exact, asymptotic, numerical, and approximate methods. The interaction free energy between two planar bodies interacting across a uniform dielectric, expressed as a sum over allowed electrodynamic modes, is interpreted in terms of reflection coefficients. It is proved that, within the approximations implied by this modal approach, the force between identical bodies interacting across a uniform dielectric is always attractive. The method of reflection coefficients is used to obtain explicit

Part I

Interactions between neutral surfaces bearing mobile charges.

Most of the material in this part has been published in the following papers:

P. Attard, R. Kjellander, and D.J. Mitchell, "Interaction between electro - neutral surfaces bearing mobile charges", Chem. Phys. Letters, **139**, 219 (1987).

P. Attard, R. Kjellander, D.J. Mitchell, and Bo Jönsson, "Electrostatic fluctuation interactions between neutral surfaces with adsorbed mobile ions or dipoles", J. Chem. Phys. (in press).

Introduction to the Thesis and to Part I

The interactions between surfaces lie at the heart of very many physical phenomena. It is a fundamental topic studied in certain branches of science and engineering including colloid science (stabilisation of sols and colloidal dispersions, mineral flotation), soil science (clay swelling), cell biology (membrane fusion, cell recognition), rheology (friction, lubrication) and physics (adhesion, wetting). An important class of systems are those where the interactions are predominantly electrostatic, where the separation and size of the interacting bodies allow them to be modelled as planar surfaces, and where the intervening medium may be regarded as a structureless fluid. Several problems which fall into this class will be addressed in this thesis.

Three topics are considered: the interaction between neutral surfaces adsorbed with mobile charges; interacting surfaces bearing mobile, orientable dipoles; and charged surfaces which interact across an electrolyte (the electric double layer). Physically, the first could model the interactions between lamellae composed of equal amounts of anionic and cationic surfactants or the classical force between metallic plates. The forces between dipolar surfaces are very important biologically, since cell membranes are composed of zwitterionic and polar lipid bilayers. Three component microemulsions and lamellar phases should also exhibit effects due to surface dipole interactions. The electric double layer occurs in all the fields listed in the preceding paragraph and could be considered a discipline in its own right.

The common theme and contribution of the present work is the inclusion of the effects of correlations (and of dielectric images) in the analyses of these systems. Classical statistical mechanics is the established theory; from this basis exact results are derived, approximate and asymptotic formulae are obtained, and numerical computations are performed. Our own interest lies in the fundamental theory and the broader

concepts rather than the particular application. Nevertheless the various approaches are compared with each other for specific parameters, and also with experiment as appropriate.

Part I of this thesis presents an analysis of the interactions between bodies with planar surfaces bearing laterally mobile charges but which are overall electrically neutral. The short-range potentials between the charges are arbitrary and there is no added electrolyte in this system. The intervening medium is characterised solely by its dielectric constant, and the two identical bodies may have a different dielectric constant beyond their surfaces. The dielectric properties at zero frequency only will be considered, so the non-zero frequency part of the van der Waals† interaction is not included. However, the higher frequency part of that interaction can, to a very good approximation, be added to the results obtained here (since the ions do not respond much to high frequency fields). This particular system is of interest as a model for interacting lamellae consisting of equimolar mixtures of anionic and cationic surfactants. It may also be considered a limiting case for diffuse double layers where the ions have a strong affinity for the surfaces.

The surfaces are overall neutral and hence the mean-field force (due to the mean charge distribution which is zero) vanishes. The force between the surfaces here arises solely from correlated fluctuations of the surface charges (and the polarisation fluctuations of the dielectric media). It is therefore essential to include correlations in any description of this system, and it is also necessary to combine the treatment of the ions with that of the dielectrics. The present problem illustrates in a hopefully transparent

---

†In this thesis I use a lower case v for van der Waals, an s in words such as polarise, and other less conventional spelling on occasion.

manner these two concepts, both of which have implications for more general systems.

The traditional DLVO (Derjaguin, Landau, Vervey, and Overbeek) theory[1,2] of colloid interaction considers the net force between particles to be the sum the double layer interaction, described by the Poisson-Boltzmann (PB) theory, and the van der Waals (vdW) interaction, treated by Hamaker theory or the more refined Lifshitz theory[3]. The latter force arises from the correlated polarisation fluctuations between the different dielectric media. In PB theory one ignores ionic correlations as well as the effects of images which arise from the different dielectric media. Hence there are fundamental inconsistencies in the traditional treatments. The coupling between the ion correlations and the polarization fluctuations will affect the static (zero frequency, classical, temperature dependent) contributions to the vdW interaction, and this should be taken into account. One can extend the Lifshitz theory to include charge - charge correlations, as has been done for neutral surfaces interacting across an electrolyte[4-7], and as is done for the more general case of charged surfaces in the latter part of this thesis. This approach does not have the inconsistencies of the DLVO theory and the zero-frequency vdW interaction now becomes screened.

Numerical treatments of the charge fluctuations are important, but leave vital, general aspects of the problem somewhat clouded since one cannot cover all possible cases. A complete, analytical solution is surely out of question, but a detailed analytical treatment is nevertheless possible. The current problem with all ions adsorbed on the surfaces is particularly well suited to illustrate several important aspects of the electrostatic fluctuation interactions between two bodies. This system is sufficiently complex and surprisingly intricate, but yields to an exact statistical mechanical analysis revealing the link between the different contributions to the interactions. The analysis also gives general, asymptotic laws for the correlation functions and for the interactions in this system, and useful, approximate formulae for

these quantities are obtained.

The layout of Part I should be easily followed. In Chapter 1 the general formalism is presented and the charge correlation functions for ionic layers analysed. Exact expressions for the pressure between the surfaces with adsorbed ionic particles are derived in §1.3 and the leading terms in the asymptotic pressure expansions for large separations are extracted. The approximate methods used for calculating the correlation functions and the interactions are described in Chapter 2, and a mean field perturbation approximation that is consistent with the exact asymptotic laws for the pressure is also derived. In §2.3 the numerical results are presented and compared to the asymptotic laws.

Chapter 1 Exact and Asymptotic Analysis

1.1 Distribution functions

The present object is to derive expressions which describe the particle distributions on, and interactions between, two planar surfaces bearing adsorbed, but laterally mobile, charged particles. The geometry of the system is illustrated in Fig. 1.1. The various surface species may be located in different layers on each surface, *i.e.* the particle centres may lie in different planes, but the motion of each species is restricted to one two-dimensional plane per surface. The particle interactions are assumed to be pairwise additive and may contain *arbitrary short range potentials*.

1.1A One surface

For a single surface with m species, one defines the position operator $\mathfrak{N}$, an m-vector with components

$$\mathfrak{N}_\alpha(\mathbf{r}) = \sum_{i=1}^{M_\alpha} \delta(\mathbf{r}-\mathbf{r}_{i,\alpha}) \qquad (1 \le \alpha \le m) \qquad (1.1.1)$$

where M_α is the number of particles of species α and where the Dirac delta function, δ, picks out the position of each particle $\mathbf{r}_{i,\alpha}$ of species α ($\mathbf{r}$ is the two-dimensional radius vector in cylindrical coordinates). The Hamiltonian of the isolated surface is

$$H_0 = \frac{1}{2}\,\mathfrak{N}^T \cdot \underline{u}_0 \cdot \mathfrak{N} = \frac{1}{2}\int d\mathbf{r}\, d\mathbf{r}'\, \mathfrak{N}^T(\mathbf{r})\, \underline{u}_0(\mathbf{r},\mathbf{r}')\, \mathfrak{N}(\mathbf{r}') \qquad (1.1.2)$$

where $\mathfrak{N}^T$ denotes the transposed vector $\mathfrak{N}$ and where $\underline{u}_0(\mathbf{r},\mathbf{r}') = \{ u_{0;\alpha\alpha'}(\mathbf{r},\mathbf{r}') \}$ is the $m \times m$ matrix of pair interactions between particles of species α and α'. The pair potential includes the interaction between α and the electrostatic image of α' (or *vice versa*) when there is a dielectric

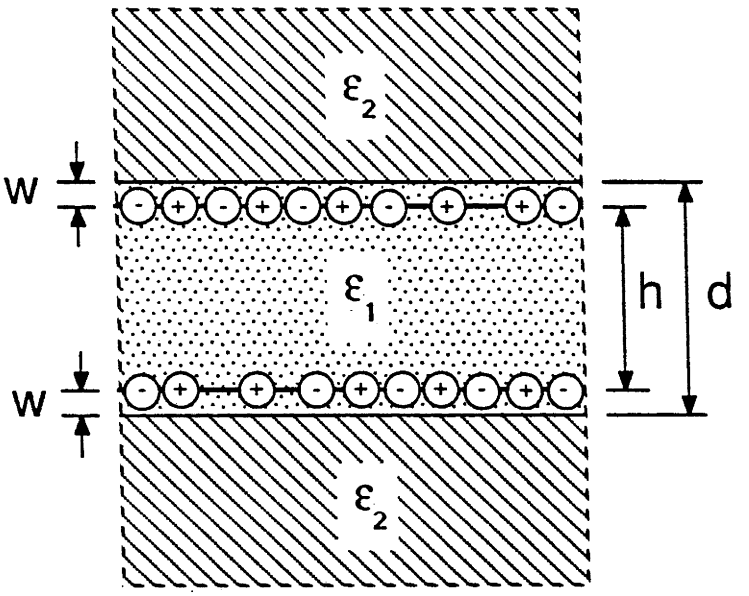

Figure 1.1 Sketch of the system composed of two surfaces with adsorbed, but laterally mobile ions. The separation between the ionic layers - as measured between the particle centers - is h, and $d = h + 2w$ is the separation between the dielectric discontinuities.

discontinuity at the single surface. No self-interaction contributions other than the interaction between a particle and its own electrostatic image (self-image interaction) should be included. The dot product denotes combined matrix multiplication and coordinate integration. In the absence of an external field, the m-vector of density distribution $\mathbf{n}_0(\mathbf{r}) \equiv \langle \mathfrak{N}(\mathbf{r}) \rangle_0 = \{ n_\alpha \}$, where n_α is the surface density of species α, is independent of $\mathbf{r}$. Here, $\langle \cdot \rangle$ denotes the ensemble average; subscript 0 shows that the average is taken for the unperturbed surface.

In the presence of an external field $\mathbf{v}(\mathbf{r}) = \{ v_\alpha(\mathbf{r}) \}$, the Hamiltonian equals $H = H_0 + H_{ext}$, where

$$H_{ext} = \mathfrak{N}^T \cdot \mathbf{v} = \int d\mathbf{r}\ \mathfrak{N}^T(\mathbf{r})\ \mathbf{v}(\mathbf{r}) \qquad (1.1.3)$$

and the density distribution becomes $\mathbf{n}(\mathbf{r}) \equiv \langle \mathfrak{N}(\mathbf{r}) \rangle$, which relation will be written $\mathbf{n} \equiv \langle \mathfrak{N} \rangle$, implicitly assuming the $\mathbf{r}$-dependence. A variation of $\delta\mathbf{v}(\mathbf{r}')$ in the external potential leads to a change $\delta\mathbf{n}(\mathbf{r})$ in the density equal to

$$\delta\mathbf{n}(\mathbf{r}) = -\beta \int d\mathbf{r}'\ \underline{\mathbf{s}}(\mathbf{r},\mathbf{r}')\ \delta\mathbf{v}(\mathbf{r}') \qquad (1.1.4a)$$

or in compact notation

$$\delta\mathbf{n} = -\beta\ \underline{\mathbf{s}} \cdot \delta\mathbf{v} \qquad (1.1.4b)$$

where $\underline{\mathbf{s}}$ is the $m \times m$ matrix of pair distribution functions

$$\underline{\mathbf{s}} = -k_B T \frac{\delta \mathbf{n}}{\delta \mathbf{v}} \equiv -k_B T \left\{ \frac{\delta n_\alpha(\mathbf{r})}{\delta v_{\alpha'}(\mathbf{r}')} \right\} = \langle \mathfrak{N}\, \mathfrak{N}^T \rangle - \langle \mathfrak{N} \rangle \langle \mathfrak{N}^T \rangle$$

$$= \left\{ n_\alpha(\mathbf{r})\, \delta_{\alpha\alpha'}(\mathbf{r},\mathbf{r}') + n_\alpha(\mathbf{r})\, n_{\alpha'}(\mathbf{r}')\, h_{\alpha\alpha'}(\mathbf{r},\mathbf{r}') \right\} \qquad (1.1.5)$$

T is the temperature, k_B is Boltzmann's constant, $\beta = (k_B T)^{-1}$, $\delta_{\alpha\alpha'}(\mathbf{r},\mathbf{r}') = \delta_{\alpha\alpha'}\, \delta(\mathbf{r}-\mathbf{r}')$ the product of the Kronecker and Dirac deltas, and $h_{\alpha\alpha'} = g_{\alpha\alpha'} - 1$ is the pair correlation function for species α and α'. Note that $\mathfrak{N}\,\mathfrak{N}^T = \{ \mathfrak{N}_\alpha(\mathbf{r}) \mathfrak{N}_{\alpha'}(\mathbf{r}') \}$, *i.e.* a dyadic product.

The inverse of $\underline{\mathbf{s}}$, $\underline{\mathbf{t}} = \underline{\mathbf{s}}^{-1}$, defined from

$$\underline{\mathbf{t}} \cdot \underline{\mathbf{s}} = \underline{\mathbf{1}} \qquad (1.1.6)$$

where $\underline{1} = \{\delta_{\alpha\alpha'}(\underline{r},\underline{r}')\}$, equals

$$\underline{t} = -\beta \frac{\delta v}{\delta n} = \left\{ \frac{\delta_{\alpha\alpha'}(r,r')}{n_\alpha(r)} - c_{\alpha\alpha'}(r,r') \right\} \qquad (1.1.7)$$

where c is the direct correlation function. Equation (1.1.6) with Eqs (1.1.5) and (1.1.7) inserted is equivalent to the Ornstein-Zernike equation for the mixture and may be taken to define the direct correlation function. For large $|\mathbf{r}-\mathbf{r}'|$ there is the well-known asymptotic relation

$$c_{\alpha\alpha'}(r,r') \sim -\beta\, u_{\alpha\alpha'}(r,r') , \qquad |r-r'| \to \infty \qquad (1.1.8)$$

which will be utilized later.

In the absence of an external potential (or when it is independent of $\mathbf{r}$), the pair functions are radially symmetric; *e.g.* $\underline{s}_0(\mathbf{r},\mathbf{r}') = \underline{s}_0(|\mathbf{r}-\mathbf{r}'|)$. Then, Eq. (1.1.6) becomes somewhat simplified in Fourier space. The Hankel transform of Eq. (1.1.6) for an unperturbed surface equals

$$\hat{\underline{t}}_0(k)\, \hat{\underline{s}}_0(k) = \hat{\underline{1}} \qquad (1.1.9)$$

where $\hat{\underline{f}}(k) = \{\hat{f}_{\alpha\alpha'}(k)\}$ with $f = t_0$ or s_0, $\hat{f}_{\alpha\alpha'}(k) = \int d\mathbf{r}\, f_{\alpha\alpha'}(r)\, J_0(kr)$, J_0 is the Bessel function of order zero, and where $\hat{\underline{1}} = \{\delta_{\alpha\alpha'}\}$ is the unit $m \times m$ matrix. Note that the product in the LHS of Eq. (1.1.9) is a simple matrix product (no integration) due to the convolution theorem. Thus, $\hat{\underline{s}}_0$ is the matrix inverse

$$\hat{\underline{s}}_0(k) = \hat{\underline{t}}_0^{-1}(k) = \left[\underline{n}^{-1} - \hat{\underline{c}}_0(k) \right]^{-1} \qquad (1.1.10)$$

where $\underline{n} = \{\delta_{\alpha\alpha'} n_\alpha\}$ (note the distinction between the matrix $\underline{n}$ and the vector $\mathbf{n}$) and $\hat{\underline{c}}_0 = \{\hat{c}_{0;\alpha\alpha'}\}$ is the direct correlation function matrix of the unperturbed surface.

1.1B Two surfaces

The above are standard expressions for the correlations on a single surface. Consider now the influence from an identical surface nearby. The basic theory for two surfaces is formally identical to that given above for one

surface with several layers of particles. It is simply a matter of convention to assign some layers to one surface and the rest to the other, and then to let the separation between the two sets vary, while keeping the internal layer separations fixed in each set. Doing so, one must allow the possibility that there may be interactions in addition to the direct pair potentials between particles on the different surfaces, for example those caused by electrostatic images induced by the approaching second surface. This effect can be included by modifying the particle interaction potentials (see below). Any direct wall-wall interaction (which is independent of the presence of the adsorbed particles) can simply be added to the pressure between the surfaces.

With this in mind, one merely introduces a special notation for the two-surface case, while the relationships above - generalized in an obvious fashion - still hold. The matrices of the total system have dimension $2m \times 2m$. The pair interaction matrix equals

$$\underline{\mathbf{U}} = \begin{bmatrix} \underline{\mathbf{u}}_s & \underline{\mathbf{u}}_c \\ \underline{\mathbf{u}}_c^T & \underline{\mathbf{u}}_s^{T'} \end{bmatrix} \qquad (1.1.11)$$

where $\underline{\mathbf{u}}_s$ is the matrix of pair potentials for particles on one surface and where $\underline{\mathbf{u}}_c$ is the corresponding potential for particles belonging to different surfaces. The superscript T' denotes reflection about the off-diagonal (NE to SW diagonal) of the minor $m \times m$ matrix. The transposition operations T' and T are done to preserve the symmetry of the system. When the surfaces constitute dielectric boundaries, the pair potential includes contributions from the interaction between one particle and the electrostatic images of the other particle, and one has $\underline{\mathbf{u}}_s \neq \underline{\mathbf{u}}_0$ since $\underline{\mathbf{u}}_0$ only contains the interaction with the primary image in the closest surface (which is independent of the surface separation h). For systems without images $\underline{\mathbf{u}}_s = \underline{\mathbf{u}}_0$.

The matrix of pair correlations for the coupled surfaces is

$$\underline{S} = -k_B T \frac{\delta N}{\delta V} = \begin{bmatrix} \underline{S}_s & \underline{S}_c \\ \underline{S}_c^T & \underline{S}_s^T \end{bmatrix}, \text{ where } N = \begin{Bmatrix} n_I \\ n_{II} \end{Bmatrix} \text{ and } V = \begin{Bmatrix} v_I \\ v_{II} \end{Bmatrix} \qquad (1.1.12)$$

(index **I** and **II** denote the two different surfaces; the two subvectors are mirror images of each other), and it describes the density response (*cf.* Eq. (1.1.4)), $\delta N = -\beta \underline{S} \cdot \delta V$, when the external potential for the whole system is varied. In analogy to Eq. (1.1.10), one has in the absence of an external field

$$\hat{\underline{S}} = \left[\underline{N}^{-1} - \hat{\underline{C}} \right]^{-1} \qquad (1.1.13)$$

where $\underline{N}$ is the diagonal matrix of densities and $\underline{C}$ is the matrix of direct correlation functions, which has the same structure as $\underline{S}$.

Finally, the pressure between the surfaces is given by

$$P = \frac{-1}{2} \int dr \, TR \left[\underline{S}(r) \frac{\partial \underline{U}(r;h)}{\partial h} \right] = \frac{-1}{8\pi^2} \int dk \, TR \left[\hat{\underline{S}}(k) \frac{\partial \hat{\underline{U}}(k;h)}{\partial h} \right] \qquad (1.1.14)$$

where $r = |\mathbf{r}-\mathbf{r}'|$ (no external field) and TR denotes the trace. Parseval's theorem has been used to transform the integral to Fourier space.

1.2 Charge-charge correlations

1.2A One surface with adsorbed ions

In the case of adsorbed ions, it is advantageous to work with charge-charge correlations rather than particle-particle correlations (here assume that all surface species on each surface lie in one plane). The charge density $\rho(\mathbf{r})$ at one surface is $\rho(\mathbf{r}) = \mathbf{q}^T \mathbf{n}(\mathbf{r})$, where $\mathbf{q}$ is the m-vector of charges $\{q_\alpha\}$ of all species $1 \le \alpha \le m$. Of course, $\rho_0(\mathbf{r}) = 0$ from electroneutrality. The only external fields considered are of electrostatic origin, and therefore $\mathbf{v}(\mathbf{r}) = \psi_{ext}(\mathbf{r})\,\mathbf{q}$, where ψ_{ext} is the external electrostatic potential at the plane of the ions. It is easy to show from Eq. (1.1.5) that the charge-charge correlation function is

$$\sigma(\mathbf{r}, \mathbf{r}') \equiv -k_B T \frac{\delta \rho(\mathbf{r})}{\delta \psi_{ext}(\mathbf{r}')} = \mathbf{q}^T \mathbf{s}(\mathbf{r}, \mathbf{r}')\,\mathbf{q} \qquad (1.2.1)$$

For an isolated surface one obtains $\hat{\sigma}_0$ from Eqs. (1.1.10) and (1.2.1):

$$\hat{\sigma}_0 = \mathbf{q}^T \hat{\underline{s}}_0 \mathbf{q} = \mathbf{q}^T \left(\underline{n}^{-1} - \hat{\underline{c}}_0 \right)^{-1} \mathbf{q} \qquad (1.2.2)$$

The large-r behaviour of $\underline{c}_0(r)$, where $r = |\mathbf{r} - \mathbf{r}'|$, is given by Eq. (1.1.8). One has

$$u_{0;\alpha\alpha'}(r) = u^{short}_{\alpha\alpha'}(r) + q_\alpha q_{\alpha'} \phi_0(r)$$

where the first term contains all non-electrostatic interactions and

$$\phi_0(r) = \frac{1}{\varepsilon_1 r} + \frac{\varepsilon_D}{\varepsilon_1 \sqrt{r^2 + (2w)^2}}$$

The second term in ϕ_0 is the image charge interaction due to the dielectric discontinuity at the single surface and $\varepsilon_D = (\varepsilon_1 - \varepsilon_2) / (\varepsilon_1 + \varepsilon_2)$. Thus, Eq. (1.1.8) implies

$$\underline{c}_0(r) \sim -\beta \phi_0(r)\, \mathbf{q}\mathbf{q}^T \sim -\frac{\beta(1+\varepsilon_D)}{\varepsilon_1 r}\, \mathbf{q}\mathbf{q}^T, \qquad r \to \infty \qquad (1.2.3)$$

provided $\varepsilon_D \neq -1$. For the case $\varepsilon_D = -1$ the pair potential ϕ_0 is identical to that of zwitterions with perpendicular orientation relative to the surface but

without images. The treatments of these two cases are therefore very similar (see part II).

Equation (1.2.3) suggests the splitting

$$\hat{\underline{c}}_0(k) = -\beta \hat{\underline{u}}_0^{el}(k) + \hat{\underline{a}}_0(k) = -\beta \hat{\phi}_0(k)\, \mathbf{q}\mathbf{q}^T + \hat{\underline{a}}_0(k) \qquad (1.2.4)$$

where $$\hat{\phi}_0(k) = \frac{2\pi\,[1 + \varepsilon_D \exp(-2w k)]}{\varepsilon_1 k}$$

and where $\hat{\underline{a}}_0(k)$ is a well-behaved (finite and continuous) function at $k = 0$. Inserting this in Eq. (1.2.2) one obtains

$$\hat{\sigma}_0(k) = \mathbf{q}^T \left(\hat{\underline{b}}_0(k) + \beta \hat{\phi}_0(k)\, \mathbf{q}\mathbf{q}^T\right)^{-1} \mathbf{q}$$

where $\hat{\underline{b}}_0(k) = \underline{n}^{-1} - \hat{\underline{a}}_0(k) = \hat{\underline{t}}_0(k) - \beta \hat{\phi}_0(k)\, \mathbf{q}\mathbf{q}^T$. The final result is obtained by using the identity

$$\underline{y}^T (\underline{M} + \underline{x}\,\underline{m}\,\underline{y}^T)^{-1} \underline{x} = (\hat{\underline{1}} + \underline{y}^T \underline{M}^{-1} \underline{x}\, \underline{m})^{-1}\, \underline{y}^T \underline{M}^{-1} \underline{x} \qquad (1.2.5)$$

which is valid for any rectangular matrices $\underline{x}$ and $\underline{y}$ and square matrices $\underline{M}$ and $\underline{m}$, where $\underline{M}$ is nonsingular. It follows that the charge-charge correlation function is

$$\hat{\sigma}_0(k) = \frac{\mathbf{q}^T \hat{\underline{b}}_0^{-1}(k)\, \mathbf{q}}{1 + \beta \hat{\phi}_0(k)\, \mathbf{q}^T \hat{\underline{b}}_0^{-1}(k)\, \mathbf{q}} = \frac{\hat{\tau}_0(k)}{1 + \beta \hat{\phi}_0(k)\, \hat{\tau}_0(k)} \qquad (1.2.6)$$

The function $\hat{\tau}_0(k) = \mathbf{q}^T \hat{\underline{b}}_0^{-1}(k)\, \mathbf{q}$ has a physical interpretation. It is not difficult to show that

$$\tau_0(\mathbf{r}, \mathbf{r}') = -k_B T \frac{\delta \rho(\mathbf{r}')}{\delta \psi_{av}(\mathbf{r})}$$

where the average electrostatic potential is defined from $\psi_{av}(\mathbf{r}) = \psi_{ext}(\mathbf{r}) + \int d\mathbf{r}''\, \phi_0(\mathbf{r}, \mathbf{r}'')\, \rho(\mathbf{r}'')$. Thus, $-\beta \tau_0(\mathbf{r}, \mathbf{r}')$ describes how the charge density "responds" to small changes in the average potential. Since the particle density does not respond directly to the average electrostatic potential but to the full potential of mean force, the function τ_0 gives the rather complex link between variations in $\psi_{av}(\mathbf{r})$ and $\rho(\mathbf{r})$. It is only in mean field theories that

the link is simple and the response is direct and local (*cf.* the weak coupling limit below).

The behaviour of $\hat{\tau}_0(k)$ at $k = 0$ is of considerable interest. As an example, let us consider the case of a two-component, symmetric electrolyte adsorbed on the surface ($q_1 = -q_2 = q$, $n_1 = n_2 = n$, $u_{11} = u_{22}$). Then, from the definition of τ one can derive

$$\hat{\tau}_0(0) = \frac{2nq^2}{1 - n\mathrm{I}_0} \tag{1.2.7}$$

where $\mathrm{I}_0 = \int (a_{0;11}(r) - a_{0;12}(r))\, dr$, and $a_{ij}(r)$ is the short range part of the direct correlation function defined in Eq. (1.2.4). With the possible exception of critical points (which will be avoided throughout), I_0 is finite, which implies that $\hat{\tau}_0(0)$ is non-zero. At low concentrations $n\mathrm{I}_0 \approx 0$ and $\hat{\tau}_0(0)$ is positive, but it may turn negative when the concentration is increased. At the point of sign change the matrix $\hat{\mathbf{b}}_0(0)$ is singular and $\hat{\tau}_0(0)$ infinite. Note that Eq. (1.2.6) implies that a point of infinite $\hat{\tau}_0(k)$ remains a regular point for $\hat{\sigma}_0(k)$. Some consequences of this behaviour will be explored later.

Returning to the general case, one sees from Eq. (1.2.6) and the small k formula $\hat{\phi}_0(k) \sim 2\pi(1+\varepsilon_D)/\varepsilon_1 k$, that

$$\hat{\sigma}_0(k) \sim \frac{k_B T\, \varepsilon_1}{2\pi\,(1+\varepsilon_D)}\, k \quad , \qquad k \to 0 \tag{1.2.8}$$

which in turn implies that

$$\sigma_0(r) \sim -\frac{k_B T\, \varepsilon_1}{4\pi^2 (1+\varepsilon_D)}\, r^{-3} \quad , \qquad r \to \infty \tag{1.2.9}$$

Note that this asymptotic law depends neither on the ion charge or concentration, nor on the short range interactions between the ions (which contribute to $\mathbf{a}_0$). Thus, the correlations in the two-dimensional charge system are universal and long-range. The physical reason for the slow decay is that in contrast to the three-dimensional bulk case, a charge cannot be shielded on all sides. The potential from an annular region of counter charge

about a fixed charge in a plane decays as the third power of the distance. The situation is similar to the case of inhomogeneous electrolytes near a surface, for which the ion-ion correlations parallel to the surface are known to be long-ranged[8,9], at least in the weak coupling limit.

The weak coupling (Debye-Hückel, DH) limit is obtained by simply neglecting the contributions from $\hat{\mathbf{a}}_0$ in $\hat{\mathbf{b}}_0$, *i.e.* take $\hat{\mathbf{b}}_0 = \mathbf{n}^{-1}$, which approximation obviously gets better as $n_\alpha \to 0$ for all α. Thus,

$$\hat{\tau}_0^{DH} = \mathbf{q}^T \underline{\mathbf{n}}\, \mathbf{q} = \sum_\alpha q_\alpha^2 n_\alpha = \kappa\varepsilon_1/2\pi\beta \qquad (1.2.10)$$

where $\kappa = (2\pi\beta/\varepsilon_1)\, \Sigma_\alpha q_\alpha^2 n_\alpha$ is the two-dimensional Debye parameter. Note that in this approximation $\tau_0(\mathbf{r},\mathbf{r}') = \delta(\mathbf{r}-\mathbf{r}')\, \Sigma_\alpha q_\alpha^2 n_\alpha$, from which follows $\delta\rho(\mathbf{r}) = \Sigma_\alpha q_\alpha n_\alpha \delta(-\beta q_\alpha \psi_{av}(\mathbf{r}))$. This local density response due to a change in ψ_{av} is assumed in the Poisson-Boltzmann approximation. Inserting Eq. (1.2.10) in Eq. (1.2.6), one obtains the DH correlation function, for which Eq. (1.2.9) is also valid (*cf.* ref. 10). However, the above derivation of the latter equation shows that it is a general asymptotic law, not dependent on the weak coupling approximation. Eq. (1.2.9) holds true simply as a consequence of Eq. (1.2.3).

1.2B Two surfaces with adsorbed ions

In the case of two interacting surfaces at separation h, one defines the electrostatic potential matrix

$$\underline{\Phi} = \begin{bmatrix} \phi_s & \phi_c \\ \phi_c & \phi_s \end{bmatrix} \qquad (1.2.11)$$

where $\phi_c = \phi_c(\mathbf{r},\mathbf{r}';h)$ is the total electrostatic potential at $\mathbf{r}$ on one surface due to a unit charge at $\mathbf{r}'$ at the other surface (including the image potential), and where $\phi_s = \phi_s(\mathbf{r},\mathbf{r}';h)$ is the corresponding potential on the same surface. Defining the charge matrix $\underline{\mathbf{Q}}$ for the whole system

$$\underline{Q} = \begin{bmatrix} q_I & 0 \\ 0 & q_{II} \end{bmatrix} \qquad (1.2.12)$$

(rectangular matrix of dimension $2m \times 2$), one can write the electrostatic part of the pair potential matrix (1.1.11): $\underline{U}^{el} = \underline{Q}\,\underline{\Phi}\,\underline{Q}^T$.

Similarly, let σ_s and σ_c be the charge-charge correlation functions within and between the surfaces, respectively, and define the 2×2 matrix

$$\underline{\Sigma} = \begin{bmatrix} \sigma_s & \sigma_c \\ \sigma_c & \sigma_s \end{bmatrix} \qquad (1.2.13)$$

It is easily seen that $\underline{\Sigma} = \underline{Q}^T \underline{S}\, \underline{Q}$, with $\underline{S}$ defined in Eq. (1.1.12). In analogy to the single surface case, introduce the matrix $\underline{B} = \underline{N}^{-1} - \underline{C} - \beta \underline{U}^{el}$ and so obtain, using Eqs (1.1.13) and (1.1.19)

$$\hat{\underline{\Sigma}} = \underline{Q}^T \left[\hat{\underline{B}} + \beta \underline{Q}\, \hat{\underline{\Phi}}\, \underline{Q}^T\right]^{-1} \underline{Q} = \left[\hat{\underline{1}} + \beta \hat{\underline{T}}\, \hat{\underline{\Phi}}\right]^{-1} \hat{\underline{T}} = \left[\hat{\underline{T}}^{-1} + \beta \hat{\underline{\Phi}}\right]^{-1} \qquad (1.2.14)$$

where the τ-matrix for the entire system $\hat{\underline{T}}(k) = \underline{Q}^T \hat{\underline{B}}^{-1}(k) \underline{Q}$ (*cf*. Eq. (1.2.6)) has been introduced. In the weak coupling limit one has $\hat{\underline{T}}^{DH} = (\kappa\varepsilon_1/2\pi\beta)\,\hat{\underline{1}}$, a constant diagonal matrix.

From Eq. (1.2.14) $\hat{\sigma}_s$ and $\hat{\sigma}_c$ can easily be expressed explicitly in terms of $\hat{\phi}_s$, $\hat{\phi}_c$, $\hat{\tau}_s$ and $\hat{\tau}_c$, the latter being the elements of $\hat{\underline{T}}$. The factor $[\underline{1} + \beta \hat{\underline{T}}\, \hat{\underline{\Phi}}^{-1}]$ in Eq. (1.2.14) describes the multiple coupling that occurs within and between the two surfaces. A consequence of the multiple coupling between the surfaces is that the tails of σ_s and σ_c, which decay like r^{-3}, have coefficients that depend on τ and hence on the ionic charges, concentrations *etc*. For instance, for large h and in absence of images one has

$$\sigma_c(r) \sim -\frac{(k_B T\, \varepsilon_1)^2}{16\pi^3\, \hat{\tau}_s(0)\, h\, r^3}, \qquad r \to \infty$$

However, $\sigma_s + \sigma_c$ has always the same, universal tail coefficient as $\sigma_0/2$ in Eq. (1.2.8).

The pressure from Eq. (1.1.14) can be written

$$P = -\frac{1}{8\pi^2}\int d\mathbf{k}\, TR\left[\underline{\hat{\Sigma}}(k;h)\frac{\partial\underline{\hat{\Phi}}(k;h)}{\partial h}\right] \qquad (1.2.15)$$

assuming h is large enough to avoid ionic core-core interactions between the two surfaces. Using Eq. (1.2.14), one can write the integrand in a useful form,

$$TR\left[\underline{\hat{\Sigma}}(;h)\frac{\partial\underline{\hat{\Phi}}(;h)}{\partial h}\right] = TR\left[\{\underline{\hat{T}}^{-1}(;h) + \beta\underline{\hat{\Phi}}(;h)\}^{-1}\frac{\partial\underline{\hat{\Phi}}(;h)}{\partial h}\right] =$$

$$= \frac{1}{\beta}\left[\frac{\partial}{\partial h}\ln DET\left[\underline{\hat{T}}^{-1}(;h') + \beta\underline{\hat{\Phi}}(;h)\right]\right]_{h'=h}$$

where only the h-dependence appears explicitly. Thus,

$$P = -\frac{k_B T}{8\pi^2}\int d\mathbf{k}\left[\frac{\partial}{\partial h}\ln DET\left[\underline{\hat{T}}^{-1}(k;h') + \beta\underline{\hat{\Phi}}(k;h)\right]\right]_{h'=h} \qquad (1.2.16)$$

1.3 Interactions

1.3A Ionic layers, no images

The first case to be treated is that of a single layer of mobile, adsorbed anions and cations on each surface. In this subsection, it will be assumed that $\varepsilon_1 = \varepsilon_2$, so image charges are absent. The electrostatic potentials in Eq. (1.2.11) then equal: $\phi_s(r) = 1/\varepsilon_1 r$ and $\phi_c(r) = 1/\varepsilon_1(r^2+h^2)^{1/2}$, where $r = |\mathbf{r} - \mathbf{r}'|$. Their Hankel transforms are $\hat{\phi}_s(k) = 2\pi/\varepsilon_1 k$ and $\hat{\phi}_c(k) = 2\pi \exp(-hk)/\varepsilon_1 k$. The ion-ion pair potentials may contain arbitrary short-ranged potentials in addition to the long-ranged electrostatic interactions.

From Eq. (1.2.16) is obtained the exact expression for the pressure between the surfaces:

$$P = -\frac{k_B T}{2\pi}\int_0^\infty \left[\frac{k^2 e^{-kh}}{1 - e^{-kh} + \dfrac{\varepsilon_1 k}{2\pi\beta(\hat{\tau}_s - \hat{\tau}_c)}} - \frac{k^2 e^{-kh}}{1 + e^{-kh} + \dfrac{\varepsilon_1 k}{2\pi\beta(\hat{\tau}_s + \hat{\tau}_c)}}\right] dk \qquad (1.3.1)$$

For large h one can expand this as an asymptotic series $P \sim \sum_{\nu\geq 3} a_\nu/h^\nu$. The coefficient a_3 is independent of the functions $\hat{\tau}_s(k;h)$ and $\hat{\tau}_c(k;h)$, which only contribute to a_ν, $\nu \geq 4$. This can be seen by making the variable substitution $k = t/h$ in the integral, whereby terms containing the τ-functions disappear from the product Ph^3 in the limit $h \to \infty$. One obtains

$$P \sim -\frac{k_B T\, \zeta(3)}{8\pi h^3}, \qquad h \to \infty \qquad (1.3.2)$$

where $\zeta(3) = 1.202...$, $\zeta(n)$ being the Riemann zeta function. This result can also be obtained as a limiting case of the classical zero frequency term of Lifshitz theory (*cf.* ref. 6). It is the analogue of the attractive quantum force (Casimir force) between conducting surfaces[11,12].

There are several points of interest in this result. First, the pressure between the surfaces follows a power law, decaying as the third power of the

separation. Second, the interaction is attractive, a consequence of the correlations between charges on the two surfaces. Third, the expression for the pressure is a *universal* law, being independent of the surface concentrations, core radii or valencies of the ions in the system. It only depends on the temperature. Here has only been considered the case when the ionic charges are confined to a single plane on each surface. However, one can show that the leading asymptotic form still holds if there is more than one layer of ions per surface (ie the ion centres lie in different planes). This could arise, for example, if the various ions adsorbed on a hard surface have different sizes.

Since Eq. (1.3.2) is independent of the concentration, the asymptotic regime lies at increasingly larger surface separations when decreasing the density (at zero density one would have to go to infinite separation in order not to violate Eq. (1.3.2)). However, it will be shown in Chapter 2 that for moderately large surface densities the asymptotic expression is valid down to surprisingly small surface separation.

The next term in the asymptotic expansion of the pressure is also easily extracted from Eq. (1.3.1). Using the fact that $\hat{\tau}_s \pm \hat{\tau}_c \to \hat{\tau}_0$ when $h \to \infty$, one obtains

$$P - a_3 h^{-3} \sim \frac{3 (k_B T)^2 \varepsilon_1 \zeta(3)}{16\pi^2 \hat{\tau}_0(0)\, h^4}, \qquad h \to \infty \tag{1.3.3}$$

Here, the concentrations, ionic charges and sizes *etc.* enter implicitly through $\hat{\tau}_0$. Note that it is sufficient to calculate $\hat{\tau}_0(0)$ for a single, isolated surface in order to obtain the term (1.3.3) for the interaction between the two surfaces. The implicit h-dependence of $\hat{\tau}_s$ and $\hat{\tau}_c$ only enters in higher order terms of the asymptotic expansion. Equation (1.3.3) shows that P will approach the limiting law (1.3.2) as $h \to \infty$ from the less attractive side for low concentrations (for which $\hat{\tau}_0(0)$ is positive), and from the more attractive side when $\hat{\tau}_0(0)$ is negative, which may occur at high concentrations.

One can obtain the Debye-Hückel approximation for the present system by using the DH expression for $\hat{\underline{T}}$ (*cf.* Eq. (1.2.10)), *i.e.* by setting $\hat{\tau}_s = \hat{\tau}_0^{DH} = \kappa\varepsilon_1 / 2\pi\beta$ and $\hat{\tau}_c = 0$ in the various expressions. The leading terms in the pressure are still given by Eqs. (1.3.2-3), but $\hat{\tau}_0^{DH}$ always remains positive. These results differ from those of Muller and Derjaguin[13], who performed a conventional Debye-Hückel analysis of this system. They obtained a pressure that decays as the fourth power in separation. The reason for the discrepancy is that they have taken the disjoining pressure to be the derivative of the internal energy of the ionic system rather than the free energy. The leading term (1.3.2) is entirely entropic.In fact, their expression for the pressure is the internal energy part of Eq. (1.3.3) in the DH limit.

1.3B Ionic layers with images

When $\varepsilon_1 \neq \varepsilon_2$ one has to include electrostatic image interactions in the treatment. The presence of two dielectric discontinuities gives rise to multiple images, and the expression for the pair potential is a slowly converging, infinite series in r-space. However, the potential can be written in closed form in Fourier space. When the discontinuities are separated by a distance d = h+2w (*cf.* Fig 1.1), the formulae for the interaction potentials equal

$$\hat{\phi}_s(k) = \frac{2\pi}{\varepsilon_1 k}\left\{1 + \frac{2\varepsilon_D}{e^{2kd} - \varepsilon_D^2}\left[\varepsilon_D + e^{kd}\cosh(hk)\right]\right\}$$

$$\hat{\phi}_c(k) = \frac{2\pi}{\varepsilon_1 k}\left\{e^{-kh} + \frac{2\varepsilon_D}{e^{2kd} - \varepsilon_D^2}\left[\varepsilon_D\cosh(hk) + e^{kd}\right]\right\} \qquad (1.3.4)$$

From Eq. (1.2.16) one can obtain an explicit expression for the pressure between the surfaces. After some algebra, the result is

$$\ln \mathrm{DET}\left[\hat{\underline{T}}^{-1} + \beta\hat{\underline{\Phi}}\right] = \ln \frac{\left[1 - H_+(k)\,e^{-kh}\right]\left[1 + H_-(k)\,e^{-kh}\right]}{1 - G^2(k)\,e^{-2hk}} + C \qquad (1.3.5)$$

where

$$G(k) = \varepsilon_D \exp(-2w\,k)$$

$$H_{\pm}(k) = G(k) - \frac{(1 + G(k))^2}{1 + G(k) + \dfrac{\varepsilon_1 k}{2\pi\beta\,(\hat{\tau}_s \pm \hat{\tau}_c)}}$$

The functions $H_{\pm}$ and G are independent of h (at least when performing the differentiation with respect to h in Eq. (1.2.16) since the implicit dependence of $\hat{\tau}_s$ and $\hat{\tau}_c$ is then ignored). Likewise, the constant C does not depend on h and disappears when taking the h-derivative.

After differentiation with respect to h one obtains the exact expression for the interaction between the ionic layers

$$P_{ionic} = \frac{k_B T}{2\pi}\left[\frac{\lambda_3(\varepsilon_D^2)}{4d^3} - \frac{1}{h^3}\sum_{\nu=\{^{+1}_{-1}}\int_0^{\infty}\frac{\nu\,\exp(-t)\,t^2\,dt}{H_\nu\,(t/h)^{-1} - \nu\,\exp(-t)}\right] \quad (1.3.6a)$$

where $\lambda_3(x) = \sum_{\nu=1}^{\infty}\frac{x^\nu}{\nu^3}$.

This result demonstrates the interdependence of the ion-image charge interactions and the vdW interactions between the dielectric media given by the Lifshitz theory[3]. The first term, which originates from the multiple image interactions, is identical to the static (zero-frequency) vdW interaction except that it has the opposite sign. Therefore, in the total interaction between the surfaces

$$P_{tot} = P_{ionic} + P_{VdW} = P_{ionic} - \frac{k_B T\,\lambda_3(\varepsilon_D^2)}{8\pi\,d^3} \quad (1.3.6b)$$

the first term in Eq. (1.3.6a) and P_{vdW} cancel each other identically. Physically, this result implies that the static vdW interaction between the dielectric media is totally screened by the ionic layers.

The additivity of P_{ionic} and P_{vdW} is most easily seen by considering the origin of the primitive model (see also the appendix to ref. 14). To derive the

Coulomb potential *in media* one takes an ensemble of ions and dipoles, and integrates over the dipolar coordinates first. For two ions in an infinite polar fluid, one would obtain the primitive model potential, $1/\varepsilon_1 r$, plus the dipolar free energy H_0, which is independent of the ions. Note that the Coulomb potential *in media* is really a free energy and that this is consistent with the fact that ε_1 is temperature dependent. If one had several polar media, one would obtain the same potential as given by Maxwell's equations, (ie with the effects due to surface polarisation at the dielectric boundaries) plus the dipolar (interaction) free energy as given by classical Lifshitz theory. One now needs to assume pairwise additivity (ie that the dielectric response is local and linear) and the primitive model for the ions follows. But there remains the zero body term H_0 which must be added to the primitive model to obtain the free energy or partition function of the full system. It is this term which has previously been (inadvertently) dropped in primitive model analyses. Since for interacting bodies it represents a power law attraction, for the present problem (as well as for dipoles, Part II, and for the electric double layer, Part III) dropping it is equivalent to including a spurious repulsion in the system. One sees that it is important to include *all* effects of the dielectric boundaries in a consistent manner when calculating the pressure between the surfaces.

The first term in Eq. (1.3.6a) therefore constitutes a fictitious pressure contribution from the image interactions. This long-range, repulsive component appears only as a consequence of the artificial splitting of the total pressure in the two terms: P_{vdW}, the interaction in absence of ions, and P_{ionic}, the correction term due to the presence of ions. In fact, the two leading terms of P_{tot} for large separations are *identical to those obtained in absence of image interactions*, Eqs. (1.3.2-3), with $\hat{\tau}_0(0)$ now refering to a single layer at a surface with a dielectric discontinuity. Thus one has

$$P_{tot} \sim -\frac{k_B T \zeta(3)}{8\pi h^3} + \frac{3(k_B T)^2 \varepsilon_1 \zeta(3)}{16\pi^2 \hat{\tau}_0(0)\, h^4}, \qquad h \to \infty \qquad (1.3.7)$$

It follows that the presence of dielectric discontinuities does not change the leading term in the pressure, which truly is a universal limiting law for the ionic system. In the next term the image interactions only enter indirectly via $\hat{\tau}_0(0)$. Accordingly, the image interactions induced by the second surface do not contribute at all to the leading terms.

As usual, one obtains the corresponding Debye-Hückel expressions by approximating $\hat{\tau}_s = \kappa\varepsilon_1 / 2\pi\beta$ and $\hat{\tau}_c = 0$ in Eqs (1.3.6). The two leading terms in the pressure, Eq. (1.3.7), remain formally the same in this approximation, but the DH value of $\hat{\tau}_0$ is only a good approximation at low concentrations. Since $\hat{\tau}_0^{DH}$ is independent of the interactions, one sees that the magnitude of the dielectric discontinuities does not affect the two leading terms of the total pressure in this approximation. The image effects enter first in the h^{-5} term.

Chapter 2 Approximate methods and results

2.1 Hypernetted chain approximation

A system composed of two coupled surfaces, each having m different adsorbed species, can formally be regarded as a 2m component, two - dimensional, homogeneous mixture with appropriate pair interaction potentials. An approximate theory that is able to accurately treat a homogeneous two-dimensional fluid, will accordingly work equally well for two coupled surfaces at both small surface separations (strong coupling) and at large separations (weak coupling). For particles interacting with long-range potentials, it is well known that the hypernetted chain (HNC) closure for the pair correlation gives an accurate description[15-19]. Therefore that approximation has been adopted in our study of the present systems†. Since it works well up to reasonably large densities, it provides a good check of the range of validity of the various asymptotic expressions derived above.

The HNC closure can be written

$$c_{ij}(r) = h_{ij}(r) - \ln[1 + h_{ij}(r)] - \beta u_{ij}(r) \qquad (2.1.1)$$

where i and j are combined species and surface indices (surface I for $1 \le i \le m$, and II for $m+1 \le i \le 2m$). This relation together with the

---

†My contribution to the HNC calculations, besides actually doing them, was to adapt a double layer programme supplied by Roland Kjellander and Stjepan Marčelja to the present problem. I also derived and implemented expressions for the free energy and pressure. I implemented a version for the single surface, and found ways to evaluate the quantity $\hat{\tau}_0(0)$ which is used in the simplified mean-field approximation (§2.2).

Ornstein-Zernike equation,

$$h_{ij}(r) = c_{ij}(r) + \sum_k n_k \int h_{ik}(|r-r'|)\, c_{kj}(r')\, dr' \qquad (2.1.2)$$

constitute the system of equations to be solved numerically. From the solutions, the matrices $\hat{\underline{b}}_s(k;h)$ and $\hat{\underline{b}}_c(k;h)$ (and for ions $\hat{\underline{t}}_s(k;h)$ and $\hat{\underline{t}}_e(k;h)$), the pressure and other quantities can be accurately determined.

It is clear from Eq. (2.1.1) that c_{ij} satisfies the relation (1.1.8), which was the basis for all asymptotic laws derived above. For instance, one is therefore guaranteed that the universal law for the ionic systems (the first term in Eq. (1.3.7)) is *exactly* fulfilled in the appropriate limit. The deviation of the HNC pressure from the universal limiting law is governed to the leading order by the second term in Eq. (1.3.7) with the HNC value of $\hat{\tau}_0(0)$ inserted.

Details about the numerical methods used to solve Eqs (2.1.1-2) are given in refs 20-23. Here, it is sufficient to say that Eq. (2.1.1) and the Hankel transform of (2.1.2) was solved by an iterative procedure. The numerical Hankel transformations involved in these iterations were performed using the orthogonal transform method of Lado[21]. The long range tails of $c_{ij}(r)$, both due to the direct Coulomb interactions and the image interactions, were subtracted off and treated analytically[20-23]. The discontinuities of $h_{ij}(r)$ and $c_{ij}(r)$ at the hard core diameter, as well as the corresponding long-range tails in Fourier space, were also eliminated and treated analytically.

In the calculations one faces the common dilemma of a large cutoff radius versus the grid size. Once the cutoff radius and the number of mesh points are specified, the actual points in both real and Fourier space are determined in Lado's Hankel transform method[21]. The cutoff radius was generally chosen to be $60 \cdot (\pi n)^{-1/2}$. For the largest separations and highest surface densities this was increased by up to 50%. Except for these latter cases, experience showed that there was negligible change in the calculated pressures when the mesh of 600 was increased to 800 points.

The calculations were performed for systems with one species of anions and one of cations on each surface,*i.e.* four distinct species in the scheme described above. The hard core diameters of all ions were identical. The pressure between the surfaces was calculated using Eq. (1.1.14). Explicit equations for the free energies within the HNC approximation are also available[20,24], and numerical differentiation of these with respect to separation is in reasonable agreement with the pressure calculated via Eq. (1.1.14).

2.2 Mean field perturbation approximation

In §1.3 it was shown that the leading terms in the (exact) pressure between two identical surfaces at large separations only contain one parameter from the corresponding single-surface system, $\hat{\tau}_0(0)$. The same formal asymptotic expressions are also valid in simple, approximate theories like the Debye-Hückel theory, but with the single-surface quantities from the same theory inserted. The limitation of that kind of theory is that it treats the single surface too simply, *i.e.* the values of $\hat{\tau}_0(0)$ are inaccurate unless the concentration is low. In this section a method will be given that combines accurate treatments of single surfaces and an approximate treatment of the interactions between the surfaces, while conforming to the asymptotic laws of §1.3. This guarantees that the calculated pressure is accurate at least in the limit of large surface separations. Since the approximate pressure formulae will contain terms additional to the (exact) leading ones, one may expect that the calculated values at small separations are better than those obtained from the leading terms alone.

Therefore assume that the (exact) pair correlations on a single, isolated surface are known, and consider the perturbation due to an identical surface nearby. All interactions between the surfaces will be included in the external potential for each surface (a mean field approximation). In addition, an arbitrary, but small, external potential will be imposed on the entire system (only a "test potential" that eventually will be put to zero). Since the total external potential remains small, one can apply Eqs (1.1.4-5), using the exact $\underline{\mathbf{s}}_0$ of the isolated surfaces, to obtain the perturbed density distribution. Define the matrix of unperturbed correlations for the entire system

$$\underline{\mathbf{S}}_0 = \begin{bmatrix} \underline{\mathbf{s}}_0 & \mathbf{0} \\ \mathbf{0} & \underline{\mathbf{s}}_0^{T'} \end{bmatrix} \qquad (2.2.1)$$

and the correlations $\underline{\mathbf{S}}$ for the coupled surfaces are given by Eq. (1.1.12). $\underline{\mathbf{S}}$

describes the density response, $\delta\mathbf{N} = -\beta\,\underline{\mathbf{S}}\cdot\delta\mathbf{V}$, when the external potential for the *total* system is varied, *i.e.* when the interaction potentials between the two surfaces are not included in the external potential **V**. On the other hand, $\underline{\mathbf{S}}_0$ describes the density response of the two individual surfaces $\delta\mathbf{N} = -\beta\,\underline{\mathbf{S}}_0\cdot\delta\mathbf{V}'$ due to the (small) potential variation around zero:

$$\delta\mathbf{V}' = \delta\mathbf{V} + \underline{\mathbf{U}}_{int}\cdot\delta\mathbf{N} = \delta\mathbf{V} - \beta\underline{\mathbf{U}}_{int}\cdot\underline{\mathbf{S}}\cdot\delta\mathbf{V}$$

where $\mathbf{V}'$ is the total external potential (including the coupling to the other surface) for the two individual surfaces and where the matrix of perturbing interaction potentials between the surfaces is $\underline{\mathbf{U}}_{int} = \underline{\mathbf{U}} - \underline{\mathbf{U}}_0$. The density variation described by $\underline{\mathbf{S}}$ and $\underline{\mathbf{S}}_0$ is approximately equal, and when the coupling between the two surfaces is weak (large separation) the approximation is very good. Since the variation in external "test potential" $\delta\mathbf{V}$ is arbitrary, it follows from the relationships above that the approximate equality

$$\underline{\mathbf{S}} = \underline{\mathbf{S}}_0 - \beta\underline{\mathbf{S}}_0\cdot\underline{\mathbf{U}}_{int}\cdot\underline{\mathbf{S}} \qquad (2.2.2)$$

is valid. Using the the fact that $\underline{\mathbf{S}}^{-1} = \underline{\mathbf{N}}^{-1} - \underline{\mathbf{C}}$ (*cf.* Eqs (1.1.6-7) and (1.1.13)), one sees that Eq. (2.2.2) implies $\underline{\mathbf{C}} = \underline{\mathbf{C}}_0 + \beta\underline{\mathbf{U}}_{int}$. If the separation between the surfaces is large enough to avoid core-core interactions between the surfaces, $\underline{\mathbf{U}}_{int}$ only contains the electrostatic interactions, and Eq. (2.2.2) is equivalent to

$$\underline{\mathbf{B}}(\mathbf{r},\mathbf{r}') = \underline{\mathbf{B}}_0(\mathbf{r},\mathbf{r}') \qquad (2.2.3)$$

where, as usual, $\underline{\mathbf{B}} = \underline{\mathbf{N}}^{-1} - \underline{\mathbf{C}} - \beta\underline{\mathbf{U}}^{el}$. Thus, the approximations are simply $\underline{\mathbf{b}}_s = \underline{\mathbf{b}}_0$ and $\underline{\mathbf{b}}_c = \underline{\mathbf{0}}$. For ionic layers this implies $\tau_s = \tau_0$ and $\tau_c = 0$. It is evident that all asymptotic formulae in §1.3 are satisfied exactly (provided the exact $\underline{\mathbf{b}}_0$ and τ_0 are used). The approximation only affects higher order terms in the pressure. The total pressure can be obtained by inserting this approximation in Eq. (1.3.6) for ions.

The approximate pair correlations for the coupled surfaces can be obtained from Eq. (2.2.2), which is easily solved in Fourier space

$$\hat{\underline{S}}(k) = [\hat{\underline{1}} + \beta \hat{\underline{S}}_0(k)\, \hat{\underline{U}}_{int}(k)]^{-1}\, \hat{\underline{S}}_0(k) \cdot \qquad (2.2.4)$$

One can also obtain an expression for the interaction free energy, F_{int}, via a coupling parameter integration. If $\underline{S}(\mathbf{r},\mathbf{r}';\eta)$ is the pair correlation when the interaction potential equals $\eta\, \underline{U}_{int}(\mathbf{r},\mathbf{r}')$, then, using Eq. (2.2.4),

$$F_{int} = \frac{1}{2} TR \int_0^1 d\eta \int dr\, dr'\, \underline{S}(r,r';\eta)\, \underline{U}_{int}(r',r) + F_{int}^{Av}$$

$$= \frac{k_B T A}{8\pi^2} \int dk\, \ln DET\, [\hat{\underline{1}} + \beta \hat{\underline{S}}_0(k)\, \hat{\underline{U}}_{int}(k;h)] + F_{int}^{Av} \qquad (2.2.5)$$

with **A** being the area of the surfaces. The last term is the "average" free energy of interaction (*i.e.* when the correlations are neglected, using smeared-out particle distributions) and equals

$$F_{int}^{Av} = \frac{1}{2} \int dr\, dr'\, \mathbf{N}^T\, \underline{U}_{int}(r,r')\, \mathbf{N}$$

It turns out to be independent of h (or even zero) in the cases considered in this work. The pressure can be obtained by differentiating the free energy with respect to the surface separation; for instance, Eq. (2.2.5) yields Eq. (1.1.14) with the approximation $\underline{S} = \underline{S}_0$ inserted.

The interaction potential $\hat{\underline{U}}_{int}(k)$, which is here assumed to be entirely electrostatic, contains a factor exp(-hk). Therefore, the small-k contributions to the integrand in Eq. (1.2.16) dominate in the pressure for large h. The mean field perturbation approximation $\hat{\underline{B}}(k) \approx \hat{\underline{B}}_0(k)$ can therefore be further simplified by inserting $\hat{\underline{B}}_0(0)$ instead of $\hat{\underline{B}}(k)$ in integrals involving the interaction potential between the surfaces. This approximation will be called the *simplified mean field perturbation theory.* In the ionic case this corresponds to the insertion of $\hat{\underline{T}}_0(0)$ instead of $\hat{\underline{T}}(k)$ in Eq. (1.2.16). Note that this can be regarded as a *modified Debye-Hückel approximation,* where the exact (or at least accurate) value of $\hat{\tau}_0(0)$ is inserted in the pressure formula rather than $\hat{\tau}_0^{DH}$. Since only the values of $\hat{\underline{B}}_0$ and $\hat{\underline{T}}_0$ at k = 0 (in terms of K_0 the compressability and $\hat{\tau}_0(0)$) enter in the asymptotic formulae

of §1.3, those formulae are still satisfied exactly. The approximations only affect higher order terms. While the pressures obtained in this approximation are guaranteed to be excellent at large separations, one would expect that they remain good also at smaller h. This is found to be true in practice (see §2.3).

When $\hat{\tau}_0(0) < 0$ (which can occur for cases of high coupling of the isolated surface) the suggested procedure introduces an artificial pole in the integrand of Eqs (1.3.1) and (1.3.6), and one has to proceed differently. One can expand P in an asymptotic series in $1/h^{\nu}$ and evaluate the coefficients using our approximation $\hat{\tau}_s(k) \exp(-hk) \approx \hat{\tau}_0(0) \exp(-hk)$ and $\hat{\tau}_c(k) \approx 0$. The leading terms of this expansion are the exact ones. By including a few more terms a good approximation for the actual pressure (see §2.3) is obtained, and a tractable expression for the pressure in terms of $\hat{\tau}_0(0)$ results.

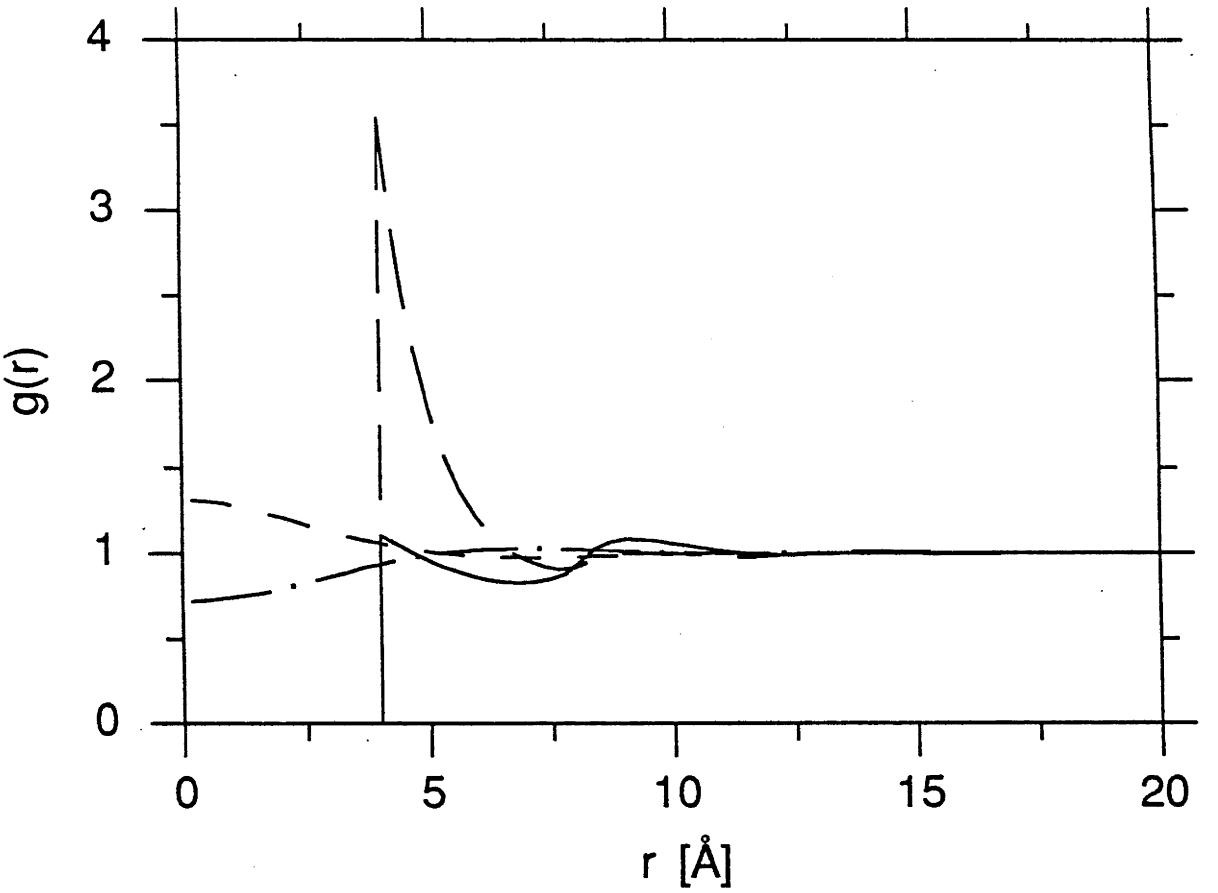

Figure 2.1a The HNC radial distribution functions $g_{ij}(r)$ for adsorbed, monovalent ions on two surfaces separated by 5Å (r is the cylindrical radial coordinate). The inverse number density (= area per ion, A) of each ion species is A = 75 Å^2, the hard sphere diameter is 4Å, and $\varepsilon_1 = \varepsilon_2 = 80$. The curves (———) and (— — — —) are for ions on the same surface (g_{11} and g_{12} respectively). The curves (— . — . — .) and (- - - - - - -) show the distribution functions between like (g_{14}) and unlike (g_{13}) ions on opposite surfaces.

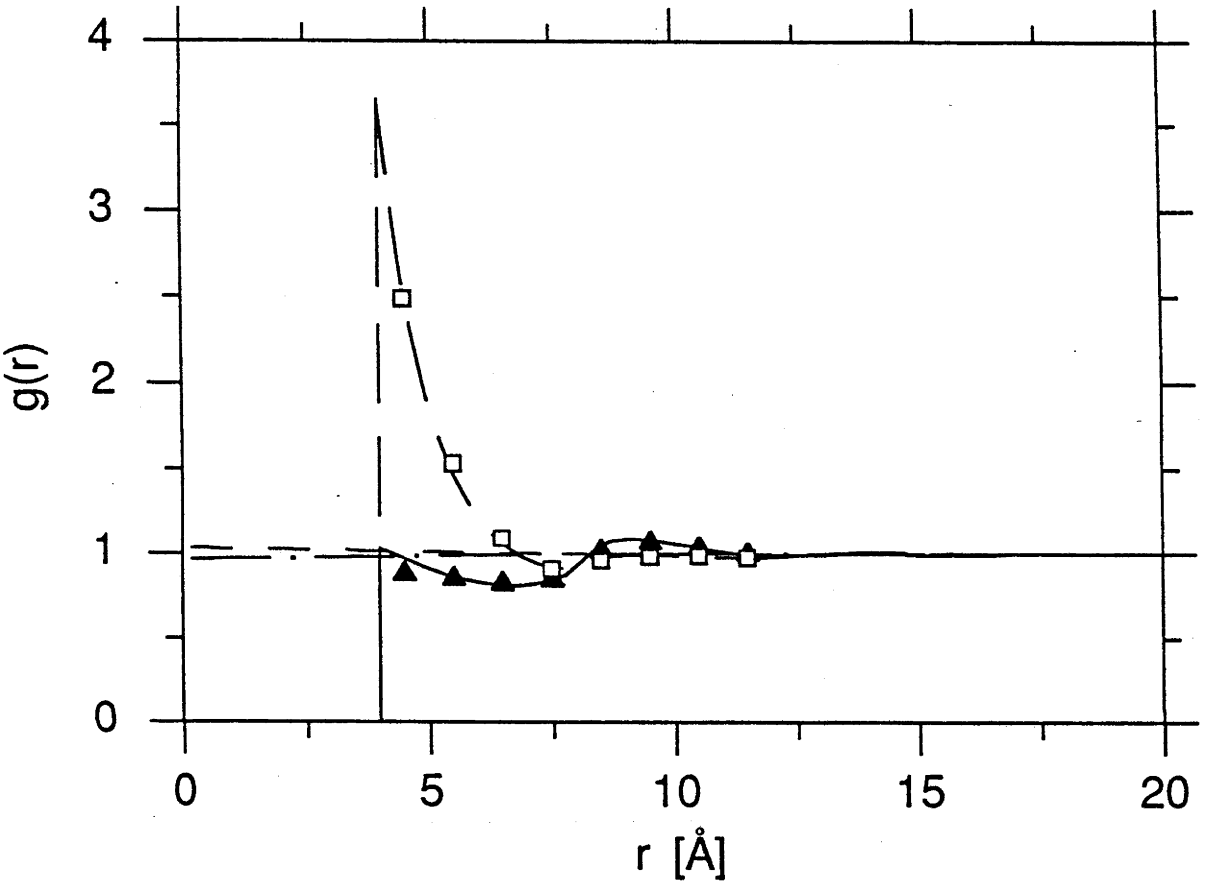

Figure 2.1b Distribution functions for the same surfaces as in fig. 2.1a separated by 10Å. The symbols (□) and (▲) show the Monte Carlo (MC) results for the corresponding single, isolated surface.

The universal, asymptotic law (1.3.2) is compared with the actual pressure for four different ion densities in Fig 2.2a, calculated in the HNC approximation. As predicted in §1.3A, the asymptotic regime moves to larger separations when the surface density is decreased. The approach of the pressure to the universal law as $h \to \infty$ is governed by the h^{-4} term given in Eq. (1.3.3). The magnitude and sign of this term are determined by $[\hat{\tau}_0(0)]^{-1}$. It is seen from the figure that the asymptote is approached from below at low densities, whereas it is approached from above at high densities. In fact, $\hat{\tau}_0(0)$ changes sign near the inverse density $A = 200$ Å^2, where the denominator of Eq. (1.2.7) passes zero. At such a point the h^{-4} term (1.3.3) vanishes and the deviation of P from the universal law (1.3.2) is determined by higher order terms only (which are small for the same reason). This is why the universal law and the actual pressure agree very well for densities around $A = 200$ Å.

The HNC pressure is compared with the results from simulations[25] in Fig. 2.2b for the case $A = 40$ Å^2. The MC calculations were done for three different sizes of the simulation cell, containing 40, 80 and 160 ions of each kind respectively. The results for 1000 Å^2 are compared in the inset. It can be seen that the MC results agree very well with the HNC curve up to a certain separation, which depends on the size of the simulation cell; the larger the cell, the larger is the range of agreement. This is an effect of the finite size of the cell and of the periodic boundary conditions used in the simulations, and it can be explained as follows. The interaction between the two surfaces at large separations is dominated by the contributions from the tails of the correlation functions. When the separation is increased, the tail segments of importance lie further and further out. Since only a limited portion of the tails can be accurately calculated in a finite cell subject to periodic boundary conditions, there will always exist a maximal separation after which the error in the MC pressure will be intolerably large.

The HNC pressure curve agrees with the MC results within the

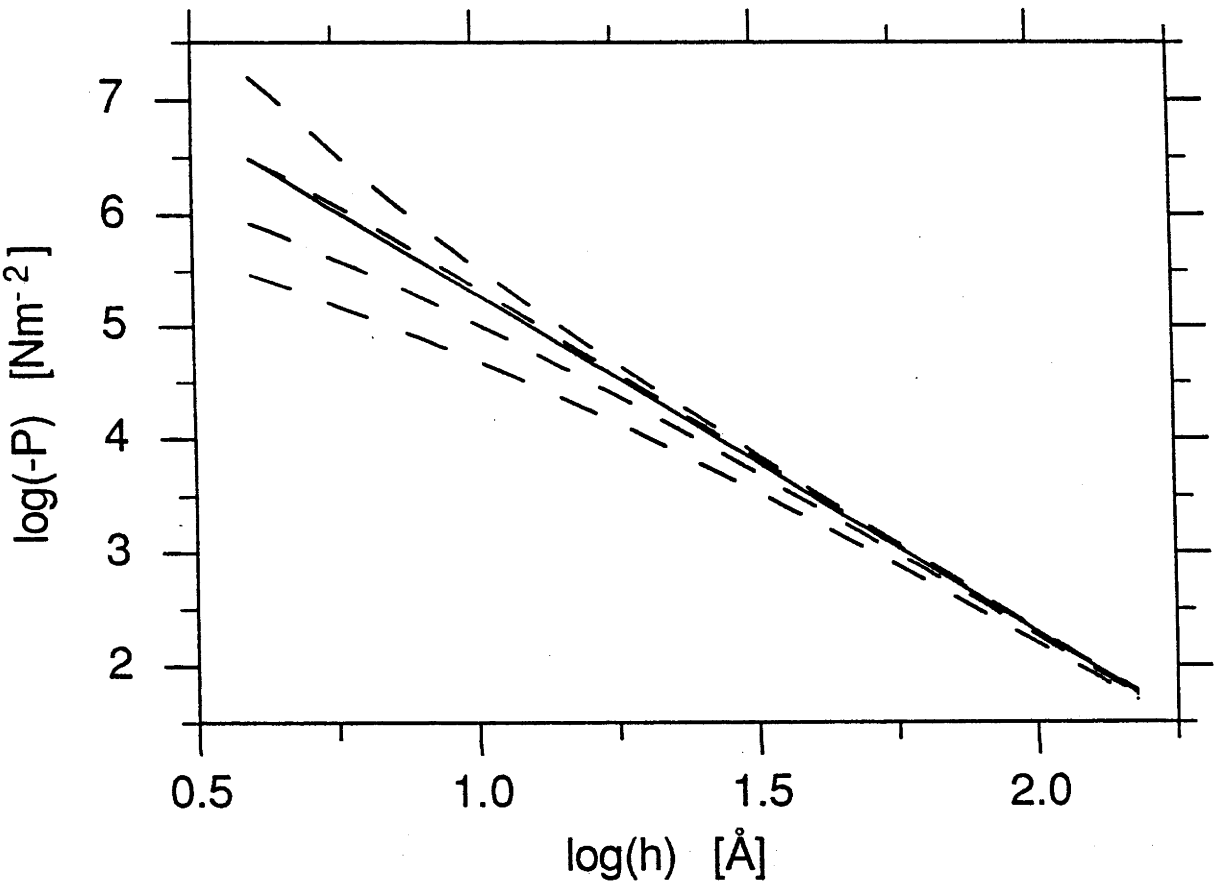

Figure 2.2a Comparison between the universal asymptotic law (———) for the attraction between two surfaces with adsorbed ions (from Eq. (1.3.2)), and the HNC results (- - - - -) for monovalent ions at four different concentrations [inverse number densities from bottom to top: 1000, 500, 200 and 40 Å^2]. The ionic diameters are 4 Å and $\varepsilon_1 = \varepsilon_2 = 80$.

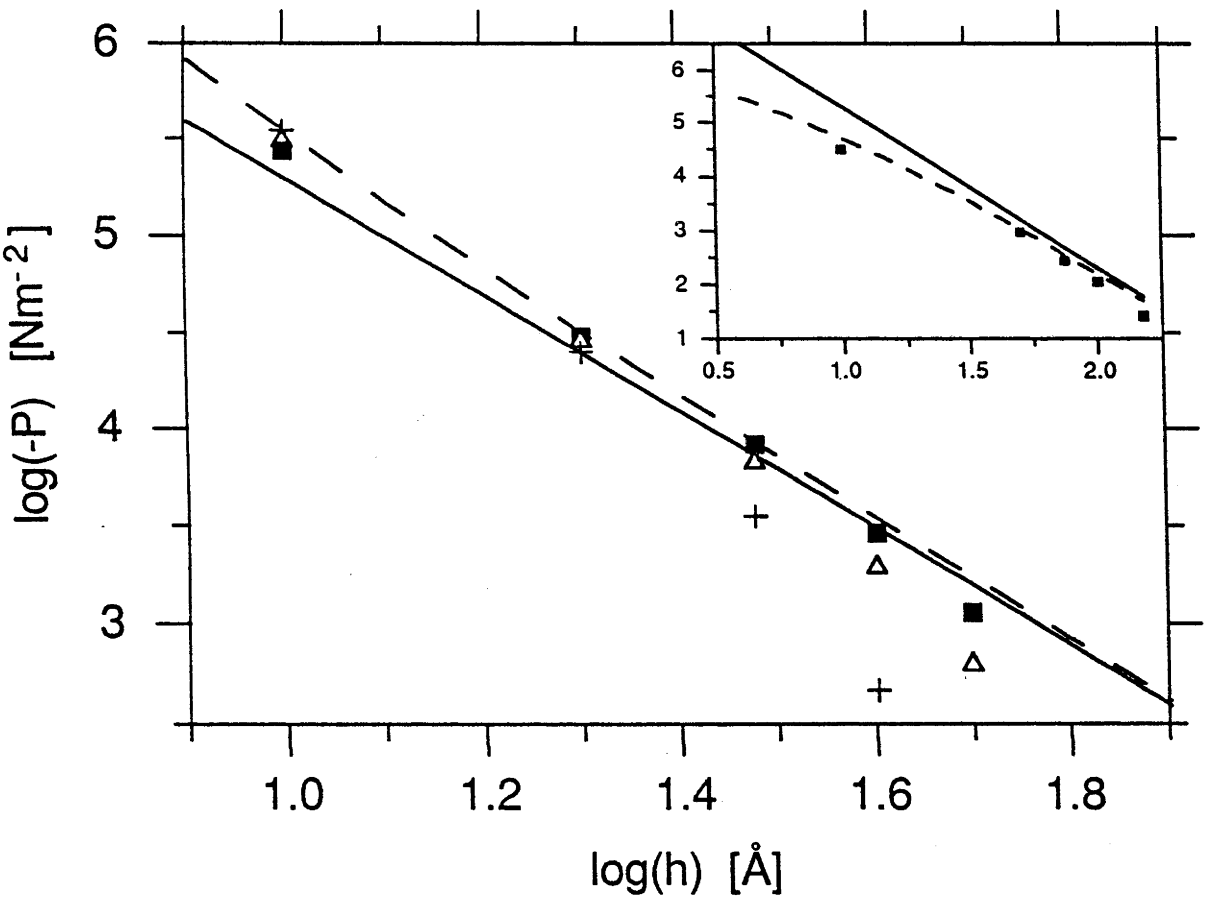

Figure 2.2b The attractive pressure, -P, for the inverse density A = 40 Å^2 calculated in the HNC approximation (- - - - -) [same as in Fig. 2.2a] and by MC simulations. Three different sizes of the simulation cell was used in the MC calculations, containing 40 (+), 80 (Δ) and 160 (■) ions of each kind respectively. The downward deviation of the MC results at larger separations is a consequence of the finite cell sizes and the periodic boundary conditions used in the simulations (see text). The universal asymptot is shown as (———). The inset shows the corresponding results for A = 1000Å (with 2×160 ions in the simulation box).

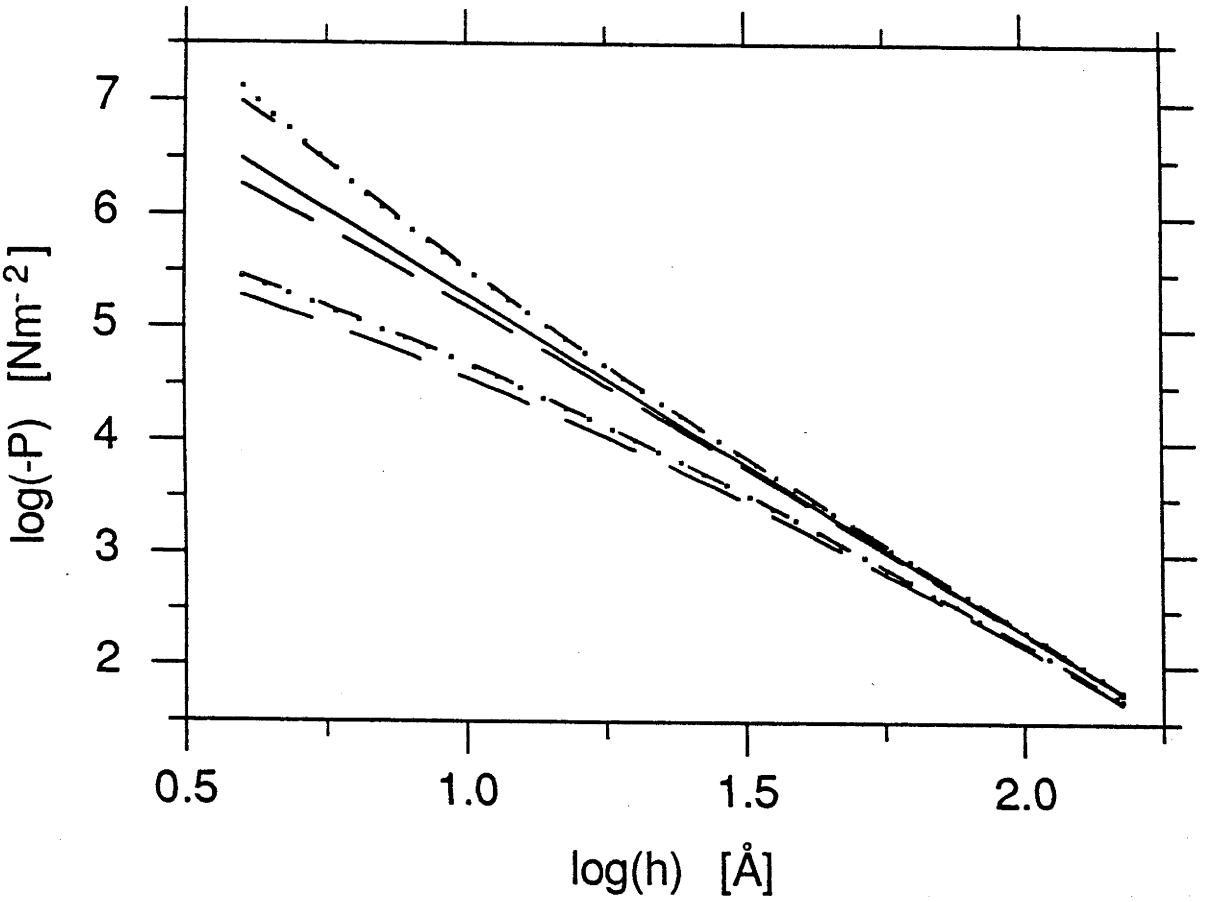

Figure 2.2c The attraction, -P, predicted by the Debye-Hückel theory (— — —) and by the mean field perturbation (MFP) theory (·····) compared to the HNC results (- - - - -). The curves are from bottom to top: DH, A= 1000Å^2; MFP & HNC (nearly coinciding), A=1000Å^2; DH, A=75Å^2; universal asymptot (————); HNC & MFP (nearly coinciding), A=75Å^2.

simulation errors. In fact, the HNC method performs much better over the whole separation range than the so-called "exact" simulations. The MC results confirm the conclusions above for the asymptotic behaviour of the pressure at large surface densities. In particular, they prove the existence of attractions larger than those given by the universal asymptote, and hence the reality of the negative $\hat{\tau}_0(0)$ values.

At low densities, the pressure curves in Fig. 2.2a agree with the asymptot only at large separations. However, at smaller separations (down to some 60 Å for the case of $A = 1000$ Å^2) the pressure is reasonably well given by the Debye-Hückel approximation, as evident from Fig. 2.2c. Note that the numerator of Eq. (1.2.7) equals $\hat{\tau}_0^{DH}$ (Eq. 1.2.10), and one sees that the DH approximation for $\hat{\tau}_0(0)$ is good when $n\mathfrak{I}_0 \approx 0$. From Eq. (1.3.1) and the fact that $\hat{\tau}_0^{DH} > 0$ it follows that the universal asymptotic law (1.3.2) is an upper bound for the attraction calculated in the DH theory, while, as has been shown above, the actual pressure may become more attractive than the value given by the asymptotic formula. For instance, $-P^{DH}$ for 75 Å^2 lies below, but close to the asymptote, while the curve for the actual attraction lie well above it since $\hat{\tau}_0(0) < 0$ in this case (Fig. 2.2c).

It is clear that the simplified mean field perturbation (modified Debye-Hückel) approximation suggested in §2.2, *i.e.* to use $\hat{\tau}_0(0)$ from an accurate calculation for a single surface instead of $\hat{\tau}_0^{DH}$, has a much larger range of validity. For the case $A = 1000$ Å^2 one can see in Fig. 2.2c that the mean field curve is virtually coinciding with the HNC curve. Equally good results are obtained down to $A \approx 200$ Å^2, where $\hat{\tau}_0(0)$ becomes negative. For higher densities, one approximates the pressure with the first few terms in its asymptotic expansion in $1/h^\nu$, using coefficients evaluated in the mean field theory (see discussion in §2.2). The results for $A = 75$ Å^2 shown in Fig. 2.2c, indicate that the agreement with the HNC curve is very good. If one only includes the h^{-3} and h^{-4} terms from Eqs. (1.3.2-3), which are independent of the mean field approximation, the resulting curve (not shown) nearly

coincides with the HNC values only above h ≈ 20 Å. For shorter separations, this curve lies between the HNC curve and the universal asymptote. Table 2.1 compares values of $\hat{\tau}_0(0)$ calculated in the Debye-Hückel and HNC approximations for various areas per ion pair.

The universal asymptotic law (1.3.2) is independent of system details like the ionic charge and size, and the number and relative positions of the ionic layers (§1.3). For example, the interaction between two surfaces containing one charged species on a neutralizing, uniform background (one-component plasma) investigated by Kjellander and Marčelja[26], obey this law. Their estimate of the coefficient ($2.2 \cdot 10^{-22}$ J) is in good agreement with the exact value ($2.0 \cdot 10^{-22}$ J). To further test how much variations in the system parameters affect the difference between the universal law and the actual pressure at moderately high densities,some calculations at A = 75 Å^2 for the two-species systems have been made. It may be seen from Fig. 2.3 that the attraction is increased when the ionic diameter or charge is increased, while it is decreased when one of the ion species on each surface is placed on a separate plane further out from the middle. However, all these pressure curves are fairly close to the asymptote above h ≈ 15Å. Quite generally, the attraction increases with the electrostatic coupling.

As shown in §1.3B, the asymptotic law, Eq. (1.3.2), is also unchanged in presence of dielectric discontinuities provided the image charge interactions for the ions as well as the static vdW interaction are included. The results for A = 75 Å^2, presented in Fig. 2.4a, show that the total attraction at all separations can be *larger* in presence of discontinuities than in their absence. The main reason is that the image charges at the nearest surface increase the electrostatic coupling in each layer. For example, the value of $q^2/\hat{\tau}_0(0)$, which determines the h^{-4} contribution in Eq. (1.3.7), changes from $-0.64 \cdot 10^{-18}$ m^2 to $-1.18 \cdot 10^{-18}$ m^2 when turning on the image interactions in this case.

It may also be seen from Fig. 2.4a that neglecting to include the vdW

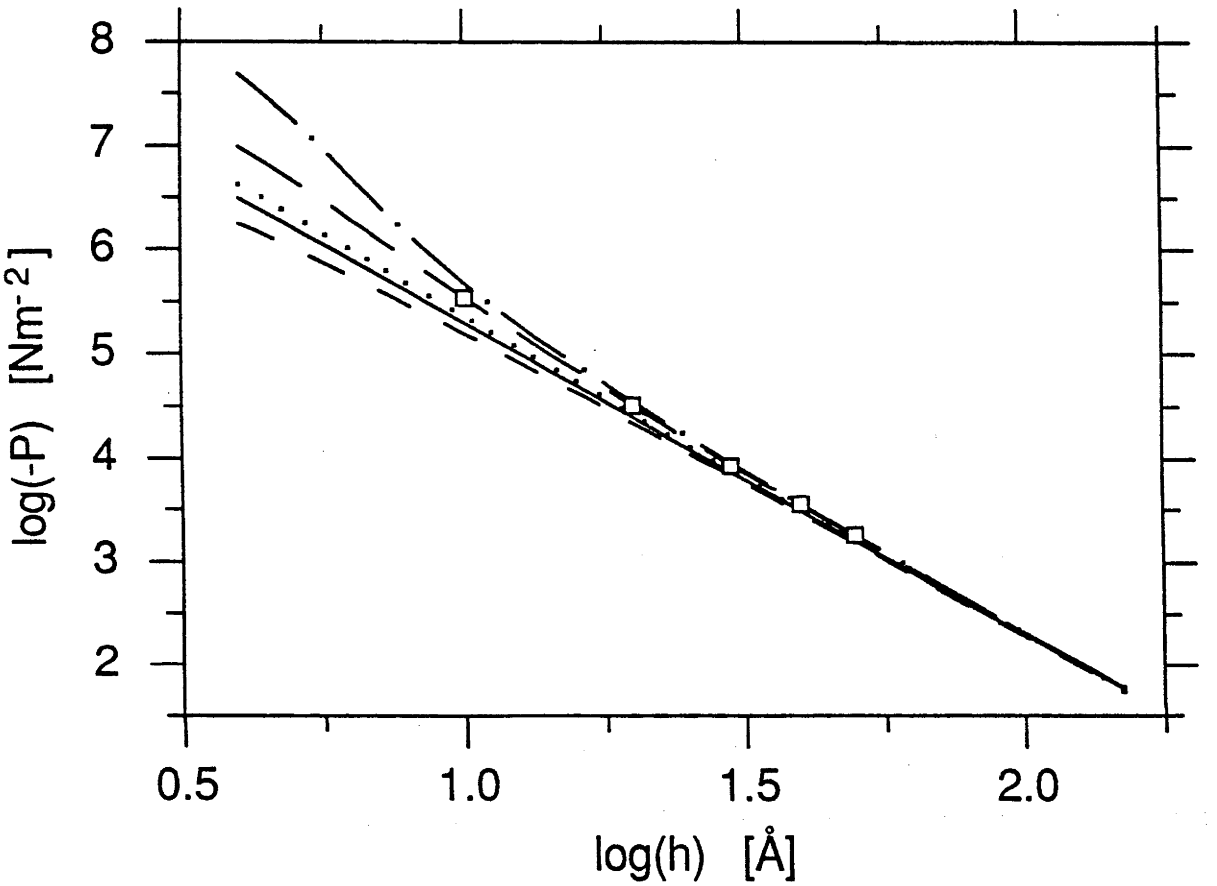

Figure 2.3 Comparison of HNC pressures for monovalent ions with diameters 2Å (·····) and 4 Å (— — — —), for divalent ions with diameters 4 Å (— . — . — .) and for 4Å monovalent ions where the cations and the anions at each surface lie in different planes separated by 4Å (- - - - -). [In the latter case the surface separation is counted between the planes closest to the middle]. The MC results for the divalent case is shown by (□) (2×160 ions in the simulation box). The inverse number density for each ionic species is 75Å^2 in all cases and $\varepsilon_1 = \varepsilon_2 = 80$. The universal asymptot is shown by (—————).

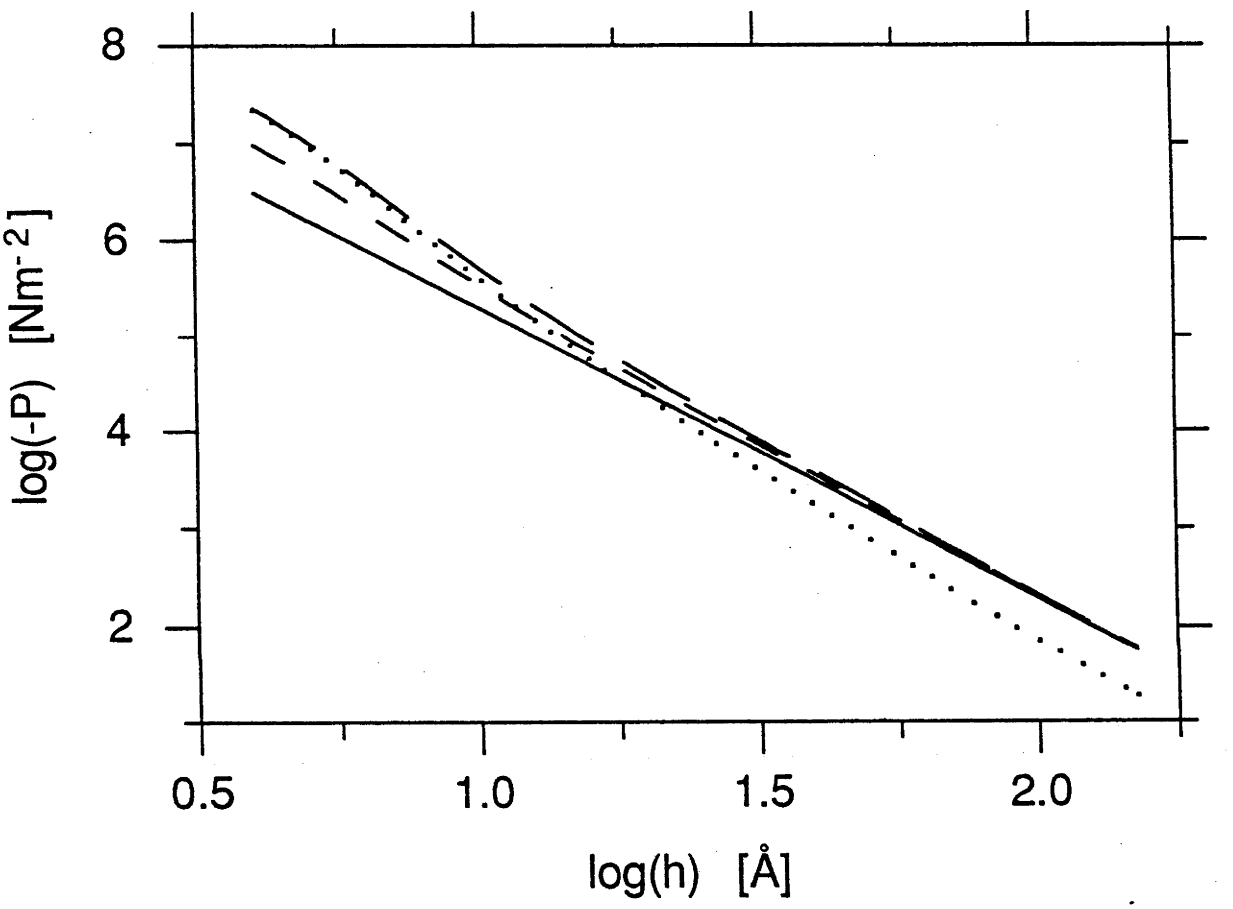

Figure 2.4a The negative pressure, -P, as a function of separation, h, between ionic layers in the presence of dielectric discontinuities, $\varepsilon_1 = 80$ and $\varepsilon_2 = 5$. The universal asymptotic law (———) is compared to the HNC results (— — —) for monovalent ions with diameters 4 Å, w = 0.5 Å and A = 75 Å^2. The pressure component P_{ionic}, *i.e.* P from the HNC calculation before addition of the static Van der Waals interaction (P_{VdW}), is shown by (·····). For reference, the pressure for the corresponding system without dielectric discontinuities is also included (- - - - -).

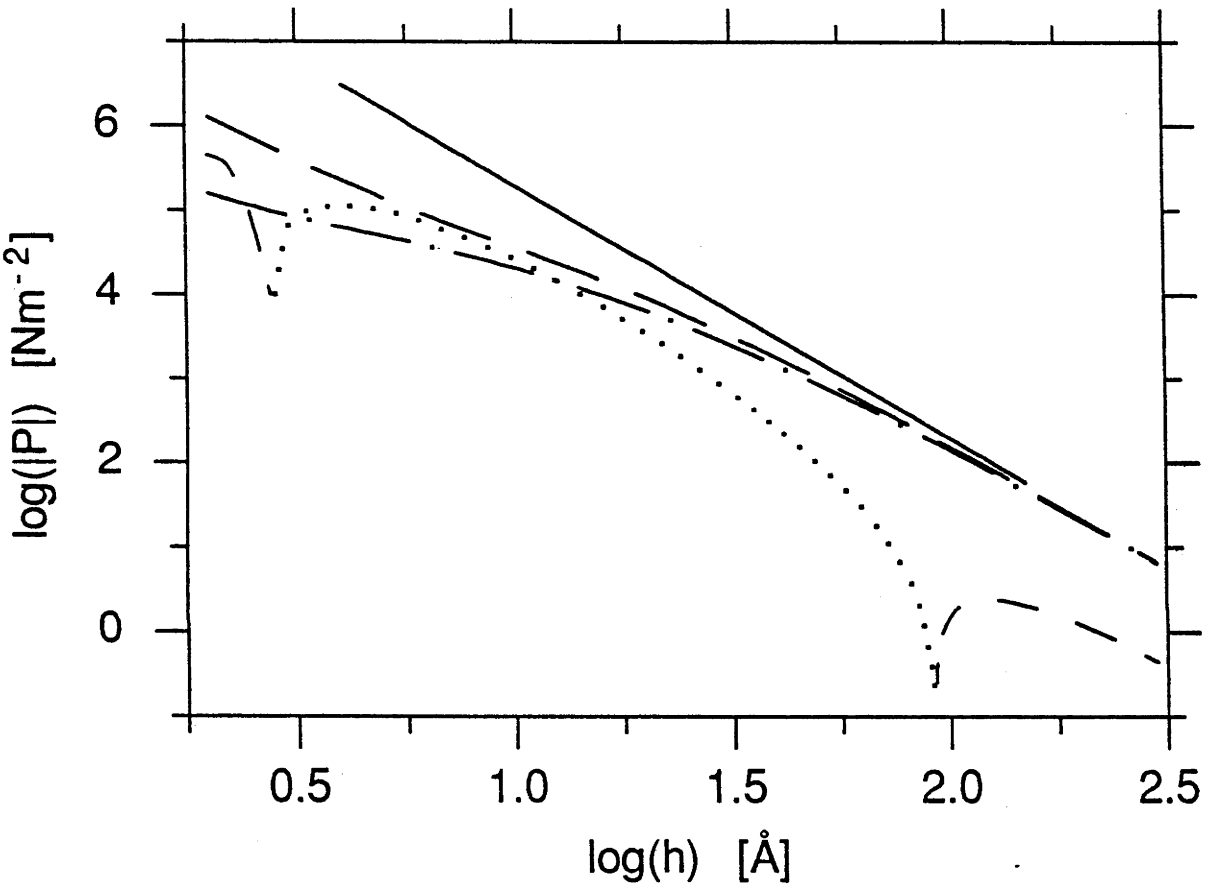

Figure 2.4b An example where P_{ionic} has both repulsive (·····) and attractive (- - - - -) regimes. The absolute value of the HNC pressure is shown as a function of the separation. The inverse density of the monovalent ions is 1000Å^2, the ionic diameters 4 Å, $\varepsilon_1 = 80$, $\varepsilon_2 = 2$ and w = 2 Å. The total pressure, $P_{ionic} + P_{VdW}$, is entirely attractive and is shown as (— — — —). The curve (— . — . — .) shows the total attractive pressure calculated by using the Debye-Hückel approximation. The universal, attractive asymptotic law is plotted as (———).

interaction, taking $P = P_{ionic}$, would lead to the erroneous conclusion that the image interactions decrease the attraction between the surfaces for separations above some 12 Å. As discussed in §1.3B, the repulsive image charge contribution is entirely fictitious. A neglect of P_{VdW} can actually lead to qualitatively wrong results for the system. This is illustrated in Fig. 2.4b, which shows the results for ionic layers with $A = 1000$ Å^2. P_{ionic} alone is repulsive in the interval 3 - 90 Å, while the total pressure is attractive throughout.

Conclusion to Part I

The leading contribution to the pressure between two surfaces with adsorbed mobile ions is universal (depending only on temperature), attractive and decays like h^{-3}, while the next order term (h^{-4}) depends on one parameter, $\hat{\tau}_0(0)$, the integral of the "mean field response function" for the corresponding isolated, single surface. The total pressure, calculated by the HNC method or by Monte Carlo simulations, is entirely attractive for the wide range of system parameters investigated. Given an accurately determined $\hat{\tau}_0(0)$, the pressure can be calculated with the mean field perturbation theory, which includes the correct h^{-3} and h^{-4} terms but approximates the higher order contributions. The agreement with the HNC and MC results is good down to surprisingly short separations.

The exact treatment of the electrostatic fluctuation interactions in this model shows that the image charge interactions of the ions and the van der Waals interaction of the dielectric media have to be treated in a consistent manner, otherwise fictitious, long range pressure contributions will be included. The zero frequency vdW interaction is screened by the ionic layers. This is caused by the coupling between ion-ion correlations and polarization fluctuations in the dielectric media, via the image interactions of the ions. From this example it is clear that one *always* has to include the vdW interaction when analyzing the image charge interactions. This holds true whether the particles are charges or dipolar (Part II) and whether they are all adsorbed on the surfaces or not. For the latter double layer problem, the screened interaction decays exponentially (see Part III), in contrast to the power-law decay found here for these interacting surfaces bearing mobile charges.

References for Part I

1 E.J.W. Verwey and J.Th.G. Overbeek, *Theory of the Stability of Lyotropic Colloids* (Elsevier, Amsterdam, 1948).

2 B.V. Derjaguin and L. Landau, Acta Phys.-Chim. USSR **XIV**, 663 (1941).

3 E.M. Lifshitz, Sov. Phys. JETP, **2**, 73 (1956); I.E. Dzyaloshinskii, E.M. Lifshitz, and L.P. Pitaevskii, Adv. Phys., **10**, 165 (1961).

4 V.N. Gorelkin and V.P. Smilga, Sov. Phys. JETP, **36**, 761 (1973).

5 B.W. Ninham and V.A. Parsegian. The original work (1972) is unpublished, but the theory is presented in Chapter 7.4 of ref. 6.

6 J. Mahanty and B.W. Ninham, Dispersion Forces (Academic Press, London, 1976).

7 B. Davies and B.W. Ninham, J. Chem. Phys., **56**, 5797 (1972).

8 B. Jancovici, J. Stat. Phys., **28**, 43 (1982).

9 S.L. Carnie and D.Y.C. Chan, Mol. Phys., **51**, 1047 (1984).

10 V.M. Muller and B.V. Derjaguin, J. Coll. Interface Sci., **61**, 361 (1977).

11 H.B.G. Casimir, Proc. Kon. Ned. Akad. Wetenschap., **51**, 793 (1948).

12 H.E. Puthoff, Phys. Rev. D **35**, 3266 (1987).

13 V.M. Muller and B.V. Derjaguin, Colloids Surf., **6**, 205 (1983).

14 B.A. Pailthorpe, D.J. Mitchell, and B.W. Ninham, J. Chem. Soc. Faraday Trans. 2 **80**, 115 (1984).

15 J.C. Rasaiah, D.N. Card, and J.P. Valleau, J. Chem. Phys., **56**, 248 (1972).

16 J.P. Valleau, L.K. Cohen, and D.N. Card, J. Chem. Phys., **72**, 5942 (1980).

17 F. Lado, Phys. Rev., B **17**, 2827 (1978).

18 R. Kjellander and S. Marčelja, Chem. Phys. Lett. **112**, 49 (1984).

19 R. Kjellander and S. Marčelja, Chem. Phys. Lett. **127**, 402 (1986).

20 R. Kjellander and S. Marčelja, J. Chem. Phys., **82**, 2122 (1985).

21 F. Lado, J. Comput. Phys., **8**, 417 (1971).

22 J.F. Springer, M.A. Pokrant, and F.A. Stevens, J. Chem. Phys., **58**, 4863, (1973).

23 K.C. Ng, J. Chem. Phys., **61**, 2680, (1974).

24 K. Hiroike, Progr. Theor. Phys., **24**, 317 (1960).

25 Bo Jönsson, *pers. com.*

26 R. Kjellander and S. Marčelja, Chem. Scripta, **25**, 112 (1985).

Part II

Interactions between dipolar surfaces.

Most of the material in this part has been published in the following papers:

P. Attard and D.J. Mitchell, "The forces between surfaces of mobile, orientable dipoles. Asymptotic expressions", Chem. Phys. Letters, **133**, 347 (1987).

P. Attard and D.J. Mitchell, "The forces between surfaces of mobile, orientable dipoles. The method of reflection coefficients", J. Chem. Phys. **88**, 4391-4396 (1988).

P. Attard, D.J. Mitchell, and B.W. Ninham, "The attractive forces between polar lipid bilayers", Biophys. J., **53**, 457-460 (1988).

P. Attard, R. Kjellander, D.J. Mitchell, and Bo Jönsson, "Electrostatic fluctuation interactions between neutral surfaces with adsorbed mobile ions or dipoles", J. Chem. Phys., (in press).

P. Attard, "Lifshitz theory for anisotropic multilayers", J. Coll. Interface Sci., (in press).

Bo Jönsson , P. Attard, and D.J. Mitchell, "The interaction between dipolar surfaces in a dielectric continuum model" J. Phys. Chem., (in press).

Introduction to Part II

Biological cells, the stuff of life, are bounded by bilayer membranes composed of surface active molecules. The forces between such surfactant membranes are implicated in many biological processes: cell-cell recognition and fusion; exo- and pinocytosis; viral infection, and the immune response; and thylakoid membrane stacking. These same forces also determine the behaviour of some microemulsions, lamellar phases for example, and are therefore of interest in colloid and surface science as well. Surfactants form bilayers in aqueous solutions because they have hydrophobic hydrocarbon tails, and polar (or zwitterionic, or charged) headgroups which are hydrophilic. One requires a model of the interacting membranes which is of sufficient complexity to show the observed forces, yet simple lest it obscure the physics. Accordingly, the important physical features of the membrane are here described by a surface of mobile, orientable dipoles (the polar headgroups) and a semi-infinite low dielectric region (the tails).

Interest in the forces between such dipolar surfaces has been stimulated by comparatively recent experimental advances. One method[1,2] measures, by X-ray scattering, the repeat distance of a lamellar phase in equilibrium with a solution of known osmotic pressure. The (repulsive) force versus distance curve is then deduced. The Canberra surface forces apparatus can also measure the forces between surfactant bilayers adsorbed to mica surfaces[3-6]. Both methods find that at short separations, large, approximately exponentially decaying repulsive forces dominate the interaction between zwitterionic bilayers[1-6]. At larger separations, the measured attractive forces[4-6] differ in magnitude and rate of decay from that predicted by the usual Lifshitz theory of van der Waals forces.

The open question is whether the short-range, repulsive "hydration" forces can arise within a continuum electrostatic model of the dipolar headgroups interacting across a uniform aqueous phase. Initially Jönsson and Wennerström[7] analysed this image charge model and answered in the

affirmative. Kjellander[8] criticised their work in some detail and showed that the asymptotic behaviour was generally characterised by power laws and hence the model predicted long ranged forces. Both analyses ignored correlations between dipoles on opposite surfaces and also the van der Waals attraction between the dielectric half spaces. Kjellander and Marčelja[9] found from numerical hypernetted chain calculations, in the case of perpendicularly constrained dipoles, that the image repulsion is dominated at short separations by the correlational attraction between dipoles on different surfaces. Granfeldt, Jönsson and Wennerström[10] have recently carried out Monte Carlo simulations for interacting zwitterionic surfaces. They were unable to reach a conclusion regarding the existence of hydration forces in this continuum image charge model. Colbow and Jones[11] were apparently the first to model the lecithin-water system by interacting surfaces of point dipoles. They attempted to explain the thickening of the bilayers associated with the small separation repulsion and calculated the fluctuations between dipoles on opposite surfaces within second order perturbation theory. Since the first order terms vanished (because the image interactions were incorrectly approximated by an effective dielectric constant for the aqueous phase), an attractive interaction free energy resulted. All these calculations (and also the ones presented here) are for rigid planar surfaces; modification of the direct forces by spontaneous bilayer undulation[12,13] is not considered.

Previous authors have used a modal approach[14] to obtain the Lifshitz result for van der Waals forces in general. It is shown in this chapter that that method may be interpreted in terms of reflection coefficients. It is then proven analytically, within the continuum electrostatic model, with the proviso that the reflection coefficients are independent of separation, that there can never be a repulsive force between identical planar bodies interacting across a uniform dielectric medium. In addition, the method is

applied to the specific problem of the interacting dipolar surfaces of the image charge model. The analysis includes both the zero frequency van der Waals force between the dielectric half-spaces, and the correlation attraction between dipoles on opposite surfaces. The contribution of the surface dipoles can be substantial, and they do appear responsible for the anomalous attractive forces measured at large separations between the polar lipid bilayers.

Section 3.1, besides the interpretation of the modal approach in terms of reflection coefficients, contains the proof that the force between identical bodies is attractive. In §3.2 the Lifshitz results for interacting dielectric half-spaces and for triple films are derived as a simple illustration of the method. The reflection coefficient of dipolar surfaces, located either in the central dielectric or in the outer media, are derived in §3.3. Section 3.4 gives the long wavelength limit of the correlation functions, and also a mean field approximation for the free energy, and a low coupling approximation for the susceptibility. The long wavelength limit is used to obtain asymptotic expansions for the free energy (§3.6). The appendix to the chapter gives an exact analysis for perpendicular dipoles similar to that of Part I. Chapter 4 contains numerical results and comparisons for the susceptibility (§4.1), the pressures between dipolar surfaces (§4.2), and an analysis of measured forces between polar lipid bilayers (§4.3).

Chapter 3 Theory

3.1 Method of reflection coefficients

The Lifshitz results for the van der Waals force between planar bodies can be found most simply via the modal method of van Kampen, Nijboer and Schraam[14]. In this approach the interaction free energy is expressed as the change in the free energies of the electromagnetic surface modes (treated as independent harmonic oscillators) allowed by the particular boundary conditions of the specific problem. Explicitly, the interaction free energy per unit area (in the non-retarded limit) is (Eq. 5.53 of ref. 15)

$$F^{int} = \frac{k_B T}{4\pi^2} \sum_{n=0}^{\infty\prime} \int dk \ln \Delta^{int}(k) \qquad (3.1.1)$$

Here k_B is the Boltzmann constant, T the temperature, and **k** the two dimensional Fourier wave vector. The interaction part of the secular determinant $\Delta^{int}(\mathbf{k})$ is an implicit function of the dielectric constants of the system $\varepsilon(i\xi_n)$ evaluated at the discrete imaginary frequencies $i\xi_n = 2\pi i n k_B T/h$ (h is Planck's constant divided by 2π). The prime on the summation indicates that the zero frequency term is to be halved. The interaction secular determinant, which by suitable choice of a multiplicative factor goes to one as the separation $h \to \infty$, gives the allowed modes and follows from the boundary conditions appropriate to each problem.

The interaction part of the secular determinant has a simple physical interpretation in terms of reflection coefficients. Consider two arbritary bodies (passive,uncharged dielectrics), 2 and 2', interacting across a central uniform dielectric medium, 1, of width h. Then the electric potential satisfies the Laplace equation $\nabla^2\psi(\mathbf{r},z)=0$, $|z|<h/2$, which in the two dimensional

Fourier space appropriate for this planar geometry, may be written

$$\frac{d^2 \hat{\psi}(k,z)}{dz^2} - k^2 \hat{\psi}(k,z) = 0 \qquad (3.1.2)$$

with solution

$$\hat{\psi}(k,z) = A \exp k(z-h/2) + B \exp -k(z+h/2) \qquad (3.1.3)$$

The first term of the potential represents the reaction of the right hand body to the second term considered as an external field. Similarly the second term represents the reaction of the left hand body to the first term. Thus if the reflection coefficient of each body is defined as the ratio of the reflected (reaction) potential to the incident potential (evaluated at the boundary), then at the left hand boundary one can write

$$B = R_{12} A e^{-kh} \qquad (3.1.4a)$$

where R_{12} is the reflection coefficient of the left hand body, and at the right hand boundary

$$A = R_{12'} B e^{-kh} \qquad (3.1.4b)$$

where $R_{12'}$ is the reflection coefficient of the right hand body. The allowed potentials which satisfy these conditions are those for which the determinant of the coefficients vanishes. This gives the secular determinant

$$\mathcal{D}^{int}(k) = 1 - R_{12} R_{12'} e^{-2kh} \qquad (3.1.5)$$

The reflection coefficients can be determined from linear response theory and each is assumed independent of the other body (ie they do not depend on h). Lifshitz theory is based upon these approximations since Maxwell's equations *in media* assume a linear response of dielectric media to external fields, a response given by local dielectric constants.

From the above it follows that, for a symmetric system ($R(k) = R_{12} = R_{12'}$), the interaction free energy per unit area is

$$F^{int} = \frac{k_B T}{4\pi^2} \sum_{n=0}^{\infty}{}' \int dk \ln \{ 1 - R^2(k) e^{-2kh} \} \qquad (3.1.6)$$

Taking the negative derivative of this with repect to separation yields for the pressure

$$P = \frac{-k_B T}{4\pi^2} \sum_{n=0}^{\infty}{}' \int dk \; \frac{2k R^2(k) e^{-2kh}}{1 - R^2(k) e^{-2kh}} \qquad (3.1.7)$$

Clearly the theory will only yield sensible (real and finite) results if the argument of the logarithm in Eq. (3.1.6) is positive. Thus within the regime of validity of the theory, Eq. (3.1.7) will always yield a negative pressure. Two identical planar bodies interacting across a uniform (dielectric) medium must always attract each other, provided the bodies have no net charge. This attractive interaction results from all the dipolar fluctuations of the dielectric media.

3.2 Lifshitz theory

It is convenient to illustrate this procedure with some well-known examples, especially since the results will prove useful later. Take the left hand body to be a semi-infinite half-space of dielectric constant ε_2 . The potential in the central medium (of dielectric ε_1) is

$$\hat{\psi}(\mathbf{k},z) = A e^{kz} + B e^{-kz} \tag{3.2.1a}$$

and that transmitted across the boundary is

$$\hat{\psi}(\mathbf{k},z) = C e^{kz} \tag{3.2.1b}$$

Now the continuity of ψ and $\varepsilon\psi'$ gives the boundary conditions (z=0)

$$A + B = C, \qquad \varepsilon_1 k (B - A) = -\varepsilon_2 k C \tag{3.2.2}$$

The reflection coefficient, which is the ratio of the response to the applied potential at the boundary, is

$$R(\mathbf{k}) = B/A = \frac{\varepsilon_1 - \varepsilon_2}{\varepsilon_1 + \varepsilon_2} \equiv \Delta_{12} \tag{3.2.3}$$

The usual Lifshitz interaction between two dielectric half-spaces is now apparent, from Eqs (3.1.6, 7). Note that the transmission coefficient (which will be required later) follows from Eq. (3.2.2) and is

$$T_{12}(\mathbf{k}) = C/A = \frac{2\varepsilon_1}{\varepsilon_1 + \varepsilon_2} \tag{3.2.4}$$

To generalise this result, one may consider a medium of dielectric constant ε_2 and of thickness w adsorbed to another body, a black box with reflection coefficient $R_{2B}(\mathbf{k})$. Then the potential in the central medium 1 is again given by Eq. (3.2.1a) while that in the adsorbed layer is now

$$\hat{\psi}(\mathbf{k},z) = C e^{k(z+w)} + R_{2B}(\mathbf{k}) C e^{-k(z+w)} \tag{3.2.5}$$

Solving the boundary conditions as above, one obtains for the full reflection coefficient

$$R(\mathbf{k}) = B/A = \frac{\Delta_{12} + R_{2B}(\mathbf{k})\, e^{-2kw}}{1 + \Delta_{12} R_{2B}(\mathbf{k})\, e^{-2kw}} \qquad (3.2.6)$$

To obtain the triple layer result, take the black box to be a half-space with dielectric constant ε_3 , and then $R_{2B}(\mathbf{k})=\Delta_{23}$ from above. The results for the general multilayer[16] follow by repeated use of Eq. (3.2.6).

These results are readily extended to include anisotropic multilayers. The procedure is very similar to the above except that one uses the more general form of the Laplace equation

$$\nabla . (\mathcal{E} \nabla\psi) = 0 \qquad (3.2.7)$$

which implies continuity of ψ and $\varepsilon_z\psi'$ at the boundaries. In place of Eq. (3.2.1a) for the potential in the central medium we now have

$$\hat{\psi}(\mathbf{k},z) = A \exp(k\beta_1 z) + B \exp(-k\beta_1 z) \qquad (3.2.8)$$

where $\beta_j = (\varepsilon_j^x / \varepsilon_j^z)^{1/2}$. Here we have assumed that the media are fluid and hence from the symmetry of the problem the two independent elements of the diagonal dielectric tensor are ε_j^x and ε_j^z. The potential transmitted across the boundary is

$$\hat{\psi}(\mathbf{k},z) = C \exp(k\beta_2 z) \qquad (3.2.9)$$

and the boundary conditions remain formally the same as Eq. (3.2.2) provided one recognises that $\varepsilon_j = (\varepsilon_j^x \varepsilon_j^z)^{1/2}$.

So the anisotropic multilayer is formally identical to the isotropic problem, provided one identifies an effective dieletric constant for each medium ε_j and multiplies each thickness by β_j (*cf* Eq. 3.2.8). One can show explicitly that the reflection coefficients are always less than unity, and hence the pressure for the symmetric anisotropic system is always well defined and attractive.

3.3 Interacting dipolar surfaces

3.3A Dipoles in central medium

The method of reflection coefficients will now be used to obtain the electrostatic free energy between two interacting planar surfaces, each containing mobile orientable dipoles (fig. 3.1). The surfaces, a distance h apart, are embedded in a central uniform dielectric ε_1 , and a distance w behind each is a semi-infinite dielectric half-space, ε_2. The separation between the half-spaces is d=h+2w. Since one cannot ascribe a bulk macroscopic dielectric constant to the dipolar surface, it is necessary to determine the analagous microscopic quantity. The polarisation - polarisation correlation function for the isolated body (ie surface plus dielectric discontinuity) can, in principle, be found at non-zero frequencies using quantum statistical mechanics. However, if only the n=0 (electrostatic) term in Eq. (3.1.6) is required, then it suffices to use classical statistical mechanics, which restricted problem is addressed henceforth.

The dipolar fluid will be described by the polarisation operator, a three component vector with component α being

$$P^*_\alpha(\mathbf{r}) = \sum_{i=1}^{N} \mu_{i\alpha}\, \delta(\mathbf{r}-\mathbf{r}_i) \qquad (3.3.1)$$

Here the Dirac delta chooses the i^{th} dipole ($\mathbf{r}$ is the cylindrical radius vector) which has moment $\mu_{i\alpha}$ in the α=x, y or z direction and the asterisk denotes an operator. Ensemble averages of operators are denoted by dropping the asterisk, and averages for isolated bodies have a zero appended. In linear response theory, the excess polarisation $\mathbf{P}^{ex}(\mathbf{r}) = \mathbf{P}(\mathbf{r}) - \mathbf{P}^0(\mathbf{r})$ induced by an external field $\mathbf{E}^{ext}(\mathbf{r})$ is given by

$$\mathbf{P}^{ex}(\mathbf{r}) = \beta \int \mathbf{G}^0(\mathbf{r}-\mathbf{s}) \cdot \mathbf{E}^{ext}(\mathbf{s})\, d\mathbf{s} \qquad (3.3.2)$$

where $\beta=1/k_BT$. The polarisation-polarisation correlation function is

$$\mathbf{G}^0(\mathbf{r}-\mathbf{s}) \equiv \langle \mathbf{P}^*(\mathbf{r})\, \mathbf{P}^*(\mathbf{s}) \rangle^0 - \mathbf{P}^0(\mathbf{r})\, \mathbf{P}^0(\mathbf{s}) \qquad (3.3.3)$$

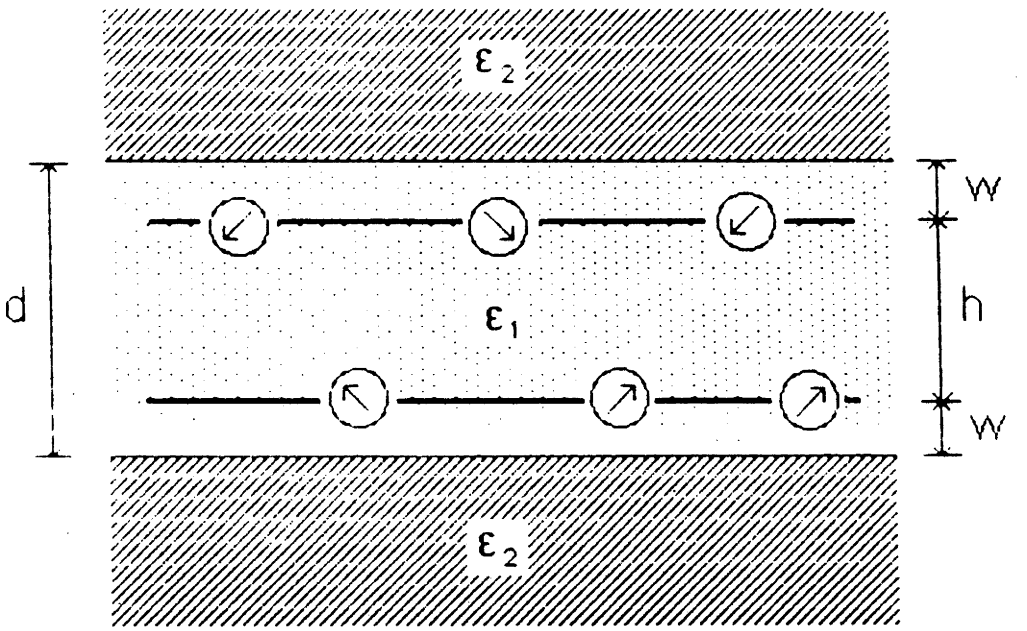

Figure 3.1 A simple diagram illustating the geometry of the model. The dipoles are on surfaces separated by a distance h and embedded in a dielectric continuum with dielectric constant ε_1. Behind each surface is a half-space with dielectric constant, ε_2. The distance between the dielectric discontinuites is d=h+2w.

In order to find the reflected potential, one requires the potential arising from an induced polarisation of the dipolar surface at z=0. One can show (eg by considering a dipole oriented in the x direction) that the direct potential due to the x component of polarisation is

$$\hat{\Phi}^{dir}_{(x)}(\mathbf{k},z) = \frac{2\pi i}{\varepsilon_1 k} e^{-k|z|} k_x \hat{P}^{ex}_x(\mathbf{k}) \qquad (3.3.4)$$

where k_x is the x component of $\mathbf{k}$. Note that this is the potential due to an ideal dipole; it is straightforward to extend the analysis to zwitterions. Since Eq. (3.2.3) enables one to find the potential reflected by the dielectric half-space, it follows that the total potential due to the x component of polarisation is

$$\hat{\Phi}_{(x)}(\mathbf{k},z) = \frac{2\pi i}{\varepsilon_1 k}(1+\Delta_{12}e^{-2kw})e^{-kz} k_x \hat{P}^{ex}_x(\mathbf{k}), \qquad z\geq 0 \qquad (3.3.5)$$

An entirely analagous expression holds for a y component. However, the potential due to a z component of polarisation is given by

$$\hat{\Phi}_{(z)}(\mathbf{k},z) = \frac{2\pi}{\varepsilon_1}(1-\Delta_{12}e^{-2kw})e^{-kz} \hat{P}^{ex}_z(\mathbf{k}), \qquad z\geq 0 \qquad (3.3.6)$$

Now a source to the right of the surface gives a potential

$$\Phi^{dir}(\mathbf{r},z) = A e^{kz} e^{-i\mathbf{k}\cdot\mathbf{r}} \qquad (3.3.7)$$

which has an associated electric field (in Fourier space)

$$\hat{E}^{dir}(\mathbf{k},z) = (ik, -k) A e^{kz} \qquad (3.3.8a)$$

This is the direct field from the source. There is also the usual reflected field from the dielectric half-space

$$\hat{E}^{im}(\mathbf{k},z) = (ik, k)\Delta_{12} e^{-2kw} A e^{-kz} \qquad (3.3.8b)$$

Using the convolution theorem, Eq. (3.3.2) gives for the induced polarisation

$$\hat{P}^{ex}(\mathbf{k}) = \beta \hat{G}^0(\mathbf{k})\cdot(\hat{E}^{dir}(\mathbf{k}) + \hat{E}^{im}(\mathbf{k})) \qquad (3.3.9a)$$

and hence for the α component at z=0

$$\hat{P}^{ex}_{\alpha}(\mathbf{k}) = A\beta \{ i(k_x \hat{G}^0_{\alpha x}(\mathbf{k}) + k_y \hat{G}^0_{\alpha y}(\mathbf{k})) (1+\Delta_{12} e^{-2kw}) - k \hat{G}^0_{\alpha z}(\mathbf{k}) (1-\Delta_{12} e^{-2kw}) \} \quad (3.3.9b)$$

Since Eqs (3.3.5-6) give the potential from an induced polarisation, the total reflected potential is

$$\hat{\Phi}^{ref}(\mathbf{k},z) = A\Delta_{12} e^{-2kw} e^{-kz} + \frac{2\pi}{\varepsilon_1}(1-\Delta_{12} e^{-2kw}) \hat{P}^{ex}_z(\mathbf{k}) e^{-kz} + \frac{2\pi i}{\varepsilon_1 k}(1+\Delta_{12} e^{-2kw}) (k_x \hat{P}^{ex}_x(\mathbf{k}) + k_y \hat{P}^{ex}_y(\mathbf{k})) e^{-kz} \quad (3.3.10)$$

It follows immediately, using the fact that $\hat{\mathbf{G}}^0(\mathbf{k})$ is hermitian, that

$$R(\mathbf{k}) = \Delta_{12} e^{-2kw} - \frac{2\pi\beta}{\varepsilon_1 k} \{ (k_x^2 \hat{G}^0_{xx}(\mathbf{k}) + k_y^2 \hat{G}^0_{yy}(\mathbf{k})) (1 + \Delta_{12} e^{-2kw})^2 + k^2 \hat{G}^0_{zz}(\mathbf{k}) (1-\Delta_{12} e^{-2kw})^2 + 2k_x k_y \hat{G}^0_{xy}(\mathbf{k}) (1+\Delta_{12} e^{-2kw})^2 + 2ik (k_x \hat{G}^0_{xz}(\mathbf{k}) + k_y \hat{G}^0_{yz}(\mathbf{k})) (1 - \Delta_{12}^2 e^{-4kw}) \} \quad (3.3.11)$$

Finally, the classical (zero frequency) interaction free energy for these interacting dipolar surfaces is

$$F^{int} = \frac{k_B T}{8\pi^2} \int dk \ \ln \{ 1 - R^2(\mathbf{k}) e^{-2kh} \} \quad (3.3.12)$$

The analysis is straightforward to carry out for zwitterions of length a and charge q. Then the polarisation is (A=1)

$$\hat{P}^{ex}_{\alpha}(\mathbf{k}) = \frac{-\beta q}{\mu^2} \{ 2iW_+ (\hat{G}^0_{\alpha x}(\mathbf{k}) \sin(k_x a/2) + \hat{G}^0_{\alpha y}(\mathbf{k}) \sin(k_y a/2)) - 2W_- \hat{G}^0_{\alpha z}(\mathbf{k}) \sinh(ka/2) \} \quad (3.3.13)$$

where $W_{\pm} \equiv 1 \pm \Delta_{12} e^{-2kw}$. The reflection coefficient may be shown to be

$$R(\mathbf{k}) = \Delta_{12} e^{-2kw} + \frac{2\pi q}{\varepsilon_1 k} \{ 2iW_+ (\sin(k_x a/2) \hat{P}^{ex}_x(\mathbf{k}) + \sin(k_y a/2) \hat{P}^{ex}_y(\mathbf{k})) + 2W_- \sinh(ka/2) \hat{P}^{ex}_z(\mathbf{k}) \} \quad (3.3.14)$$

For zwitterions constrained to point perpendicular to the surface, this reduces to

$$R(\mathbf{k}) = \Delta_{12} e^{-2kw} - \frac{8\pi\beta q^2 \hat{G}^0_{zz}(\mathbf{k})}{\mu^2 \varepsilon_1 k} W_-^2 \sinh^2(ka/2) \quad (3.3.15)$$

3.3B Dipoles in outer media

Now consider dipolar surfaces embedded in the outer dielectric half-spaces ε_2, with separation between the surfaces h=d+2w (d is still the thickness of the central medium ε_1). A source to the right of the surfaces, $\Phi=Ae^{kz}$ is transmitted across the dielectric boundary, with a coefficient given by Eq. (3.2.4), and produces a field

$$\hat{\mathbf{E}}^{\text{trans}}(\mathbf{k}) = (\mathrm{i}\mathbf{k}, -k)\, T_{12}\, e^{kz} \tag{3.3.16}$$

The induced polarisation is then $\hat{\mathbf{P}}^{\text{ex}}(\mathbf{k}) = \beta\, \hat{\mathbf{G}}^0(\mathbf{k}) \cdot \hat{\mathbf{E}}^{\text{trans}}(\mathbf{k})$, or in component form

$$\hat{P}_\alpha(\mathbf{k}) = \beta \left\{ ik_x \hat{G}_{\alpha x}(\mathbf{k}) + ik_y \hat{G}_{\alpha y}(\mathbf{k}) - k \hat{G}_{\alpha z}(\mathbf{k}) \right\} A\,(1+\Delta_{12})\, e^{-kw} \tag{3.3.17}$$

where $T_{12}=1+\Delta_{12}$ has been used. Each component of polarisation gives rise to a direct potential (cf Eq. (3.3.4)) which is transmitted across the boundary with coefficient $T_{21}=1-\Delta_{12}$. Hence the total reflected potential is

$$\hat{\Phi}^{\text{ref}}(\mathbf{k},z) = A\,\Delta_{12}\, e^{-kz} + (1-\Delta_{12})\, e^{-kw}\, \frac{2\pi}{\varepsilon_2 k}\, e^{-kz} \left\{ ik_x \hat{P}_x(\mathbf{k}) + ik_y \hat{P}_y(\mathbf{k}) + k \hat{P}_z(\mathbf{k}) \right\} \tag{3.3.18}$$

This yields for the reflection coefficient

$$R(\mathbf{k}) = \Delta_{12} - (1-\Delta_{12}^2)\, e^{-2kw}\, \frac{2\pi\beta}{\varepsilon_2 k} \left\{ k_x^2 \hat{G}^0_{xx}(\mathbf{k}) + k_y^2 \hat{G}^0_{yy}(\mathbf{k}) + k^2 \hat{G}^0_{zz}(\mathbf{k}) + 2k_x k_y \hat{G}^0_{xy}(\mathbf{k}) + 2ik \left(k_x \hat{G}^0_{xz}(\mathbf{k}) + k_y \hat{G}^0_{yz}(\mathbf{k}) \right) \right\} \tag{3.3.19}$$

which when inserted in Eq. (3.3.12) gives the interaction free energy between dipolar surfaces embedded in the outer dielectric half-spaces, provided the present distance between the boundaries, d (rather than h) is used in the exponential.

3.4 Limits and approximations

3.4A Long wavelength limit

The expression for the classical interaction free energy requires the polarisation correlations as functions of **k**. A considerable simplification results if the small **k** limit of $\hat{\mathbf{G}}^0(\mathbf{k})$ is taken instead, since this reduces the requirement to just two parameters, the susceptibilities. For large separations between the surfaces one expects that only the long wavelength correlations will contribute to the interaction free energy. And indeed the factor e^{-2kh} does damp the large **k** behaviour of R(**k**) and hence $\hat{\mathbf{G}}^0(\mathbf{k})$. The limiting result is here derived for the dipolar surfaces in the central medium. The analogous expressions for the dipoles in the outer media follow by interchanging the subscripts 1 and 2.

The polarisation-polarisation correlation function gives the induced polarisation in terms of the applied field, Eq. (3.3.2). As in Part I, one can define a response function τ which gives it in terms of the mean field:

$$\mathbf{P}^{ex}(\mathbf{r}) = \beta \int \tau(\mathbf{r}-\mathbf{s}) \cdot \mathbf{E}^{mean}(\mathbf{s})\, d\mathbf{s} \qquad (3.4.1)$$

The usual expression for the mean field is

$$\mathbf{E}^{mean}(\mathbf{r}) = \mathbf{E}^{ext}(\mathbf{r}) + \int \mathbf{T}(\mathbf{r}-\mathbf{s}) \cdot \mathbf{P}^{ex}(\mathbf{s})\, d\mathbf{s} \qquad (3.4.2)$$

where **T** is the dipole field tensor which here implicitly includes hard core or other short range effects. These equations (3.3.2, 3.4.1-2) may be solved in Fourier space

$$\hat{\mathbf{G}}^0(\mathbf{k}) = (\mathbf{I} - \beta\, \hat{\tau}(\mathbf{k})\, \hat{\mathbf{T}}(\mathbf{k}))^{-1}\, \hat{\tau}(\mathbf{k}) \qquad (3.4.3)$$

Now it was shown in Part I that $\tau(\mathbf{r})$ is a short ranged function (it is related to the short range part of the Ornstein-Zernike direct correlation funtion). It then follows that its Fourier transform possesses a Taylor series about k=0, $\hat{\tau}(\mathbf{k}) \sim \hat{\tau}(0) + \mathcal{O}(k^2)$. From the symmetry of the problem, $\hat{\tau}(0)$ is diagonal with only two independent entries (the parallel components being equal). On the other hand, the dipole field tensor is long ranged, its components decaying as

inverse cubics in r, and hence its Fourier transform has a mod k singularity at the origin. It therefore follows that the required small k limit of the correlation function is

$$\hat{G}^0(k) \sim \hat{G}^0(0) + \beta \hat{G}^0(0)\, \hat{T}'(k)\, \hat{G}^0(k) + \mathcal{O}(k^2) \qquad (3.4.4)$$

The typical components of the long range part of the interaction tensor $\hat{T}'(k)$ (which is hermitian) are

$$\hat{T}'_{xx}(k) = \frac{-2\pi k_x k_x}{\varepsilon_1 k} \left(1 + \Delta_{12} e^{-2kw} \right) \qquad (3.4.5a)$$

$$\hat{T}'_{xz}(k) = \frac{-2\pi i k_x}{\varepsilon_1} \Delta_{12} e^{-2kw} \qquad (3.4.5b)$$

$$\hat{T}'_{zz}(k) = \frac{2\pi k}{\varepsilon_1} \left(1 - \Delta_{12} e^{-2kw} \right) \qquad (3.4.5c)$$

These equations show that, like the dipole field tensor itself, the correlation function has a mod k singularity. It is therefore long ranged in real space, decaying as r^{-3} along the surface. This result is analagous to known results for three dimensional homogeneous fluids[17] where the isothermal compressability κ_T replaces the susceptibility $\hat{G}^0(0)$ above. One could now take $\hat{G}^0(k)$ to be given by Eq. (3.4.3) and insert it directly into the reflection coefficient (3.3.11) and thence obtain the free energy (3.3.12). However since the long wavelengths become dominant at larger separations, one could also use this form as the basis for an asymptotic expansion (§3.5 below). We first derive a simplified mean field approximation (analgous to that given for ions in §2.2). These two approaches (asymptotic and approximate) only involve two parameters:- the parallel $\hat{G}^0_{xx}(0)$ and perpendicular $\hat{G}^0_{zz}(0)$ components of the susceptibility. These can be found numerically (§4.1) or from a low coupling approximation (§3.4C).

3.4B Mean field perturbation approximation

The preceding analysis has been for ideal (point) dipoles. We now give

the simplified mean field approximation for zwitterions of length a and moment $\mu=qa$ interacting only via electrostatic potentials. Then components of the dipole field tensor are

$$\hat{T}_{xx}(k) = \frac{-2\pi}{\varepsilon_1 k a^2} 2(1-\cos(k_x a))(1+\Delta_{12} e^{-2kw}) \qquad (3.4.6a)$$

$$\hat{T}_{xz}(k) = \frac{2\pi}{\varepsilon_1 k a^2} 2i \sin(k_x a/2)\, 2\sinh(ka/2)\, \Delta_{12} e^{-2kw} \qquad (3.4.6b)$$

$$\hat{T}_{zz}(k) = \frac{-2\pi}{\varepsilon_1 k a^2}\left(2-2e^{-ka}-\Delta_{12}e^{-2kw}(2-e^{-ka}-e^{ka})\right) \qquad (3.4.6c)$$

The simplified mean field approximation then consists of inserting these into the formula for the polarisation correlation function (3.4.3) and taking the reponse function to be given by its value at k=0, $\hat{\tau}(0)$. This is related to the susceptibility by Eq. (3.4.3) at k=0, or explicitly

$$\hat{G}_{xx}(0) = \hat{t}_{xx}(0) \;, \quad \hat{G}_{zz}(0) = \frac{\hat{\tau}_{zz}(0)}{1+4\pi\beta\,\hat{\tau}_{zz}(0)/(\varepsilon_1 a)} \qquad (3.4.7)$$

Hence an accurate numerical calculation of the susceptibility will give the value of $\hat{\tau}(0)$ and the pressure in the simplified mean field approximation follows, by replacingf $\hat{\tau}(\mathbf{k})$ by $\hat{\tau}(0)$ in Eq. (3.4.3).

3.4C Low coupling approximation

The parallel and perpendicular components of the susceptibility can be estimated in the low coupling regime. The short ranged response function τ is not only independent of the long range tail of the interaction potential, but is determined approximately by the system interacting with a truncated potential (see Part I). Therefore, to a first approximation, its value is given by that of an ideal dipolar gas in which all orientations are equally likely

$$\hat{\tau}^{id}_{xx}(0) = \hat{\tau}^{id}_{yy}(0) = \hat{\tau}^{id}_{zz}(0) = \frac{1}{3}\rho\,\mu^2 \qquad (3.4.8)$$

This approximation is analogous to the Debye-Hückel theory of electrolytes.

The dipole field tensor **T** includes short range potentials, and these contribute to $\hat{\mathbf{T}}(0)$. If the sytem is not too highly coupled, then the core repulsions may be neglected. There then remains an electrostatic term in the zz component. Zwitterions of length a (and fixed moment μ) have $\hat{T}_{zz}(0) = -4\pi/\varepsilon_1 a$. Hence for freely orientable dipoles one has the approximations

$$\hat{G}^0_{xx}(0) = \hat{G}^0_{yy}(0) \approx \frac{1}{3}\rho\mu^2 \quad , \quad \hat{G}^0_{zz}(0) \approx \frac{\rho\mu^2/3}{1 + 4\pi\beta\rho\mu^2/3\,\varepsilon_1 a} \qquad (3.4.9a)$$

and for perpendicularly constrained dipoles one has

$$\hat{G}^0_{xx}(0) = \hat{G}^0_{yy}(0) \equiv 0 \quad , \quad \hat{G}^0_{zz}(0) \approx \frac{\rho\mu^2}{1 + 4\pi\beta\rho\mu^2/\varepsilon_1 a} \qquad (3.4.9b)$$

Note that this approximation predicts that the zz component of the susceptibility goes to zero in the limit of point dipoles. This limit is a high coupling limit (since the charge must increase if the dipole moment μ=qa is held fixed) and in actual fact the susceptibility becomes constant at sufficiently high coupling (see §4.1).

3.5 Asymptotic results

The long wavelength limit of the correlation function can be inserted into the reflection coefficient and the interaction free energy determined numerically from Eq. (3.3.12). However, since the contribution from long wavelengths becomes increasingly dominant at larger separations, one could argue that an asymptotic expansion in powers of separation would be more consistent. To obtain this, one expands the logarithm in Eq. (3.3.12), and collects from each term coefficients with the same power of k. From scaling arguments (change variables, k=q/h), each power of k corresponds to successive terms in the asymptotic expansion. Note that in this derivation the nearest images, which are independent of separation, are included in the reference system.

First for the case of the dipolar surfaces embedded in the central dielectric medium (h=d-2w). Using the long wavelength limit of the correlations Eq. (3.4.4) in the formula for the reflection coefficient Eq. (3.3.11), one obtains the first several terms in the asymptotic expansion. The leading term is

$$F_0^{int} = \frac{-k_B T}{8\pi^2} \sum_{n=1}^{\infty} \frac{1}{n} \int dk\, \Delta_{12}^{2n}\, e^{-2nkd} = \frac{-k_B T}{16\pi d^2}\, \zeta_3(\Delta_{12}^2) \qquad (3.5.1)$$

where $\zeta_3(x)=\sum x^n/n^3$ which may be considered to be a generalised Riemann zeta function. This is the usual Lifshitz zero frequency result for the interaction between two half-spaces (*cf* Eq. (1.3.6)); it is independent of the dipolar surfaces. The next order term, where the coefficients contribute a factor of k, is

$$F_{10}^{int} = \frac{1}{\varepsilon_1} \int_0^{\infty} k^2\, \frac{\Delta_{12}\, e^{-kh}\, e^{-kd}}{1-\Delta_{12}^2\, e^{-2kd}} \left\{ X W_+^2 + Z W_-^2 \right\} dk \qquad (3.5.2)$$

Here and after we use the notation $X \equiv \hat{G}^0{}_{xx}(0)$, $Z \equiv \hat{G}^0{}_{zz}(0)$, $W_{\pm} \equiv 1 \pm \Delta_{12}\, e^{-2kw}$. This term corresponds to first order perturbation theory, keeping only the terms linear in k. Asymptotically, this term decays as an inverse cubic in

separation.

To obtain the terms which asymptotically go like h^{-4}, one must collect coefficients quadratic in k. Then one obtains

$$F_{11}^{int} = \frac{-2\pi\beta}{\varepsilon_1^2}\int_0^\infty k^3 \frac{\Delta_{12} e^{-kd} e^{-kh}}{1-\Delta_{12}^2 e^{-2kd}} \left\{ (X W_+ + Z W_-)^2 \Delta_{12} e^{-2kw} + X^2 W_+^2 - Z^2 W_-^2 \right\} dk \tag{3.5.3}$$

$$F_{20}^{int} = \frac{-\pi\beta}{\varepsilon_1^2}\int_0^\infty k^3 \frac{(1+\Delta_{12}^2 e^{-2kd}) e^{-2kh}}{(1-\Delta_{12}^2 e^{-2kd})^2} \left\{ X W_+^2 + Z W_-^2 \right\}^2 dk \tag{3.5.4}$$

The first of these arises in first order perturbation theory, from that part of the polarisation correlation function linear in k, Eq. (3.4.4). The other comes from second order perturbation theory with only the (k=0) susceptibility. Of the above, this term is the only one non-zero if $\varepsilon_1=\varepsilon_2$, since it includes the direct correlational attraction between the two dipolar surfaces.

For the dipolar surfaces embedded in the outer dielectric media (h=d+2w), the corresponding terms (in addition to the Lifshitz zero frequency contribution (3.5.1)) are:

$$F_{10}^{int} = \frac{X+Z}{\varepsilon_2}\int_0^\infty k^2 \frac{\Delta_{12} e^{-2kd}}{1-\Delta_{12}^2 e^{-2kd}} (1-\Delta_{12}^2) e^{-2kw} dk \tag{3.5.5}$$

$$F_{11}^{int} = \frac{-2\pi\beta}{\varepsilon_2^2}\int_0^\infty k^3 \frac{\Delta_{12} e^{-2kd}}{1-\Delta_{12}^2 e^{-2kd}} (1-\Delta_{12}^2) e^{-2kw} \left\{ X^2 - Z^2 - (X-Z)^2 \Delta_{12} e^{-2kw} \right\} dk \tag{3.5.6}$$

$$F_{20}^{int} = \frac{-\pi\beta}{\varepsilon_2^2}(X+Z)^2 \int_0^\infty k^3 \frac{1+\Delta_{12}^2 e^{-2kd}}{1-\Delta_{12}^2 e^{-2kd}} (1-\Delta_{12}^2)^2 e^{-2kh} dk \tag{3.5.7}$$

The long wavelength limit of the correlation function is an exact result and yields the correct interaction free energy asymptotically. To obtain the strict asymptotic results, one should expand all the e^{-2kw} in powers of w/h (see the appendix to this Chapter). However, the results presented in this

section are more accurate than the strict asymptotic form over the separations of the order of Ångstroms that one is usually interested in (see Chapter 4).

Appendix

3.A Perpendicular dipoles, exact results

Dipoles which are constrained to point perpendicularly to the surfaces interact with radially symmetric potentials. The pair correlations then also have this symmetry in the absence of an external field. Here is investigated systems consisting of two surfaces with laterally mobile perpendicular dipoles in the formally exact manner of Part I. The general theory of §1.1 will be applied here for particles that interact with a combination of ideal point-dipole and short range core potentials, but the treatment can be easily generalized to zwitterionic particles. Only the restricted problem of a single particle species will be examined, and the first case to be treated will be the one without electrostatic image interactions ($\varepsilon_1 = \varepsilon_2$).

The pair interactions in Eq. (1.1.11) now equal $u_s = u_s^{short} + \mu^2\phi_s$ and $u_c = u_c^{short} + \mu^2\phi_c$, where u^{short} contains all non-electrostatic interactions, μ is the dipole moment of the particles, and ϕ_s and ϕ_c are the unit dipole-dipole potentials. Explicitly

$$\hat{\phi}_s(k) = -\frac{2\pi k}{\varepsilon_1}, \qquad \hat{\phi}_c(k) = \frac{2\pi k e^{-kh}}{\varepsilon_1} \tag{3.A.1}$$

In ϕ_s contributions from the inaccessible region around r = 0 are excluded. Since the results are valid for all u_s^{short} this is of no consequence. As before, define the matrix $\underline{B} = \underline{N}^{-1} - \underline{C} - \beta\underline{U}^{el}$, where $\underline{U}^{el} = \mu^2\underline{\Phi}$ is the electrostatic part of the pair interaction matrix (*cf.* Eq. (1.2.11)). The function $\underline{B}(r)$ is relatively short ranged, and using Eqs (1.1.8) and (3.A.1) one finds that $\hat{\underline{B}}(k) \sim \hat{\underline{B}}(0) + \mathcal{O}(k^2)$ for small k. From Eq. (1.1.13) follows

$$\hat{\underline{S}}(k) = [\hat{\underline{B}}(k) + \beta\hat{\underline{U}}^{el}(k)]^{-1} \tag{3.A.2}$$

and after a matrix inversion and Hankel transformation one finds that the pair distribution functions have r^{-3} tails. For instance, the single surface correlation function has the asymptotic behaviour (cf Eq. (3.4.4))

$$s_0(r) \sim -\frac{k_B T \mu^2 K_0^2 n^4}{\varepsilon_1 r^3}, \qquad r \to \infty \tag{3.A.3}$$

where the density $n \equiv \rho$ and K_0 is the isothermal compressibility for the isolated surface (*cf.* the general arguments by Stell[17]). Here have been used $1/\hat{b}_0(0) = \hat{s}_0(0)$, valid for ideal dipoles with ϕ_s from Eq. (3.A.1), and the general relationship $\hat{s}_0(0) \equiv \hat{G}^0_{zz}(0)/\mu^2 = n + n^2 \int h_0(r) dr \equiv k_B T K_0 n^2$.

When calculating the pressure, the main interest is in the behaviour when the surface separation is large enough to avoid core-core interactions between the surfaces. Then, using Eq. (3.A.2) the pressure from Eq. (1.1.14) can be written (in analogy to Eq. (1.2.16))

$$P = -\frac{k_B T}{8\pi^2} \int \left[\frac{\partial}{\partial h} \ln \mathcal{D}\mathrm{et} \left(\underline{\hat{B}}(k;h') + \beta \underline{\hat{U}}^{el}(k;h) \right) \right]_{h'=h} dk \tag{3.A.4}$$

Inserting $\underline{\hat{U}}^{el}$, one obtains the exact expression

$$P = -\frac{k_B T}{2\pi h^4} \int_0^\infty \frac{\left[\frac{\hat{b}_c}{\alpha} + \frac{t}{h} e^{-t} \right] t^3 \, dt}{\left[\frac{\hat{b}_s}{\alpha} - \frac{t}{h} \right]^2 - \left[\frac{\hat{b}_c}{\alpha} + \frac{t}{h} e^{-t} \right]^2} \tag{3.A.5}$$

where $\alpha = 2\pi\beta\mu^2/\varepsilon_1$, the variable $t = hk$ has been substituted, and where $\hat{b}_s(k;h)$ and $\hat{b}_c(k;h)$ are elements of $\underline{\hat{B}}(k;h)$. To extract the leading term for large h from Eq. (3.A.5), expand $\hat{b}_\eta(t/h;h) = \hat{b}_\eta(0;h) + \mathcal{O}(t^2/h^2)$, $\eta = s$ or c. When $h \to \infty$ one has $\hat{b}_c(0;h) \to 0$ more rapidly than h^{-1} and $\hat{b}_s(0;h) \to \hat{b}_0(0)$. (The former statement is a consequence of that $b_c(r;h)$ behaves like $[u_c(r;h)]^2$ for large h.) It follows that the leading term in the pressure is

$$P \sim -\frac{3\pi k_B T \mu^4 n^4 K_0^2}{2\varepsilon_1^2 h^5}, \qquad h \to \infty \tag{3.A.6}$$

The attractive interaction decays as the fifth power of separation when the surfaces are sufficiently far apart. It is a consequence of the correlations between the dipolar particles at the two surfaces. In contrast to the case of

ionic layers on the surfaces (§1.3), the pressure law is not universal since it depends on the details of the system via K_0.

Now include the effect of image interactions. The electrostatic interaction potentials for ideal point dipoles are (*cf.* Eq. (1.3.4))

$$\hat{\phi}_s(k) = -\frac{2\pi k}{\varepsilon_1}\left\{1 + \frac{2\varepsilon_D}{e^{2kd} - \varepsilon_D^2}\left[\varepsilon_D - e^{kd}\cosh(hk)\right]\right\}$$

$$\hat{\phi}_c(k) = \frac{2\pi k}{\varepsilon_1}\left\{e^{-kh} + \frac{2\varepsilon_D}{e^{2kd} - \varepsilon_D^2}\left[\varepsilon_D\cosh(hk) - e^{kd}\right]\right\} \quad (3.A.7)$$

where $\varepsilon_D \equiv \Delta_{12}$. Using these potentials, one defines the matrices $\hat{\mathbf{B}}$ and $\hat{\mathbf{U}}^{el}$ as in the previous section. $\hat{\mathbf{B}}$ still has the properties mentioned there and Eqs (3.A.2) and (3.A.4) remain valid. After some algebra one obtains the following exact expression for the interaction between the dipolar layers

$$P_{dipolar} = -\frac{k_B T}{4\pi h^4}\sum_{\nu=\{^{+1}_{-1}}\int_0^\infty \frac{\nu\, t^3 e^{-t} E_\nu^2\, dt}{\frac{\varepsilon_1(\hat{b}_s - \nu\hat{b}_c)}{2\pi\beta\mu^2} - \frac{t}{h}\left[1 + \nu e^{-t}\right]E_\nu} \quad (3.A.8)$$

where the variable $t = hk$ and the functions

$$E_\pm(k,hk) = \frac{1 - G(k)}{1 \pm G(k)\, e^{-hk}}, \qquad G(k) = \varepsilon_D e^{-2wk}$$

have been introduced. It is straightforward to extract the leading term for large h, namely

$$P_{dipolar} \sim \frac{3 k_B T\, \mu^2 n^2 K_0\, (1 - \varepsilon_D)^2\, \zeta_3(\varepsilon_D^2)}{4\varepsilon_1\, h^4\, \varepsilon_D}, \qquad h \to \infty \quad (3.A.9)$$

where $\zeta_n(x) = \sum_{j>0}\,(x^j / j^n)$ is like a Riemann zeta function.

This asymptotic law has been previously obtained by Kjellander[8]. It originates from the interaction of each dipole with the image charges induced by all dipoles located at the same surface. (The interactions with its own images are here included). One can see that the power law changes

from h^{-5} without images to h^{-4} with images. However, in a consistent treatment of this system one should include all contributions due to the presence of the dielectric discontinuities. As discussed in §1.3b, the image charge interactions and the vdW interactions are intimately related. Therefore, we must at least add the zero frequency vdW interaction

$$P_{tot} = P_{dipolar} + P_{VdW} = P_{dipolar} - \frac{k_B T \zeta_3(\varepsilon_D^2)}{8\pi d^3} \qquad (3.A.10)$$

In contrast to the case of ionic layers, §1.3b, there is no contribution from the image charge interactions that becomes cancelled by the vdW pressure. This means that the vdW interaction is not screened by the dipolar layers. The leading image interaction term, Eq. (3.A.9), goes as h^{-4} when $h \to \infty$. Since P_{vdW} goes as h^{-3}, it will dominate the interaction between the surfaces for large h, and the total pressure is always attractive there.

To make the link with the case without images, the h^{-5} term from Eq. (3.A.8) will also be extracted. After some calculus, making use of the fact that both $\hat{b}_c(0;h)$ and $\hat{b}_s(0;h) - \hat{b}_0(0)$ approach zero more rapidly than h^{-1}, one obtains

$$P_{dipolar} - a_4 h^{-4} \sim$$

$$- \frac{3 k_B T \mu^2 n^2 K_0 (1 - \varepsilon_D)}{2\varepsilon_1} \left[\frac{\pi \mu^2 n^2 K_0 (1 - \varepsilon_D)^2}{\varepsilon_1} + 2w\varepsilon_D \right] \theta(\varepsilon_D)\, h^{-5} \qquad (3.A.11)$$

where $x^2\theta(x) = 2(1-x)\,\zeta_3(x^2) - (1+x)\,\zeta_4(x^2)$ and a_4 is the coefficient in Eq. (3.A.9). Note that K_0 here refers to a single, isolated surface with a dielectric discontinuity.

Chapter 4 Comparison of results

4.1 Susceptibility and distribution functions

The susceptibility for perpendicular dipoles is simply related to the isothermal compressibility, $\chi_{zz} \equiv \hat{G}^0{}_{zz}(0)/\rho\mu^2 = \rho k_B T K_T$, which in turn is just an integral of the indirect correlation function. In the HNC scheme† this was found to be the most accurate method to evaluate this quantity, specifically

$$\chi_{zz} \equiv 1 + \rho \int h(r)\, dr$$

$$= 1 + 2\pi\rho \int_0^R h(r)\, r\, dr - 2\pi\rho\beta\mu^2 \chi_{zz}^2 \,(1-\Delta_{12}) / (\varepsilon_1 R) \qquad (4.1.1)$$

This follows by analytically integrating the $1/r^3$ tail of the correlation function (*cf* Eqs (3.4.4, 3.A.3)) from some large cutoff R. The larger root of the quadratic is the correct value for the susceptibility and this is usually insensitive to the value of R. Note that this refers to a single isolated surface and is therefore, in some sense, independent of the HNC calculations of the pressure for the interacting system.

---

† The original HNC program written by Roland Kjellander and Stjepan Marčelja contained errors and these effected the published results[9]. I corrected the bugs in the input (the calculations were effectively performed for ~10 times smaller dipole moment than specified) and the potential (incorrect for no images; appproximately correct when images were present) routines. I also rewrote the algorithm for solving the HNC equation, the routines for subtracting the long-range tails, and the pressure routine. I implemented a version for a single dipolar surface and devised accurate methods to calculate the new quantity, the compressability.

Tables 4.1a and b exhibit the susceptibility for perpendicular dipoles of moment 1eÅ and 5eÅ respectively. The Monte Carlo simulations were performed by Bo Jönsson and the ideal gas results are from Eq. (3.4.9b). This is certainly a worthwhile approximation at these couplings, as evinced by its agreement with the MC and HNC results. These latter two accurate approaches converge to the ideal gas value of unity as the surface density of dipoles goes to zero.

If one fixes the zwitterion dipole moment $\mu=qa$ and sends the dipole length to zero (point dipole limit), the ideal gas value goes to zero. However, this is a high coupling limit, and that approximation is not expected to then be valid. Indeed, calculation with the HNC method shows the susceptibility to become constant in this limit. As an example, for zwitterions with μ=5eÅ and density $\rho^{-1}=75Å^2$, for lengths of a= 10, 5, 2.5, 1, and 0.5 Å, the HNC susceptibility is χ_{zz} = .29, .20, .17, .161, and .159 respectively, whereas the ideal gas estimate is χ_{zz} = .26, .15, .08, .03, and .02 . This also explains why the MC results for point dipoles are in such good agreement with the HNC calculations for zwitterions.

Bo Jönsson has also included a soft core repulsion with length scale 4Å in the simulations, and this decreases the susceptibility. The effect is less marked for the 5Å case where the electrostatics keep the dipoles far enough apart anyway. No hard core was considered in any of the HNC calculations for dipoles. Images slightly increase the susceptibility although their effect can clearly be ignored to a first approximation (at least for perpendicular dipoles).

The susceptibility for orientable point dipoles (with 4Å soft core and no images) has been simulated by Jönsson and this is shown in Table 4.2. There is a noticable anisotropy present for 5eÅ dipoles. The parallel component of the susceptibility is approximately the same as the ideal gas estimate for μ=1eÅ but there is a noticable deviation for the system with the larger moment. The simulation data for the perpendicular component has also

Area [Å^2]	Ideal	MC	MC[a]	HNC	HNC[b]
25	0.2223	0.44	0.067	0.4204	0.4726
40	0.3138	-	0.14	0.5501	0.6078
50	0.3637	0.62	-	0.6092	0.6666
75	0.4616	0.71	0.28	0.7064	0.7571
100	0.5334	0.77	-	0.7651	0.8093
200	0.6957	0.84	-	0.8698	0.8980

[a]Includes effects of 4Å soft core [b]Includes images, ε_2=2, w=1Å

Table 4.1a The non-dimensional susceptibility $\chi_{zz}=\hat{G}^0{}_{zz}(0)/\mu^2\rho$ for perpendicular dipoles with moment 1eÅ at various surface densities. The Monte Carlo results are for point dipoles, and the hypernetted chain and ideal gas estimates are for monovalent zwitterions (ie 1Å in length with unit charge). The temperature is 300K and ε_1=80.

Area [Å^2]	Ideal	MC	MC[a]	HNC	HNC[b]
25	0.0541	0.047	0.013	0.0695	0.0741
40	0.0838	-	0.043	0.1123	0.1241
50	0.1026	0.12	-	0.1400	0.1565
75	0.1464	0.18	0.12	0.2046	0.2338
100	0.1861	0.24	0.18	0.2624	0.3019
150	0.2554	0.34	-	0.3587	0.4125
200	0.3138	0.42	0.35	0.4342	0.4956

[a]Includes effects of 4Å soft core [b]Includes images, ε_2=2, w=3Å

Table 4.1b Same as the preceding table but for dipoles of moment 5eÅ.

Area [Å^2]	1 eÅ			5 eÅ		
	χ_{xx}	χ_{zz}		χ_{xx}	χ_{zz}	
25	0.40	0.27	(0.1539)	0.64	-	(0.0488)
40	0.36	0.28	(0.1928)	0.65	0.10	(0.0718)
75	0.36	0.33	(0.2400)	0.66	0.15	(0.1132)
100	-	-	(0.2581)	0.50	0.18	(0.1356)
200	-	-	(0.2909)	0.42	0.25	(0.1928)

Table 4.2 Monte Carlo susceptibility $\chi=\hat{G}^0(0)/\mu^2\rho$ for orientable point dipoles (with 4Å soft core) at various surface densities. The figures in brackets are the ideal gas estimate for the perpendicular component (monovalent zwitterions); for the parallel component this is χ_{xx} = 1/3 everywhere. The temperature is 300K, ε_1=80 and no images are included.

been compared with the ideal gas estimate for monovalent zwitterions, and the utility of this latter approximation is again apparent.

The radial distribution functions for 1eÅ zwitterions on the same and on opposite surfaces are shown in figs 4.1. The HNC results (h=5Å and Δ_{12} =0) are compared to the mean field asymptotic forms which are

$$g_{11}(r) \sim 1 - \frac{\beta \mu^2 \chi_{zz}^2}{\varepsilon_1 r^3} \qquad (4.1.2a)$$

$$g_{12}(r) \sim 1 - \frac{\beta\mu^2\chi_{zz}^2 (2h^2-r^2)}{\varepsilon_1 (h^2+r^2)^{5/2}} \qquad (4.1.2b)$$

with χ_{zz}=0.7064 in this case. Note that to this leading order $g_{11}(r)$ is the same as that for an isolated surface (*cf* Eq. (3.4.4)). For dipoles on the same surface, the asymptotic form is here unphysical for r < 2Å, but the HNC results rapidly go over to the large r limiting form. About a dipole, there is a depletion of the uniform surface density on the same surface, and a positive adsorption excess beyond r=h$\sqrt{2}$ on the opposite surface.

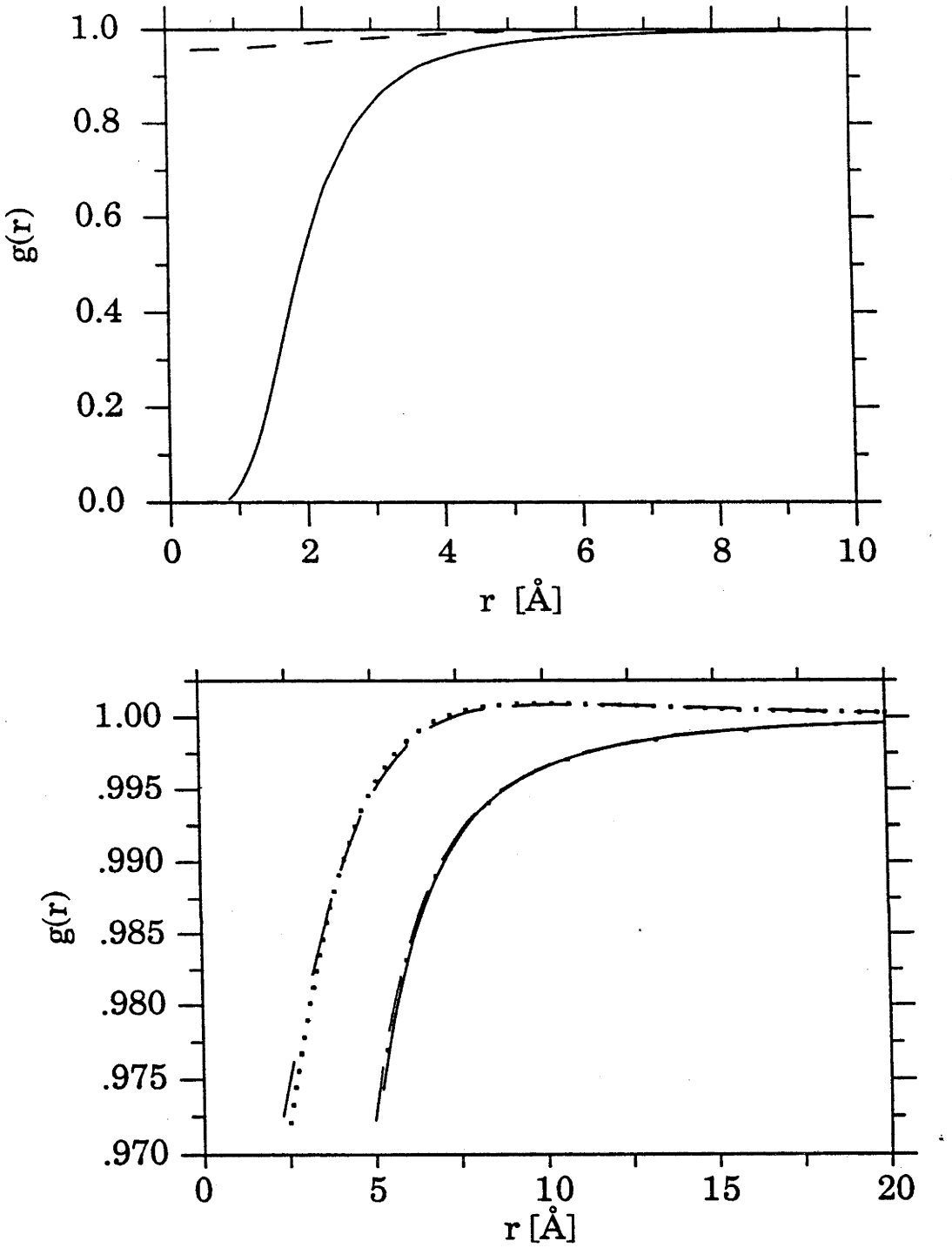

Figures 4.1 Radial distribution functions for 1Å monovalent zwitterions on the same and on opposite surfaces (ρ^{-1}=75Å^2, T=300K, $\varepsilon_1 = \varepsilon_2$=80) at a surface separation of 5Å. The HNC results (solid curve, same surface; dashed curve, opposite surfaces) are shown. These are compared to their respective asymptotic forms (curves with dots) in the lower graph with the expanded vertical scale.

4.2 Pressure between dipolar surfaces

One can calculate the interaction free energy (and hence the pressure by differentiation) using the various approximations of the preceding chapter. First concentrate on dipoles constrained to point perpendicular to the surfaces (hence the parallel components of the susceptibility are zero). The HNC results will be compared with the following approximations:

(a) Ideal dipoles, second order perturbation theory. This is just Eqs (3.5.2) and (3.5.4), but doesn't include the asymptotic part of the correlation function Eq. (3.5.3).

(b) Zwitterions, second order perturbation theory. This uses the reflection coefficient (3.3.15), together with the approximation $\hat{G}^0_{zz}(k) = \hat{G}^0_{zz}(0)$, and the expansion of the logarithm in the free energy expression (3.3.12) through to terms of order $(\hat{G}^0_{zz}(0))^2$.

(c) Zwitterions, perturbation theory, including the asymptotic part of the correlation function. Same as (b) but includes the term linear in k (Eq. (3.4.4) using Eq. (3.4.6c)). This approximation is the analogue of Eqs (3.5.2-4), generalised to zwitterions.

(d) Zwitterions, infinite order perturbation theory. $G^0_{zz}(\mathbf{k})$ as in (c) inserted into the reflection coefficient (3.3.15) and the full logarithm expression (3.3.12) is used for the free energy.

(e) Simplified mean field perturbation approximation. The $G^0_{zz}(\mathbf{k})$ is obtained from $\hat{\tau}(0)$ (using $G^0_{zz}(0)$ from table 4.1 in Eq. (3.4.7)) inserted into Eq. (3.4.3) using the zwitterion potentials (3.4.6). Then the reflection coefficient and free energy are determined as in (d).

All of these approximations are identical in the asymptotic limit of large separations. However the accuracy at smaller separations is expected to improve in going from a to e, as we now explicitly show. As before, the HNC is considered to be a benchmark against which to test the other approximations. This is reasonable since the hypernetted chain closure is

known to work well in general for systems with long range interactions (see Part I and references therein). In addition, HNC results for the susceptibility of these particular two dimensional dipolar systems have already been favourably compared with simulation data (§4.1).

Figures 4.2 show the pressure between surfaces of perpendicular dipoles at an area per dipole of 75Å^2 (chosen to reflect the surface density of polar lipid bilayers) and for moments of μ=1 and 5 eÅ. Since there are no images here, the attraction arises from the correlations between dipoles on opposite surfaces, and asymptotically decays as h^{-5}. For the 1Å zwitterions, we see that the ideal dipolar approximation (a) is already very good at 10Å separation (always measured between the zwitterion midpoints) and that the simplified mean field perturbation approximation (e) is excellent over nearly the whole regime shown. For the system with the higher moment, μ= 5 eÅ, the ideal dipole is within an order of magnitude of the HNC at 10Å, and is virtually coincident with it by about 30Å separation. The approximations progressively improve, and again (e) gives virtually exact agreement with the HNC even at very small separations.

Figures 4.3 show the effect of images on the pressure due to the surface dipoles alone. It is desirable to highlight these novel surface effects and so the zero frequency Lifshitz term has not yet been added (but see fig. 4.4 below). In the attractive (small separation) regime, the difference between the various approximations is most apparent. However, by the time the image repulsion dominates, all the approximations agree, and now the pressure goes asymptotically as h^{-4}. Figure 4.4 shows the total pressure for the 5Å zwitterions in the HNC approximation. Below about 15Å the pressure for the cases with and without dielectric discontinuities are quite similar. Here it is obviously dominated by the direct correlational attraction between dipoles on opposite surfaces in both cases. Beyond that separation, the pressure for the case with images is essentially given by the zero frequency van der Waals attraction. This decays as h^{-3} and dominates the more rapidly

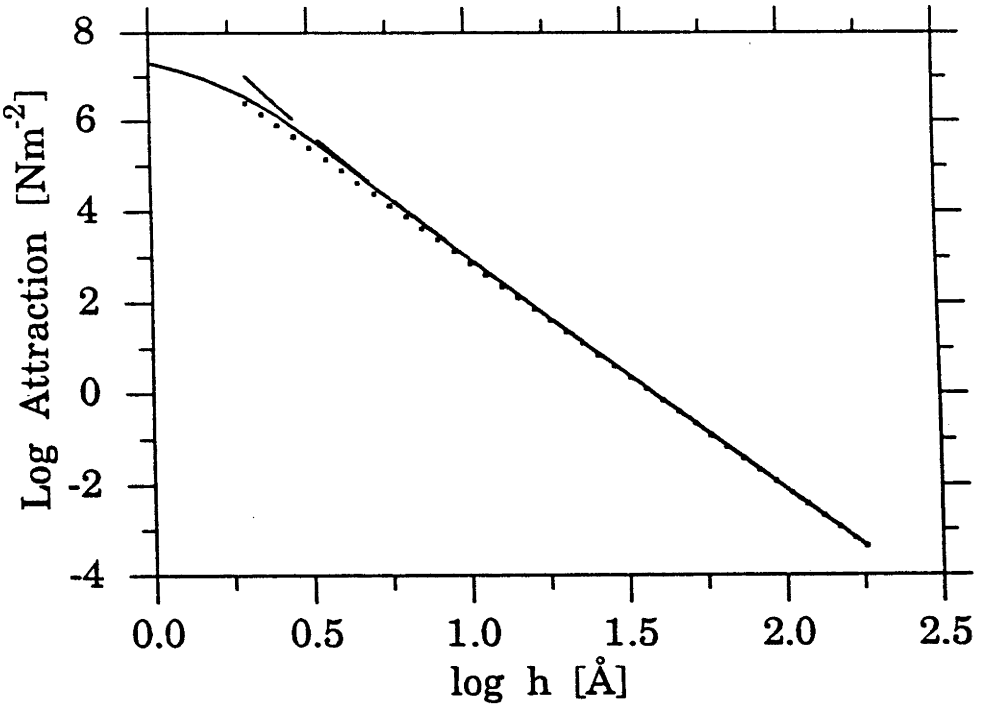

Figure 4.2a The attractive pressure between surfaces of perpendicular dipoles (μ=1Å) versus separation (log scales). The HNC results for monovalent zwitterions (————) are compared to the ideal dipole approximation (a, · · · · ·) and the simplified mean field perturbation approximation (e, — — —). The area per diopole is 75Å^2, ε_1=ε_2=80 (no images) and T=300K. The susceptibility used in the approximations is taken from the HNC results in Table 4.1.

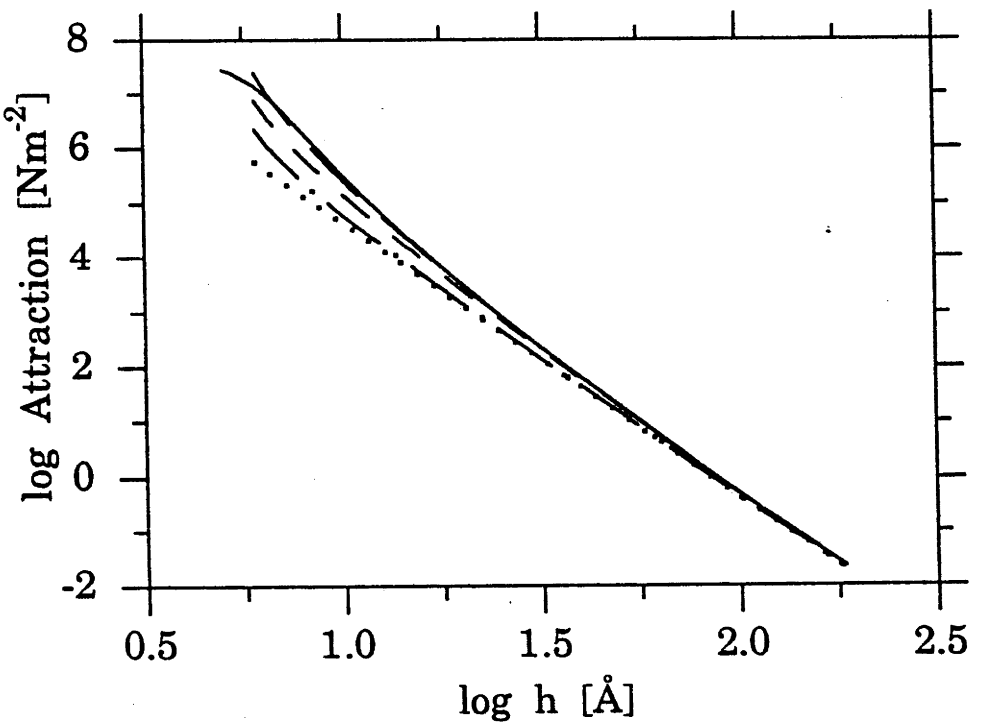

Figure 4.2b Same as preceding figure but for μ=5Å. The HNC zwitterion results (————) are compared to four approximate formulae (given in the text): a (· · · · ·); b (— · — · —) (would be coincident with approximation c); d (— — — —); and e (— — —).

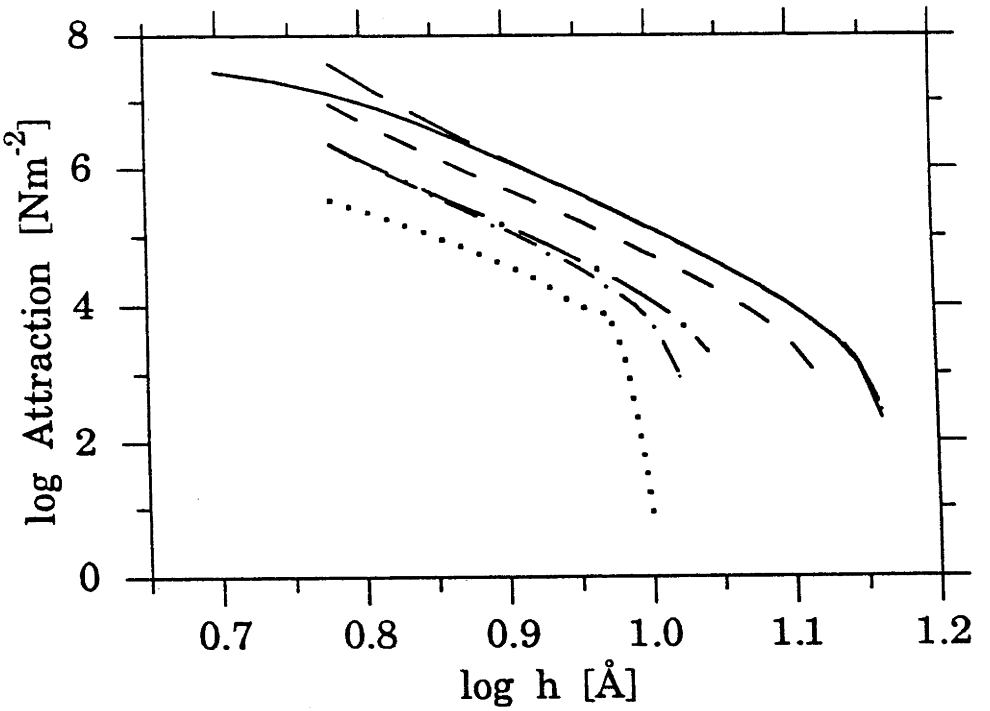

Figure 4.3a The attractive pressure between surfaces of perpendicular dipoles (μ=5Å) versus separation (log scales). The HNC results for monovalent zwitterions (————) are compared are compared to five approximate formulae: a (· · · · ·); b (— · — · —); c (— · — · — · —); d (— — — —); and e (— — — —). The area per diopole is 75Å^2, ε_1=80, ε_2=2, w=3Å and T=300K. The susceptibility used in the approximations is taken from the HNC results in Table 4.1b. The zero frequency van der Waals attraction is not included.

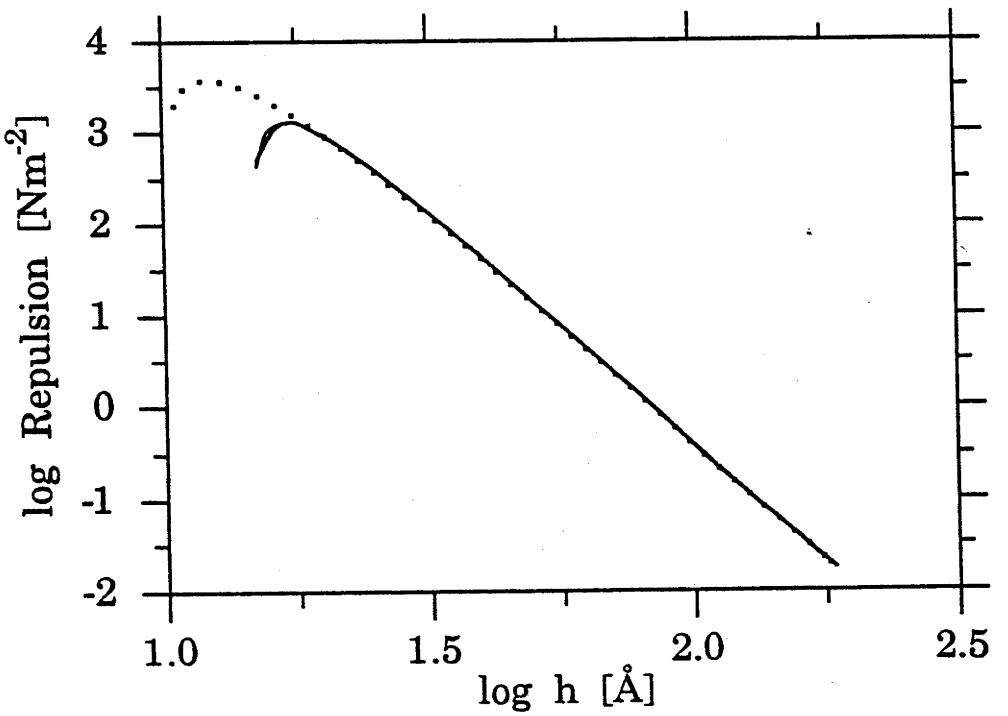

Figure 4.3b Same system as above but in the repulsive regime (the zero frequency van der Waals attraction is not included). The ideal dipole prediction (a, · · · · ·) is compared to the HNC (————) and the simplified mean field perturbation approximation (e, — — — —), the latter two virtually coincident.

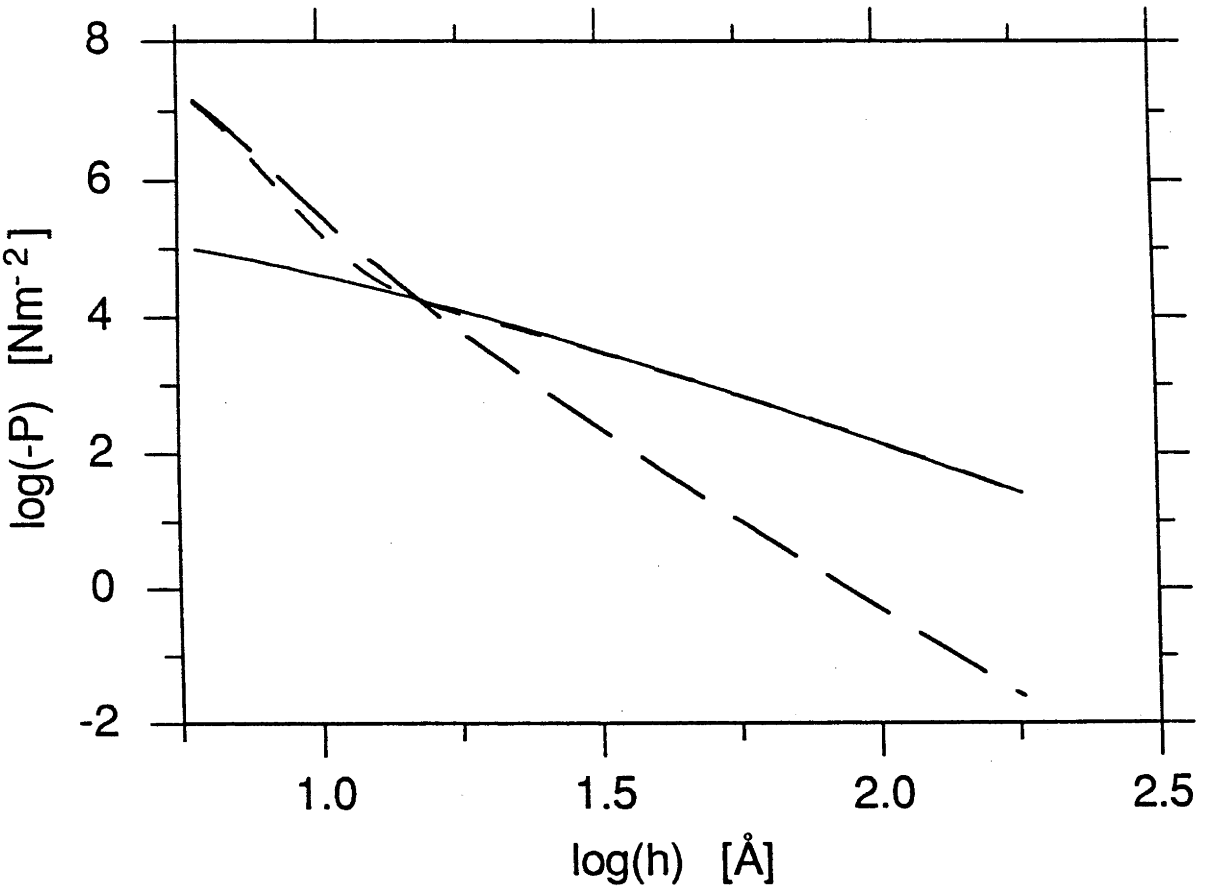

Figure 4.4 HNC results for the attractive pressure, -P, as a function of separation, h, between two surfaces with perpendicular 5Å zwitterions in the presence of dielectric discontinuities ($\varepsilon_1 = 80$, $\varepsilon_2 = 2$ and $w = 3$ Å). The inverse density is 75 Å^2 and T=300K. The total pressure (– – –), $P_{dipolar} + P_{VdW}$, is compared to the static VdW interaction, P_{VdW}, alone (————). As a reference, we have also included the pressure curve (— — — —) for the system in absence of discontinuities [same as in fig. 4.2b].

decaying dipolar self image repulsion.

One can compare the HNC results with the Monte Carlo data of Granfeldt et al.[10]. These authors have recently simulated 5Å perpendicular zwitterions, at an area per dipole of 60Å^2, a separation of h=11Å, with images (ε_1=80, ε_2=2, without van der Waals). For w=2.6Å (the distance from the zwitterion midpoint to the dielectric discontinuity) they obtained a pressure of $-1\pm2\times10^4$ Nm^{-2} and we find the HNC pressure to be -3.15×10^4 Nm^{-2} . When the dielectric discontinuity is further removed (w=4.5Å), the MC simulation gives $-4\pm2\times10^4$ Nm^{-2} and the HNC -7.76×10^4 Nm^{-2}. The agreement is satisfactory considering the difficulties in simulating this system with long ranged correlation and electrostatic interactions. The model examined by the HNC method does not have any hard cores. Hence the compressibility there will be larger than in the simulated model which includes a 2Å radius hard core repulsion. The correlational attraction is proportional to the square of the susceptibility (Eq. 3.5.7), which for perpendicular dipoles is directly related to the compressibility. This may be the reason why the simulated attractions appear to lie below the HNC, at least for these two data.

Figure 4.5 compares the pressure between perpendicular and orientable dipoles, using the asymptotic formulae (3.5.2-4) and susceptibilities from tables 4.1, 4.2. The surface contribution to the pressure is here repulsive for both the perpendicular and orientable 1eÅ dipoles. The enhanced repulsion for the latter arises because the image charges reinforce parallel orientations of the dipoles, whereas they tend to cancel the perpendicular ones. However, for 5eÅ dipoles, the inclusion of the extra orientational degrees of freedom leads to a substantially increased correlational attraction. Figure 4.6 shows calculated pressures Eqs (3.5.5-7) when the dipoles are confined to the outer low dielectric region. The susceptibility used was χ_{xx}=0.0023 and χ_{zz}=0.0025 (Bo Jönsson, pers. com.). Here the surface contribution to the force is repulsive down to very small separations, in contrast to the results for dipoles in the aqueous phase.

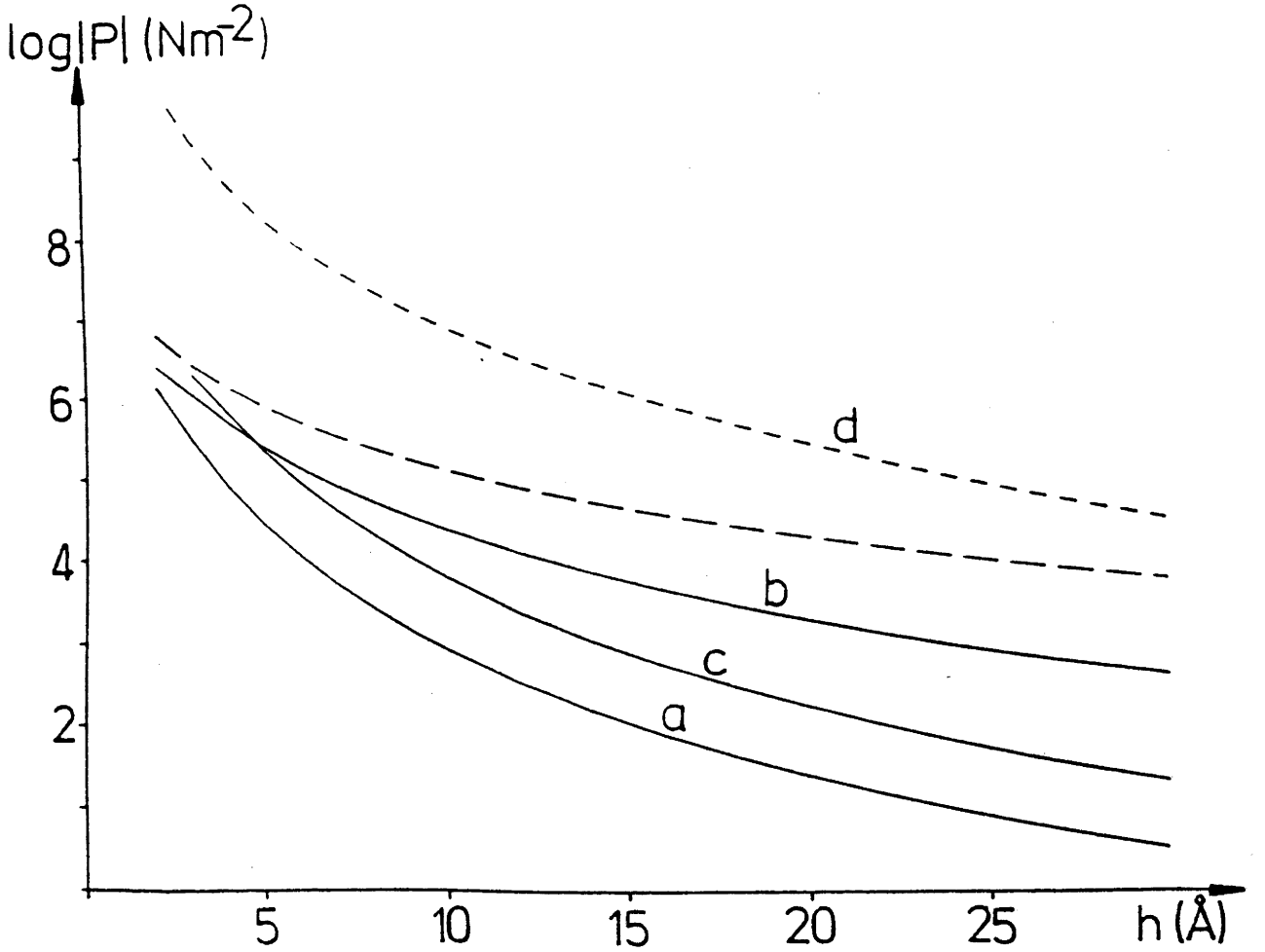

Figure 4.5 A comparison of the contributions to the pressure between surfaces with perpendicular and freely orientable dipoles as a function of their separation. Solid lines (——) represent a positive and dashed lines (- - -) a negative surface contribution to the total pressure. (a) perpendicular, 1eÅ dipoles; (b) freely orientable 1eÅ dipoles; (c) perpendicular 5eÅ dipoles; and (d) freely orientable 5eÅ dipoles. These curves are for the dipoles in the aqueous region and r_c=4Å, ε_1=80, ε_2=2 w=0.5Å and ρ^{-1}=75Å^2. The remaining curve (— — —) is the zero frequency Lifshitz attraction between the dielectric half spaces.

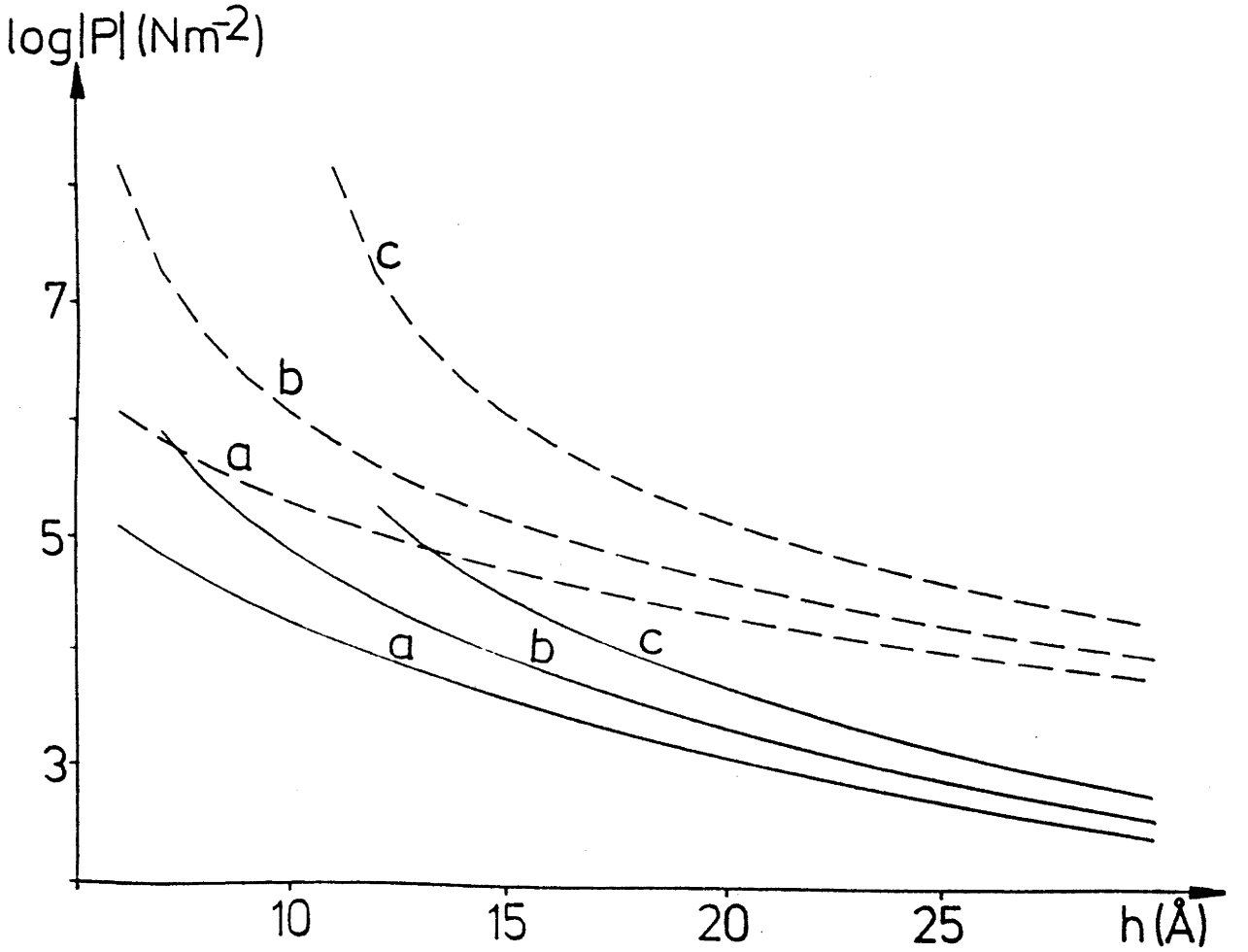

Figure 4.6 Contributions to the pressure between surfaces with freely orientable dipoles in the low permittivity region as a function of the separation. The repulsive contribution from the dipoles (——) is dominated by the zero frequency Lifshitz attraction (— — —) in each case: (a) w=0.5Å; (b) w=2.5Å; and (c) w=5.0Å. The dipole moment is 5eÅ, r_c=4Å, ε_1=80, ε_2=5 and ρ^{-1}=40Å^2.

However the zero frequency van der Waals still dominates so that the total force is always attractive, as it should be.

An attempt was made to compare the results for orientable dipoles with the recent simulation data of Granfeldt et al.[10]. For 5Å monovalent zwitterions, with $\rho^{-1}=60Å^2$, $\varepsilon_1=80$, $\varepsilon_2=2$, and $w=4.5Å$, at separations of $h=9$, 11 and 16Å, the Swedes find attractive pressures -0.54, -0.29, and -0.03×10^5 Nm^{-2}. If one uses the susceptibilities given by Jönsson ($\chi_{xx}=0.65$ and $\chi_{zz}=0.13$ table 4.2) one is unable to find pressures within an order of magnitude of these results. The reason may lie with the model treated by Granfeldt et al.[10], in which the 5Å zwitterions pivot about one end. Since the dielectric discontinuity lies just 2Å beyond this pivot, there is a substantial loss of orientational freedom in this model. Consequently the susceptibility should be smaller than those simulated by Jönsson for freely orientable point dipoles (table 4.2). Indeed, using values of $\chi_{xx}=0.14$ and $\chi_{zz}=0.17$ the asymptotic formulae (3.5.2-4) predict pressures of -2, -0.6, and -0.02×10^5 Nm^{-2}. One can't really expect any better agreement than this since the differences in the two models are exacerbated at these small separations.

4.3 Forces between polar lipid bilayers

The attractive forces operating between lipid bilayers inferred from osmotic pressure experiments[1,2] or measured directly [3-6] show up some puzzling anomalies. For the first class of experiments[1,2], the Hamaker constants are deduced by balancing an extrapolated repulsive hydration force with an assumed van der Waals force at the equilibrium bilayer separation. The magnitude of the forces so deduced varies by a factor of about five above or below that expected from Lifshitz theory for hydrocarbon-water systems, depending on the lipid involved[2]. For the second set of experiments, the attractive forces have been measured accurately over a water thickness range from 20Å to 60Å. Again there are anomalies:- sometimes the forces are about an order of magnitude larger than expected, and sometimes lower[4-6]; More importantly, the decay with distance does not follow the power law dependence predicted by theory .

The strongly repulsive short range hydration force operating between lipids is of no concern here. The (larger) separation regimes where attractive forces dominate can be clearly demarked. In this distance regime it will be shown that the apparent anomalies disappear if a previously neglected component of the forces is taken into account. These additional contributions arise from correlations between polar headgroups which have been treated explicitely in Chapter 3. In §4.2 the analytic approximations were shown to be accurate over experimental distance regimes of interest. The effect of the headgroup correlations is to give a force contribution that is at first attractive but which turns over to a repulsion at larger separations. The Lifshitz interaction can be substantially changed when the polar headgroup contribution is added, although the total force is always attractive.

Here are reexamined the measured attractive forces between bilayers deposited on mica surfaces [4-6]. Data for plant digalactosyl-diglyceride (DGDG), L-α-dipalmitoyl-phosphatidyl-choline (DPPC), and L-α-dipalmitoyl-phosphatidyl-ethanolamine (DPPE) are analysed.

The attractive pressures between bilayers deposited on mica substrates were originally analysed[4-6] using simple Hamaker theory for half spaces,

$$P = \frac{-A}{6\pi d^3} \qquad (4.3.1)$$

where d is the thickness of the aqueous phase and the Hamaker constant for hydrocarbon - water is $A \sim 6 \cdot 10^{-21}$J. We show below that this value does not fit the data. More suggestive is the difference in the qualitative behaviour, since it will be shown that the measured pressures decay faster than the cubic law predicted by the Hamaker theory. Since this theory is a very crude approximation to the van der Waals forces acting between the bilayers, before seeking an alternative explanation for the data it is first necessary to compute the predictions of the complete Lifshitz theory. The retarded Lifshitz theory for a mica - hydrocarbon - water triple film[15,16] is used. The required dielectric data is taken from the literature, for mica[18], and for water[19], and no ultraviolet interpolation is used[19]. For the hydrocarbon, the measured[6] thickness, ~50Å, and dielectric data for bulk hexane (ε_{hc}=1.89, ω_{uv} = $1.54 \cdot 10^{16} s^{-1}$) are required. There is a slightly larger attraction if values for bulk dodecane (ε_{hc}=2.04, ω_{uv}=$1.40 \cdot 10^{16} s^{-1}$) are used instead. Since Lifshitz theory is formulated to describe interactions between uniform macroscopic dielectric media, it is more appropriate to use these bulk values than, for example, the value ascribed[20] to lecithin bilayers, ε_{hc}=2.143. The latter contains contributions from the polar headgroups, and these are here treated separately. Also, this value taken together with a hydrocarbon ionisation potential, ω_{uv}, predicts too large an attraction for the phospholipid data at large separations.

The experimental data presented in fig. 4.7 is derived from Marra[6]. The measurements were made via the jump method; ie by measuring the

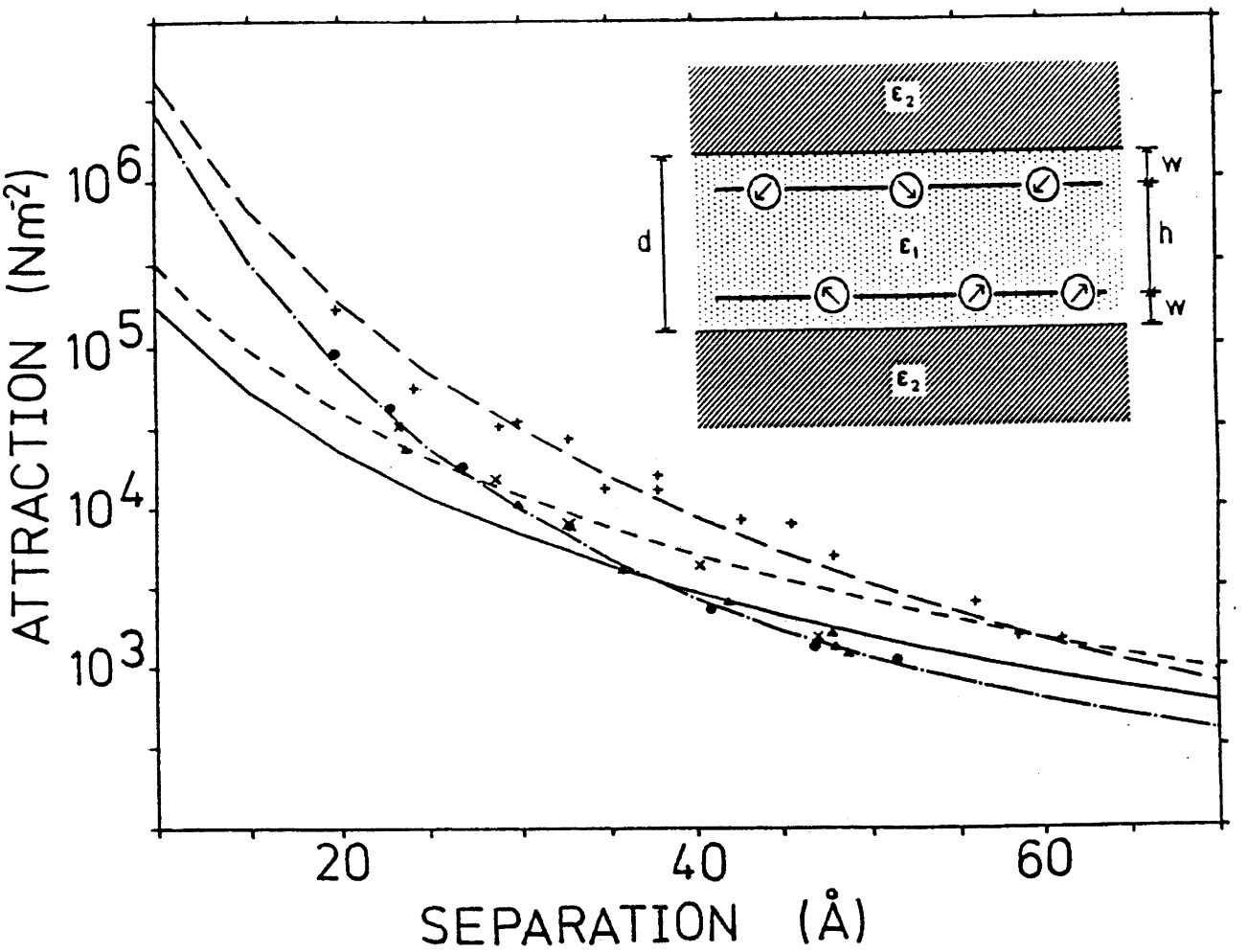

Figure 4.7 Direct force measurements[6] of the attractive pressure between digalactosyl-diglyceride (DGDG, +), phosphatidyl-choline (DPPC, O) and phosphatidyl-ethanolamine (DPPE, Δ) bilayers compared to various theories. Simple Hamaker theory, $A=6.0 \cdot 10^{-21}$J (- - - -) does not have the correct decay, and neither does the retarded, triple-film Lifshitz theory (——). The data can be described by adding to the Lifshitz result the pressure due to zero frequency correlations between dipoles of the polar headgroups. Thus for DGDG (– – – –) the susceptibility fitted was $\hat{G}(0)=0.8\times10^{-38}$, and the distance of the dielectric discontinuity behind the dipoles was w=4Å. For the phospholipids (– · – · – · –) the parameters fitted were $\hat{G}(0)=0.3\times10^{-38}$ and w=0.1Å. Note that the data for DGDG in 0.2M NaCl (×, no fit attempted), indicates some additional headgroup contribution to the attraction at non-zero frequencies. **Inset.** Geometry of the primitive model of the polar headgroup interactions.

separation at which the gradient of the attractive force equalled the spring constant K_s. Then using the Derjaguin approximation, the pressure between two flat surfaces at that separation is $P=-K_s/2\pi R$, (R is the mean radius of the crossed mica cylinders). Plotting the data in the present form no longer implies a particular theory of the attractive force. However, experimental scatter and departure from theory are more apparent here than in the original presentation[4-6]. It can be seen that the results for the two phospholipids lie on approximately the same curve and this is substantially below the data for the galactolipid. Upon the addition of 0.2M NaCl, the attraction for DGDG is reduced. The separation is the experimental distance from D=0, the anhydrous bilayer contact. Ambiguities in the interpretation of this distance (in the context of the point dipole model for the headgroups) have minimal effect at these large separations. These ambiguities do become more severe in interpreting the osmotic pressure experiments[1,2]. Note that the large separation experimental attractions were measured by a quite different method to that used to measure the small separation adhesion energies. The latter are not analysed here.

The simple Hamaker theory (4.3.1) is compared with the Lifshitz triple film calculation. It can be seen that a traditional value of the Hamaker constant ($A=6\cdot10^{-21}J$) overestimates the van der Waals attraction. Note that if the Lifshitz data is fitted to a Hamaker form, the Hamaker "constant" varies from $3.4\times10^{-21}J$ at a separation of 10Å to $4.0\times10^{-21}J$ at 60Å. The Hamaker "constant" should decay with separation due to retardation. The weak variation is due to the simultaneous increase in the relative contribution of the mica to the triple film calculation. Previous authors[4-6] claimed a good description of the data was given by simple Hamaker theory but close inspection shows this to be untrue. Even by moving the so called plane of origin of the van der Waals force (with respect to D=0), or by choosing a different Hamaker constant, the data cannot be fitted. This is because the measured force decays faster than that given by Hamaker (or Lifshitz) theory

between half-spaces. Since the contributions from surfaces decay faster than those from semi-infinite half-spaces[16], the measured data indicates that there is a substantial effect from the headgroups. Also the quantitative differences between the various lipids can be understood because of their different polar headgroups.

The data have been fitted by adding the contribution from the headgroup correlations Eqs (3.5.2-4) to the Lifshitz results. While the model is fully anisotropic, only isotropic susceptibilies have been considered here. For DGDG a susceptibility of $\hat{G}^0(0)=0.8\times10^{-38}\ C^2$ has been used and the effective dielectric discontinuity has been located w=4Å behind the surfaces containing the dipoles. For the phospholipids the fitted parameters are $\hat{G}^0(0)=0.3\times10^{-38}\ C^2$ and w=0.1Å. Note that while the data for DGDG is always above the Lifshitz result, the phospholipid data lies below it for larger separations. Thus here with this choice of parameters, and indeed generally for this model, the phospholipid headgroups must experience an image repulsion (ΔF_1 dominates). This lowers the net attractive force for these lipids in this large distance regime. Changing to w=1Å decreases the fitted attraction by 30%. This is for the phospholipids at small separations; at larger separations the results are quite insensitive to the value of w. Similarly, doubling the susceptibility increases the attraction by about 70%. The fitted values for the susceptibility are of the same order as those found by Monte Carlo simulations of the model system (table 4.2). The qualitative behaviour of the curves, in particular the initially steep decay, is similar for any other reasonable parameters.

These parameters enable one to obtain quite a good fit to the experimental data, but their actual value obviously has to be treated with caution. The primitive model is a gross simplification of reality. Besides this, it is clear that there must be some further effects not taken into account. To see this consider the forces in the presence of high salt. Here all the zero

frequency terms (including the polar headgroup correlations) should be completely screened[16]. Since the data for DGDG in 0.2M NaCl remains above the Lifshitz result (at smaller separations at least) and still exhibit a faster decay, it can be presumed that the measured forces include additional contributions from higher frequency correlations associated with the headgroups. In principle these could be treated by the Lifshitz theory for anisotropic multilayers (§3.2), provided the dielectric data were available. Since here all of these effects are subsumed in the zero-frequency model dipolar correlation term, the parameters must be regarded as effective rather than literal.

The primitive model perturbation analysis predicts that correlations between the dipolar headgroups can give rise to attractions many times larger that the conventional van der Waals force between dielectric half-spaces. Here data for some polar lipid bilayers has been analysed and shown to be well described when these surface terms are included. The actual values taken by these fitted parameters are not as important as is the main theme:- that headgroup correlations must be involved in order to account for both the variation with lipid type and especially the rate of decay of the forces. The data cannot be described by the Lifshitz theory of macroscopic media. The different susceptibilities fitted reflect a specificity of the polarisation correlations due to the different lipid headgroups (size, polarity, mobility and flexibility), as one might expect. Depending on the particular headgroup, and on the separation, the attractive force can be above or below the usual Hamaker or Lifshitz prediction. It appears that one cannot ignore the contributions of the polar headgroup correlations to the attractive forces between lipid bilayers.

Conclusion to Part II

It has been shown (in the linear continuum electrostatic approximation) that similar dielectric bodies interacting across a uniform dielectric medium must always attract each other. While the result does not prove that the primitive model can never give a repulsion for this system (the independence of the reflection coefficients of separation precludes absolute rigor), it now appears unlikely that continuum electrostatics can account for the repulsive "hydration" force at short separations.

Analytic formulae for the interaction free energy between dipolar surfaces have been derived in various approximations and asymptotic limits. These have been compared to numerical computations and shown to be surprisingly good, even down to quite small separations. The puzzling anomalies in the measured long range attractive forces between polar lipid bilayers have been explained by taking into account the effects of the surface dipoles.

References for Part II

1. D.M. LeNeveu, R.P. Rand, and V.A. Parsegian, Nature (Lond.), **259**,601 (1976).
2. L.J. Lis, M. McAlister, N. Fuller, R.P. Rand, and V.A. Parsegian, Biophys. J. **37**, 657 (1982).
3. R.G. Horn, Biochim. Biophys. Acta. **778**, 224 (1984).
4. J. Marra and J.N. Israelachvili, Biochemistry **24**, 4608 (1985).
5. J. Marra, J. Colloid Interface Sci. **107**, 446 (1985).
6. J. Marra, J. Colloid Interface Sci. **109**, 11 (1985).
7. Be. Jönsson and H. Wennerström, Faraday Trans II **79**, 19 (1983).
8. R. Kjellander, J. Chem. Soc. Faraday Trans. II **80**, 1323 (1984).
9. R. Kjellander and S. Marčelja, Chemica Scripta. **25**, 112 (1985).
10. M. Granfeldt, Bo. Jönsson and H. Wennerström, Mol. Phys., (submitted).
11. K. Colbow and B.L. Jones, Biochim. Biophys. Acta **345**, 91 (1974).
12. W. Helfrich, Z. Naturforsch. **A33**, 305 (1978).
13. D. Sornette and N. Ostrowsky, J. Chem. Phys. **84**, 4062 (1986).
14. N.G. van Kampen, B.R.A. Nijboer and K. Schram, Phys. Lett. **26a**, 307 (1968).
15. J. Mahanty and B.W. Ninham, *Dispersion Forces* (Academic Press, London, 1976).
16. V.A. Parsegian and B.W. Ninham, J. theor. Biol. **38**, 101 (1973).
17. G. Stell, in "Statistical Mechanics, Part A: Equilibrium Techniques", ed. B.J. Berne (Plenum Press, New York, 1977)
18. P. Richmond and B.W. Ninham, J. Colloid Interface Sci., **40**, 406 (1972).
19. D. Gingell and V.A. Parsegian, J. theor. Biol., **36**, 41 (1972).
20. R.J. Cherry and D. Chapman, J. Mol. Biol. **40**, 19 (1969).

Part III

Correlations and images in the electric double layer.

Most of the material in this part has been published in the following papers:

P. Attard, D.J. Mitchell, and B.W. Ninham, "Beyond Poisson-Boltzmann: Images and correlations in the electric double layer. I Counterions only", J. Chem. Phys., (in press).

P. Attard, D.J. Mitchell, and B.W. Ninham, "Beyond Poisson-Boltzmann: Images and correlations in the electric double layer. II Symmetric electrolyte", J. Chem. Phys., (submitted).

Introduction to Part III

The DLVO[1,2] theory of the interaction between charged particles across an electrolyte includes two independent forces: a repulsive "double layer" interaction and an attractive van der Waals interaction. The first, considered as a repulsion due to the overlapping of electric double layers around the charged particles, is calculated using a primitive model in which the solvent, usually water, is treated as a continuum macroscopic dielectric. Furthermore the interaction is calculated using the classical (non-quantum mechanical) mean field theory of Gouy[3] and Chapman[4] based on the Poisson-Boltzmann equation. In this theory pair correlations and image interactions are ignored. The van der Waals interaction is calculated according to the simple Hamaker theory[5] as a sum of the pairwise (quantum mechanical) London interactions[6] between molecules.

Lifshitz developed a more rigorous theory for the van der Waals interaction between dielectric bodies across a dielectric medium, using quantum statistical mechanics[7]. Lifshitz theory employs an approximation in which the dipole-dipole correlation function (which gives the linear response to an external field) is calculated according to the macroscopic electromagnetic theory of dielectric continua. Consequently the Lifshitz theory is valid only asymptotically for large separations. The van der Waals interaction is expressed as a sum over discrete imaginary frequencies of a functional of the frequency dependent dielectric constants of the system. The zero frequency term is the classical (non-quantum mechanical) limit of the Lifshitz theory. It arises from thermal fluctuations (or dipole correlations), and is approximately proportional to temperature. The remaining terms are predominatly due to quantum mechanical fluctuations and are approximately independent of temperature. Ninham and Parsegian[8] have shown that the zero frequency term can be significant, at least for some systems involving polar media (eg oil-water).

When ions are added to the dielectric medium, because the ions are slow moving, they will not affect the non-zero frequency contributions to the Lifshitz theory, except through their polarizabilities. On the other hand we can expect the ions to dramatically modify the classical zero frequency contribution. For this reason Ninham and Parsegian[9,10] extended the Lifshitz theory to include the effects of ions in the solvent, at least in the case of uncharged particles (see also refs 11, 12). They found that the zero frequency term is screened by the electrolyte so that this term decays exponentially with distance. This theory was extended by Barouch, Perram, and Smith[13] and by Mitchell and Richmond[14] to include the case of charged particles. The latter paper addressed the problem of the relationship between the double layer interaction and the van der Waals interaction explicitly. Note that in these approaches the effects of ion-ion correlations and image interactions ommited in the DLVO theory are included as part of the van der Waals interaction.

More recently others have proceeded differently, including the effects of ion-ion correlations and image interactions as part of the *double layer* interaction. Guldbrand et al.[15] have done Monte Carlo simulations of the primitive model, one component (counterions only) double layer between walls (without dielectric discontinuities) and Kjellander and Marčelja have treated the same system via the anisotropic HNC equation[16]. The latter authors have also included multiple images due to dielectric discontinuities[17], and more recently, examined the more general problem with a two component electrolyte between the surfaces[18]. These essentially exact approaches involve lengthy numerical computation.

What is hidden in these numerical approaches is the intimate relationship between the classical double layer and the van der Waals forces. The primitive model used to calculate the double layer interactions gives, in some approximation, the difference in the free energies of the system with and without the ions. Thus one should add to the double layer interaction

given by the primitive model the free energy of interaction of the system in the absence of the ions. This is given asymptotically by the Lifshitz theory. The Lifshitz interaction, especially the zero frequency term, cannot be considered to be unrelated to the double layer interaction. It involves the same parameters, namely the dielectric constants of the media. As in the earlier parts of this thesis, the intimate connection between the zero frequency Lifshitz and the primitive model is apparent in the analytic approach we take to the double layer.

Here is used the Debye-Hückel closure to the inhomogeneous Ornstein - Zernike equation and the free energy is expressed as an integral of the secular determinant over Fourier space. This is very similar to the van Kampen modal method[19], and so the rigorous approach taken here may be seen as a continuation of the work started by Ninham and Parsegian some fifteen years earlier[9,10]. It is important to clearly delineate the differences to similar work of others. Barouch, Perram, and Smith[13] addressed the relationship between interacting double layers and van der Waals forces. However they had a spurious divergence in their results (and hence their answers depend on an artificial cutoff) which has precluded any actual calculation from being made. Barnes and Davies[20] analysed the problem but they found a repulsion which decays with the fifth power of separation, which is absurd. Mitchell and Richmond[14] used a Green's function approach in a route to the thermodynamics which was not robust. Consequently when they approximated the profile by the PB form, the double layer and van der Waals forces became simply additive. The modified PB theory of Outhwaite et al.[21] is a numerical scheme which has been used to study the ionic profiles of isolated double layers. It is roughly equivalent to the analytic approach taken here, except that it also treats volume exclusion effects. Carnie and Chan[22] have studied ionic correlations *per se* in inhomogeneous electrolytes, effectively using the Debye-Hückel closure (as is done here).

Over many years, *ad hoc* corrections to DLVO theory have been suggested to account for one physical effect or another. Such procedures may be viewed as modifying the primitive model and are generally of unknown validity or accuracy. For these reasons such corrections will not be reviewed in this work. Nor will be mentioned integral equation schemes which use bulk correlation functions. These are at the singlet level and the validity and accuracy of this approach *is* known. In this part of the thesis systematic corrections to DLVO theory are considered within the primitive model (ions between charged planar walls embedded in continuum macroscopic dielectrics). It is hoped that such accurate solutions can distinguish between experimental data which indicate a breakdown in the DLVO approximation, and those data which truly herald behaviour beyond the continuum model.

The three chapters which make up this part comprise general theory and particular analysis. Chapter 5 sets out a general formalism for inhomogeneous fluids. From this emerges the mean field Poisson-Boltzmann (PB) analysis (§5.2) and the next order approximation, which includes both images and correlations (§5.3). That section concludes with an explicit general solution for the zero size mean spherical model (Debye-Hückel theory) for an arbitrary inhomogeneous electrolyte profile.

Chapter 6 illustrates the application of the theory for a particular limiting case: the one component double layer. The Poisson-Boltzmann approximation (§6.1) and our extension of it (§6.2) are given in turn. Numerical comparisons are made between the present theory and 'exact' HNC calculations for parameters of experimental interest (§6.3). Those results allow a demarkation of regimes in which the theory provides an adequate description of the primitive model, and estimates of the error in Gouy-Chapman theory.

Chapter 7 applies the theory to the symmetric electrolyte. In §7.1 we solve the mean field Poisson-Boltzmann equation giving expressions for the profile, the pressure, and the bulk, surface and interaction free energies,

along with asymptotic expansions for the pressure and interaction free energy. In §7.2 is derived the extended Poisson-Boltzmann expression for the free energy. This involves solutions of Lamé's equation. The surface free energy in this theory is given, and the generalisation of the Onsager - Samaras result that emerges is discussed. The leading asymptotic expression for the interaction free energy is then presented. Numerical results of the theory are given in §7.3, together with a comparison with HNC and PB calculations. There also we give a method for estimating the real surface charge from the effective surface charge deduced by fitting experimental data to PB theory.

Chapter 5 Theoretical Analysis

5.1 Formalism

The thermodynamics of a multicomponent inhomogeneous fluid at a given temperature T, in a given region of space with volume V, with chemical potential μ_α and thermal wavelength λ_α for each species α, interacting with pair potentials $u_{\alpha\gamma}(\mathbf{r},\mathbf{s})$ and in an external potential $\Phi_\alpha(\mathbf{r})$, can, according to classical statistical mechanics, be determined from the grand potential $\Omega = -k_B T \ln \Xi$. The grand partition function is given by

$$\Xi = \sum_{\{N_\alpha\}} \prod_\alpha \left[\frac{\lambda_\alpha^{-3N_\alpha}}{N_\alpha!} \right] \int\!\cdots\!\int \{ d\mathbf{r}_{\alpha i} \} \exp \{ -\beta [H - \sum_\alpha \mu_\alpha N_\alpha] \} \quad (5.1.1)$$

where $\beta = 1/k_B T$ is the inverse temperature and the integrations are over the coordinates of the N_α particles of each species present in each ensemble. The configurational Hamiltonian is

$$H = H_0 + \sum_{\alpha,i} \Phi_\alpha(\mathbf{r}_{\alpha i}) + \frac{1}{2} \sum_{\alpha,\gamma} \sum_{i,j} u_{\alpha\gamma}(\mathbf{r}_{\alpha i}, \mathbf{r}_{\gamma j}) \quad (5.1.2)$$

$$(\alpha,i) \neq (\gamma,j)$$

H_0 is the zero body free energy (effective Hamiltonian) which may depend on geometry but not on the configurations of the solute species $\{\alpha\}$. This form ignores bulk self energy terms like the Born energy of an ion, or the dispersion self energy[10]. These are constant and therefore irrelevant. However when dielectric discontinuities are present self-image terms arise which will be incorporated into the external potential. The intrinsic chemical potential $\mu_\alpha(\mathbf{r}) \equiv \mu_\alpha - \Phi_\alpha(\mathbf{r})$ ultimately determines the density profile[23] and in terms of this entity one can write

$$H - \sum_{\alpha} \mu_{\alpha} N_{\alpha} = H_0 - \sum_{\alpha} \int \hat{\rho}_{\alpha}(\mathbf{r})\, \mu_{\alpha}(\mathbf{r})\, d\mathbf{r} + \frac{1}{2} \sum_{\alpha,\gamma} \int \hat{\rho}^{(2)}_{\alpha\gamma}(\mathbf{r},\mathbf{s})\, u_{\alpha\gamma}(\mathbf{r},\mathbf{s})\, d\mathbf{r}\, d\mathbf{s} \qquad (5.1.3)$$

with the density and pair correlation operators defined as

$$\hat{\rho}_{\alpha}(\mathbf{r}) = \sum_{i=1}^{N_{\alpha}} \delta(\mathbf{r} - \mathbf{r}_{\alpha i}) \,, \quad \hat{\rho}^{(2)}_{\alpha\gamma}(\mathbf{r},\mathbf{s}) = \hat{\rho}_{\alpha}(\mathbf{r})\, \hat{\rho}_{\gamma}(\mathbf{s}) - \hat{\rho}_{\alpha}(\mathbf{r})\, \delta_{\alpha\gamma}\, \delta(\mathbf{r}-\mathbf{s}) \qquad (5.1.4)$$

using the standard Dirac and Kronecker deltas. Ensemble averages of these two operators are the equilibrium density profile $\rho_{\alpha}(\mathbf{r})$, and the pair distribution function $\rho^{(2)}_{\alpha\gamma}(\mathbf{r},\mathbf{s}) = \rho_{\alpha}(\mathbf{r})\, \rho_{\gamma}(\mathbf{s})\, (h_{\alpha\gamma}(\mathbf{r},\mathbf{s}) + 1)$, $h_{\alpha\gamma}$ being the usual indirect correlation function.

The thermodynamic potential $\Omega = -k_B T \ln \Xi$ is more easily obtained from $\rho^{(2)}$ rather than directly from the partition function. One approach is to express Ω in terms of $\rho^{(2)}$ by considering its change due to a shift in the Hamiltonian, viz

$$\delta\Omega = \langle \delta H \rangle = -\sum_{\alpha} \int \rho_{\alpha}(\mathbf{r})\, \delta\mu_{\alpha}(\mathbf{r})\, d\mathbf{r} + \frac{1}{2} \sum_{\alpha,\gamma} \int \rho^{(2)}_{\alpha\gamma}(\mathbf{r},\mathbf{s})\, \delta u_{\alpha\gamma}(\mathbf{r},\mathbf{s})\, d\mathbf{r}\, d\mathbf{s} \qquad (5.1.5)$$

whence in principle Ω follows from a coupling constant integration that switches on the pair potential. This route to thermodynamics is also difficult, because $\rho^{(2)}$ is a functional of the profile. As shown by Evans[23], it is more convenient to express the system as a functional of the density profile. The idea is that since the external potential prescribes the profile uniquely, an alternate description is through the density profile rather than through the external field. To see this, define a free energy $\mathcal{F}$, where

$$\mathcal{F} \equiv \Omega + \sum_{\alpha} \int \rho_{\alpha}(\mathbf{r})\, \mu_{\alpha}(\mathbf{r})\, d\mathbf{r} - H_0 \qquad (5.1.6)$$

$$\equiv F - \sum_{\alpha} \int \rho_{\alpha}(\mathbf{r})\, \Phi_{\alpha}(\mathbf{r})\, d\mathbf{r} - H_0$$

The functional $\mathcal{F}$ is the internal part of the Helmholtz free energy F, since the second term represents the mean contribution from the external potential. From Eq. (5.1.5)

$$\delta\mathcal{F} = \sum_{\alpha}\int \mu_{\alpha}(r)\ \delta\rho_{\alpha}(r)\ dr + \frac{1}{2}\sum_{\alpha,\gamma}\int \rho^{(2)}_{\alpha\gamma}(r,s)\ \delta u_{\alpha\gamma}(r,s)\ dr\, ds \qquad (5.1.7)$$

in which form it is evident that $\mathcal{F} = \mathcal{F}[\rho]$ is a functional of the profile. If the profile is known $\mathcal{F}[\rho]$ can be obtained by calculating the correlation functions *at fixed* $\rho_{\alpha}(\mathbf{r})$ as the pair potential coupling constant is turned on. Inversion of Eq. (5.1.6) now defines a thermodynamic potential functional

$$\Omega[\rho] = \mathcal{F}[\rho] - \sum_{\alpha}\int \rho_{\alpha}(r)\,\mu_{\alpha}(r)\ dr + H_0 \qquad (5.1.8)$$

with the property that $\Omega[\rho] = \Omega$ at the equilibrium density profile. The profile is given by Eq. (5.1.7), or explicitly as

$$\frac{\delta\mathcal{F}[\rho]}{\delta\rho_{\alpha}(r)} = \mu_{\alpha}(r) \qquad (5.1.9)$$

Hence by taking the functional derivative of Eq. (5.1.8), it is clear that $\Omega[\rho]$ is optimised at the equilibrium profile. An advantage of this variational formulation is that the thermodynamic potential functional is relatively insensitive to the approximations to the density profile. This fact will be exploited later. To proceed further one requires the Ornstein-Zernike equation which relates the direct (c) and indirect (h) correlation functions:

$$h_{\alpha\gamma}(r,s) = c_{\alpha\gamma}(r,s) + \sum_{\delta}\int c_{\alpha\delta}(r,t)\,\rho_{\delta}(t)\,h_{\delta\gamma}(t,s)\ dt \qquad (5.1.10)$$

Also required is the density-density correlation function which gives the linear response of the density to the external field (intrinsic chemical potential):

$$\delta\rho_{\alpha}(r) = \beta\sum_{\gamma}\int\left[\,\rho_{\alpha}(r)\,\delta_{\alpha\gamma}\,\delta(r-s) + \rho_{\alpha}(r)\,\rho_{\gamma}(s)\,h_{\alpha\gamma}(r,s)\,\right]\delta\mu_{\gamma}(s)\ ds \qquad (5.1.11)$$

Using Eq. (5.1.10), this can be inverted to give

$$\delta\mu_{\alpha}(r) = k_B T\sum_{\gamma}\int\left[\,\frac{\delta_{\alpha\gamma}\,\delta(r-s)}{\rho_{\alpha}(r)} - c_{\alpha\gamma}(r,s)\,\right]\delta\rho_{\gamma}(s)\ ds \qquad (5.1.12)$$

whence follows the compact form for the direct correlation function

$$c_{\alpha\gamma}(\mathbf{r},\mathbf{s}) = -\beta \frac{\delta^2(\mathcal{F}-\mathcal{F}^{id})}{\delta\rho_\alpha(\mathbf{r})\,\delta\rho_\gamma(\mathbf{s})} \tag{5.1.13}$$

Here $\mathcal{F}^{id}$ is the ideal gas $\mathcal{F}$:

$$\mathcal{F}^{id} = k_B T \sum_\alpha \int \rho_\alpha(\mathbf{r}) \left[\ln\{ \lambda_\alpha^3 \rho_\alpha(\mathbf{r}) \} - 1 \right] d\mathbf{r} \tag{5.1.14}$$

This completes the required formalism. Successive approximations that describe the electric double layer will now be given.

5.2 Mean field approximation

In lowest order approximation correlations are ignored so that $\rho^{(2)}_{\alpha\gamma}(\mathbf{r},\mathbf{s}) = \rho_\alpha(\mathbf{r})\,\rho_\gamma(\mathbf{s})$. Then with the ideal gas as a reference system ($u_{\alpha\gamma}(\mathbf{r},\mathbf{s}) = 0$) integration of Eq. (5.1.7) yields the mean field result

$$\mathcal{F}^{mf} = \mathcal{F}^{id} + \frac{1}{2}\sum_{\alpha,\gamma}\int \rho_\alpha(\mathbf{r})\,\rho_\gamma(\mathbf{s})\,u_{\alpha\gamma}(\mathbf{r},\mathbf{s})\,d\mathbf{r}\,d\mathbf{s} \qquad (5.2.1)$$

with the equilibrium profile determined from Eq. (5.1.9) as

$$\mu_\alpha(\mathbf{r}) = \mu_\alpha - \Phi_\alpha(\mathbf{r}) = k_B T \ln\left\{\lambda_\alpha^3 \rho_\alpha(\mathbf{r})\right\} + \psi_\alpha(\mathbf{r}) \qquad (5.2.2)$$

$$\psi_\alpha(\mathbf{r}) = \sum_\gamma \int \rho_\gamma(\mathbf{s})\,u_{\alpha\gamma}(\mathbf{r},\mathbf{s})\,d\mathbf{s} \qquad (5.2.3)$$

In mean field theory the pair potential contributes to the profile only through the mean potential $\psi_\alpha(\mathbf{r})$. Rearranging gives the Boltzmann equation

$$\rho_\alpha(\mathbf{r}) = z_\alpha \exp -\beta\{\psi_\alpha(\mathbf{r}) + \Phi_\alpha(\mathbf{r})\} \qquad (5.2.4)$$

In the absence of any mean or external potentials, the fugacity $z_\alpha = \lambda_\alpha^{-3}\exp\{\beta\mu_\alpha\}$ reduces to the density of species α in a uniform bulk fluid.

The Poisson-Boltzmann (PB) description of the double layer follows if all short range interactions and image potentials due to dielectric discontinuities are ignored. Note that the self image interaction (part of the external field) should remain in any rigorous mean field analysis. However, since in reality this is screened, including it while ignoring correlations gives strange results at large separations. Hence image charge effects are not yet considered, and the pair potential is taken to be the Coulomb interaction in an infinite medium with uniform dielectric constant ε_1

$$u_{\alpha\gamma}(\mathbf{r},\mathbf{s}) = \frac{q_\alpha q_\gamma}{\varepsilon_1\,|\mathbf{r}-\mathbf{s}|} \qquad (5.2.5)$$

where q_α is the charge of the species α. Taking the total mean electrostatic potential as $\psi(\mathbf{r}) = (\,\psi_\alpha(\mathbf{r}) + \Phi_\alpha(\mathbf{r})\,)\,/\,q_\alpha$ the non-linear PB equation emerges as

$$\nabla^2\psi(\mathbf{r}) = -\frac{4\pi}{\varepsilon_1}\sum_\alpha q_\alpha z_\alpha \exp\{-\beta q_\alpha \psi(\mathbf{r})\} \qquad (5.2.6)$$

The PB result for the thermodynamic potential is now obtained. To do this, substitute $\mathfrak{F}^{mf}$ Eq. (5.2.1) into Eq. (5.1.8), and take H_0 to be the external, configuration independent, electrostatic free energy only. Then the thermodynamic potential consists of an ideal term (less the chemical potential part) and mean electrostatic terms; i.e. with the ionic charge density $Q(\mathbf{r}) \equiv \sum q_\alpha \rho_\alpha(\mathbf{r})$, and an external charge density $\sigma(\mathbf{r})$, we have

$$\Omega^{PB} = \mathfrak{F}^{id} - \sum_\alpha \mu_\alpha \int \rho_\alpha(r)\ dr + \frac{1}{2}\int Q(r)\,\psi(r)\ dr + \frac{1}{2}\int \sigma(r)\,\psi(r)\ dr \qquad (5.2.7)$$

Use of the optimised profile Eq. (5.2.2), gives

$$\Omega^{PB} = -k_B T \sum_\alpha \int \rho_\alpha(r)\ dr - \frac{1}{2}\int Q(r)\,\psi(r)\ dr + \frac{1}{2}\int \sigma(r)\,\psi(r)\ dr$$

$$= -k_B T \sum_\alpha \int \rho_\alpha(r)\ dr - \frac{1}{8\pi}\int \varepsilon(r)\,(\nabla\psi(r))^2\ dr + \int \sigma(r)\,\psi(r)\ dr \qquad (5.2.8)$$

In obtaining the final line, the middle term has been identified with the mean electrostatic energy. The PB pressure is obtained by differentiation with respect to separation.

The term H_0 we have used above does not include the Lifshitz interaction. The reason is that the Coulomb potential Eq. (5.2.5) is that for a infinite uniform dielectric medium. Since the image interactions have been excluded in the PB analysis, it is not appropriate to add here the Lifshitz interaction which also arises from dielectric discontinuities. It is also inconsistent to include dipolar fluctuations while ignoring those due to ions. In next approximation both image charge effects and correlations in the electrolyte will be included. It is then essential to include the Lifshitz contribution in H_0. Otherwise, as will be made explicit, when dielectric discontinuities are present the primitive model gives a spurious long range repulsion which is cancelled identically by the zero frequency Lifshitz term (see parts I and II).

5.3 Images and correlations

The mean field approximation above includes no correlations. Both the direct and indirect correlation functions were taken to be zero. A better approximation follows from Eq. (5.1.13) if we take the second functional derivative of the non-ideal part of the mean field free energy Eq. (5.2.1). This gives

$$c_{\alpha\gamma}(\mathbf{r},\mathbf{s}) = -\beta u_{\alpha\gamma}(\mathbf{r},\mathbf{s}) \tag{5.3.1}$$

Note that this closure is a Debye-Hückel approximation which is equivalent to the mean spherical model with no hard core radius. In fact, this is the correct asymptotic form for the direct correlation function, which is to be expected since the mean field superposition approximation for the pair correlation function is also exact for large particle separations. Use of this closure provides an improved description of the double layer. For bulk electrolytes Debye-Hückel theory fails at high concentrations because short range effects become important. However, the thermodynamics is given correctly in the low dilution limit, since there the system is dominated by the tail of the Coulomb potential. This provides some motivation for persisting with this approximation. However, the real justification will come *a posteriori*, when the results are compared with more sophisticated calculations.

One proceeds by substituting Eq. (5.3.1) into the Ornstein-Zernike equation and obtain an expression for the indirect correlation function. The pair potential coupling constant integral can then be formally evaluated to give the next approximation for $\mathcal{F}$.

To turn on the pair potential, invoke a coupling constant i.e. $u_{\alpha\gamma}(\mathbf{r},\mathbf{s};\lambda)=\lambda\, u_{\alpha\gamma}(\mathbf{r},\mathbf{s})$. Then if $\mathcal{F} = \mathcal{F}^{mf} + \mathcal{F}^{corr}$, with the mean field free energy given by Eq. (5.2.1), one has

$$\mathcal{F}^{corr} = \frac{1}{2}\sum_{\alpha,\gamma}\int_0^1 d\lambda \int \rho_\alpha(\mathbf{r})\,\rho_\gamma(\mathbf{s})\,h_{\alpha\gamma}(\mathbf{r},\mathbf{s};\lambda)\,u_{\alpha\gamma}(\mathbf{r},\mathbf{s})\;d\mathbf{r}\,d\mathbf{s} \tag{5.3.2}$$

The required partially coupled indirect correlation function $h_{\alpha\gamma}(\mathbf{r},\mathbf{s};\lambda)$ follows from the Ornstein-Zernike equation (with $c_{\alpha\gamma}(\mathbf{r},\mathbf{s};\lambda) = -\beta\lambda u_{\alpha\gamma}(\mathbf{r},\mathbf{s})$) as

$$h_{\alpha\gamma}(\mathbf{r},\mathbf{s};\lambda) = -\beta\lambda u_{\alpha\gamma}(\mathbf{r},\mathbf{s}) - \beta\lambda \sum_{\delta} \int u_{\alpha\delta}(\mathbf{r},\mathbf{t})\, \rho_{\delta}(\mathbf{t})\, h_{\delta\gamma}(\mathbf{t},\mathbf{s};\lambda)\, d\mathbf{t} \qquad (5.3.3)$$

Integration of this equation, substitution into Eq. (5.3.2), followed by the coupling constant integration, then gives for the correlation free energy

$$\mathcal{F}^{corr} = \frac{-\beta}{4} \sum_{\alpha,\gamma} \int \rho_{\alpha}(\mathbf{r})\, \rho_{\gamma}(\mathbf{s})\, u_{\alpha\gamma}(\mathbf{r},\mathbf{s})\, u_{\gamma\alpha}(\mathbf{s},\mathbf{r})\, d\mathbf{r}\, d\mathbf{s}$$

$$+ \frac{\beta^2}{6} \sum_{\alpha,\gamma,\delta} \int \rho_{\alpha}(\mathbf{r})\, \rho_{\gamma}(\mathbf{s})\, \rho_{\delta}(\mathbf{t})\, u_{\alpha\gamma}(\mathbf{r},\mathbf{s})\, u_{\gamma\,\delta}(\mathbf{s},\mathbf{t})\, u_{\delta\alpha}(\mathbf{t},\mathbf{r})\, d\mathbf{r}\, d\mathbf{s}\, d\mathbf{t} \ldots\ldots \qquad (5.3.4)$$

By discretising this expression (replace the integrals by Riemann sums), it becomes clear that it represents a sum of traces of powers of a matrix. The expression can be resummed if we determine the eigenvalues Λ of the integral equation

$$-\beta \sum_{\gamma} \int \rho_{\gamma}(\mathbf{s})\, u_{\alpha\gamma}(\mathbf{r},\mathbf{s})\, f_{\gamma}(\mathbf{s})\, d\mathbf{s} = \Lambda f_{\alpha}(\mathbf{r}) \qquad (5.3.5)$$

Then the correlation free energy may be rewritten as sums of powers of the eigenvalues

$$\mathcal{F}^{corr} = \frac{-k_B T}{2} \sum_{n=2}^{\infty} \frac{1}{n} \sum_{i=1}^{\infty} \Lambda_i^n = \frac{k_B T}{2} \sum_{i=1}^{\infty} \ln\{1-\Lambda_i\} + \Lambda_i \qquad (5.3.6)$$

Note that the term in Λ_i represents the self interaction which cancels the first term in the expansion of the logarithm. Since the self image interaction will later be added via the external field, it is actually only the (infinite) direct Coulombic self interaction which is excluded from the free energy.

Further progress requires determination of the eigenvalues. For notational convenience first write the pair potential as $u_{\alpha\gamma}(\mathbf{r},\mathbf{s}) = q_{\alpha}\, q_{\gamma}\, u(\mathbf{r},\mathbf{s})$ and define the local inverse Debye length by

$$\kappa^2(\mathbf{r}) = \frac{4\pi\beta}{\varepsilon_l} I(\mathbf{r}) = \frac{4\pi\beta}{\varepsilon_l} \sum_{\alpha} q_{\alpha}^2\, \rho_{\alpha}(\mathbf{r}) \qquad (5.3.7)$$

where $I(\mathbf{r})$ is the ionic strength. Then the eigenvalue equation (5.3.5) for the

eigenfunction $f_\alpha(\mathbf{r}) = q_\alpha f(\mathbf{r})$ may be rewritten

$$-\beta \int I(s)\, u(\mathbf{r},\mathbf{s})\, f(s)\, ds = \Lambda\, f(\mathbf{r}) \qquad (5.3.8)$$

Note that the profile remains unspecified in the present analysis.

Now particularise to planar geometry. The electrolyte is confined to a region of dielectric constant ε_1 of width $d = h + 2w$ separating two half spaces of dielectric constant ε_2 (fig. 5.1) with the distance of closest approach of the ions to each surface being w (the zeroth order Stern layer). As the area A of the planar surfaces becomes infinite, the spectrum of the eigenvalues becomes continuous in the (x,y) direction parallel to the interfaces. Then in Fourier space the sum over wave vectors **k** is replaced by a two-dimensional integral with a density of modes $A/(2\pi)^2$. The correlation free energy can then be written (with $d\mathbf{k}=2\pi k dk$)

$$\mathfrak{F}^{corr} = \frac{k_B T A}{8\pi^2} \int \sum_{i=1}^{\infty} \{ \ln[\,1 - \Lambda_i(k)\,] + \Lambda_i(k) \}\, d\mathbf{k} \qquad (5.3.9)$$

and the eigenvalue equation becomes

$$-\beta \int \hat{u}(k,z_1,z_2)\, I(z_2)\, f(z_2)\, dz_2 = \Lambda(k)\, f(z_1) \qquad (5.3.10)$$

The circumflex denotes the two dimensional Fourier transform of the cylindrically symmetric potential, and the eigenfunction is an implicit function of k.

Because $u(\mathbf{r},\mathbf{s})$ is the potential at **r** due to a charge in the electrolyte at **s**, it satisfies $\nabla^2 u = 0$, $|z| > h/2$, and, $\nabla^2 u = -(4\pi/\varepsilon_1)\,\delta(\mathbf{r}-\mathbf{s})$, $|z| < h/2$. In Fourier space these equations can be written

$$\hat{u}''(k,z,z_1) - k^2\, \hat{u}(k,z,z_1) = \frac{-4\pi}{\varepsilon_1}\, \delta(z-z_1) \qquad (5.3.11)$$

and the boundary condition can be shown to be

$$k\,\varepsilon_2\, \hat{u}(k,d/2,z_1) + \varepsilon_1\, \hat{u}'(k,d/2,z_1) = 0 \qquad (5.3.12)$$

Using these results the eigenvalue equation (5.3.10) can be rewritten as

$$f''(z) - (k^2 + \lambda\, \kappa^2(z))\, f(z) = 0 \qquad (5.3.13)$$

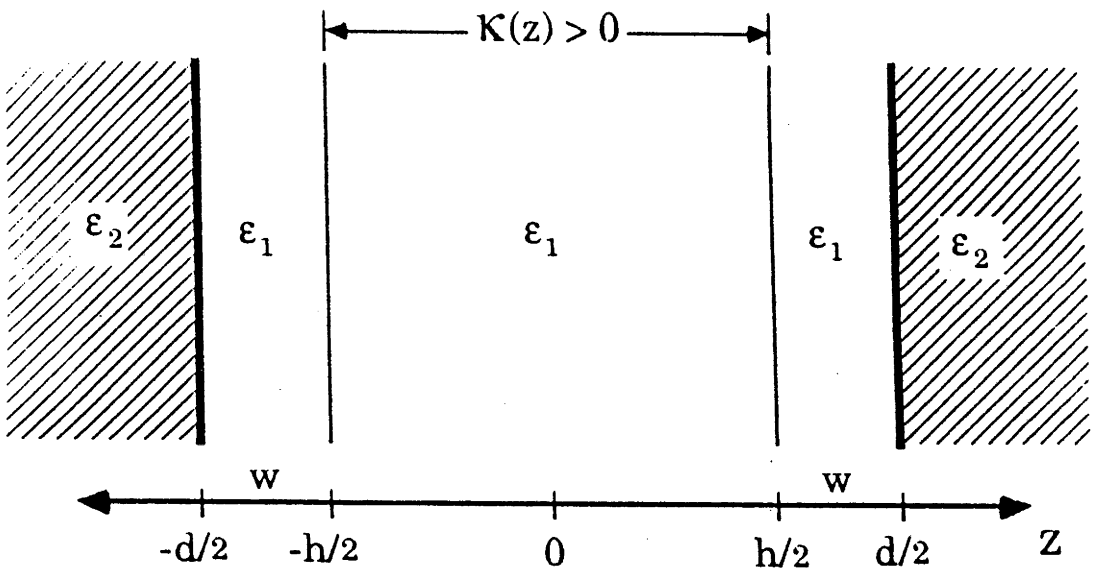

Figure 5.1 In planar geometry, the width of the electrolyte is h and that of each Stern layer (from which the ions are excluded) is w. The separation of the surfaces is d=h+2w, which is also the width of the intervening uniform dielectric ε_1. This region separates two half-spaces with dielectric constant ε_2.

where $\lambda=1/\Lambda$, and the same boundary condition holds.

Now define $C_\lambda(z)$ and $S_\lambda(z)$ as the (even and odd) solutions which satisfy the initial conditions at the midpoint:

$$C_\lambda(0) = 1 \qquad C'_\lambda(0) = 0 \tag{5.3.14a}$$

$$S_\lambda(0) = 0 \qquad S'_\lambda(0) = 1 \tag{5.3.14b}$$

These functions are defined between the surfaces, and their k dependence has not been shown explicitly. The initial conditions, together with the differential equation (5.3.13), completely determine the $C_\lambda(z)$ and the $S_\lambda(z)$. The eigenvalues are those values of λ for which the solutions satisfy the boundary condition Eq. (5.3.12), and this requirement yields the secular determinant

$$\mathfrak{D}_\lambda(k) = \{ k\varepsilon_2 C_\lambda(d/2) + \varepsilon_1 C'_\lambda(d/2) \} \{ k\varepsilon_2 S_\lambda(d/2) + \varepsilon_1 S'_\lambda(d/2) \} \tag{5.3.15}$$

It is desirable to have the functions evaluated at the boundary of the Stern layer rather than at the surface. Since $\kappa(z)=0$ within the Stern layer, each of $C_\lambda(z)$ and $S_\lambda(z)$ are here a sum of exponentials. Then from their continuity (and that of their first derivative), we can express Eq. (5.3.15) in terms of functions evaluated at h/2. This gives for the secular determinant

$$\mathfrak{D}_\lambda(k) = Y \{ C'_\lambda(h/2) + k C_\lambda(h/2) + \Delta_{12} [C'_\lambda(h/2) - k C_\lambda(h/2)] e^{-2kw} \}$$
$$\times \{ S'_\lambda(h/2) + k S_\lambda(h/2) + \Delta_{12} [S'_\lambda(h/2) - k S_\lambda(h/2)] e^{-2kw} \} \tag{5.3.16}$$

Here $Y=k^2(\varepsilon_2+\varepsilon_1)^2 e^{2kw}/4$ is independent of λ. Since secular determinants are determined up to an arbitrary constant, it is only their ratio that will prove physically meaningful. We have also defined $\Delta_{12}=(\varepsilon_1-\varepsilon_2)/(\varepsilon_1+\varepsilon_2)$.

The allowed eigenvalues are then the zeros $\mathfrak{D}_\lambda(k)=0$. Using this, the sum over the possible modes Eq. (5.3.9) can be expressed as a contour integral in the complex λ-plane (fig. 5.2). By the Cauchy residue theorem we have

$$\sum_i \ln\{ 1 - 1/\lambda_i(k) \} = \frac{1}{2\pi i} \int_C \frac{\dot{\mathfrak{D}}_\lambda(k)}{\mathfrak{D}_\lambda(k)} \ln\{ 1-1/\lambda \} \, d\lambda \tag{5.3.17}$$

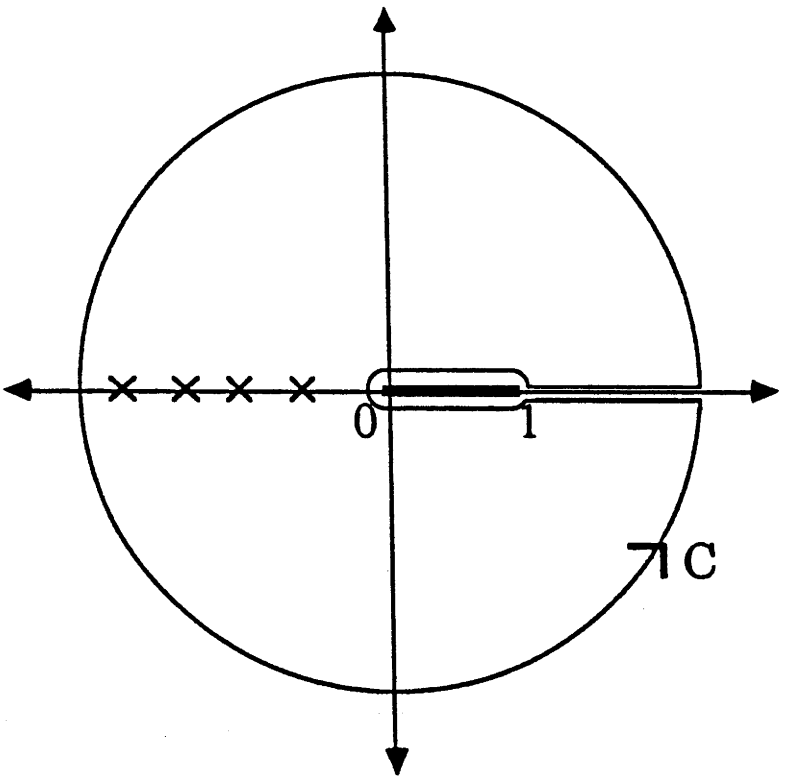

Figure 5.2 The contour in the complex λ-plane used to rewrite the sum over the eigenvalues as an integral Eq. (5.3.19). The allowed modes lie on the negative real axis.

where the dot denotes differentiation with respect to λ. Spurious zeros of the secular determinant have been excluded by fixing the initial conditions, and this precludes trivial solutions. It remains to show that there are no unwanted residues by showing that $\mathfrak{D}_\lambda(k)$ has no poles. If in addition the integral around the arc vanishes (as its radius is taken to infinity), then what is left is an integral around the branch cut between 0 and 1, and the problem of evaluating $\mathfrak{F}^{corr}$ reduces to a tractable form.

To do this the following argument is made. From the form of the secular determinant Eq. (5.3.16) it is sufficient to show that each of the functions $C_\lambda(k)$, $C'_\lambda(k)$, $S_\lambda(k)$ and $S'_\lambda(k)$ is entire. As solutions of a differential equation, these functions must be finite, continuous and single valued (from the initial conditions Eq. (5.3.14)) for any finite value of λ. To show that they are analytic it must be shown that their derivatives with respect to λ exist. Accordingly differentiate Eq. (5.3.13) to obtain

$$\frac{d^2 \dot{f}(z)}{dz^2} - (k^2 + \lambda \kappa^2(z))\, \dot{f}(z) = \kappa^2(z)\, f(z) \qquad (5.3.18)$$

Now with f(z) equal to $C_\lambda(z)$ or $S_\lambda(z)$, it has already been shown that the right hand side is finite, continuous and single valued. Hence the solutions to the equation, which must be $\dot{C}_\lambda(z)$ and $\dot{S}_\lambda(z)$ respectively, are also finite and continuous functions of λ. The conclusion also holds for their z derivatives. That they are single valued follows by taking the derivative with respect to λ of the initial conditions Eq. (5.3.14). Finally, since a function is analytic if its derivative exists, we conclude that the four functions which comprise the secular determinant Eq. (5.3.16) are entire, and that the contour integral Eq. (5.3.17) contains no spurious contributions from poles.

Next consider the behaviour of the secular determinant for large λ. The differential equation (5.3.13) is analysed using a WKB approximation. Let f(z)=exp w(z). Then (since $\kappa(z)$ is non zero within the electrolyte)

$$\frac{f''(z)}{f(z)} = w''(z) + (w'(z))^2 \approx \lambda \kappa^2(z) \qquad (5.3.19)$$

It follows that $w'' << (w')^2$, and that $w' \sim \lambda^{1/2}$. Thus $C_\lambda(h/2)$ and $S_\lambda(h/2)$ behave as $\exp\{a\lambda^{1/2}\}$, $(a=\int_0^{h/2} \kappa(z)\, dz)$. Then $\mathcal{D}_\lambda(k) \sim \exp\{2a\lambda^{1/2}\}$, and the vanishing of the integral Eq. (5.3.17) around the outer contour as $\lambda \to \infty$ is assured.

There remains the integral around the branch cut between 0 and 1 (fig.5.2) which gives the final result for the correlation free energy

$$\mathcal{F}^{corr} = \frac{A k_B T}{8\pi^2} \int \ln\left[\frac{\mathcal{D}_1(k)}{\mathcal{D}_0(k)}\right] dk \; - \; \mathcal{F}^{self} \qquad (5.3.20)$$

Here the sum over the eigenvalues themselves gives the self interaction term, which, from Eq. (5.3.4) may be written

$$\mathcal{F}^{self} = \frac{1}{2}\sum_\alpha \int \rho_\alpha(r)\, u_{\alpha\alpha}(r,r)\, dr = \frac{A}{8\pi^2}\iint I(z)\, \hat{u}(k,z,z)\, dk\, dz \qquad (5.3.21)$$

Note that when the external term is added, $\mathcal{F}^{self}$ will be partially cancelled by the self image interaction. This will leave only the divergent Coulombic self energy term in which $\hat{u}$ is replaced in the above by $\hat{u}^{Coul}(k,z,z) = 2\pi/\varepsilon_1 k$. The free energy contains bulk and surface as well as separation dependent contributions. The main concern is with the pressure between the surfaces, and therefore most interest lies in the interaction part of $\mathcal{F}^{corr}$ above.

Consider then the structure of Eq. (5.3.20). It involves $\mathcal{D}_0(k)$, the secular determinant evaluated at $\lambda=0$, which case is equivalent to one of no electrolyte between the surfaces. The expression for $\mathcal{F}^{corr}$ Eq. (5.3.20) includes a repulsive contribution $-\Omega^{Lif}$ where

$$\Omega^{Lif} = \frac{A k_B T}{8\pi^2}\int \ln\{\mathcal{D}_0(k)/(Y\, k e^{kh})\}\, dk = \frac{A k_B T}{8\pi^2}\int \ln\{1 - \Delta_{12}^2 e^{-2kd}\}\, dk \qquad (5.3.22)$$

and $C_0(z) = \cosh(kz)$, $S_0(z) = \sinh(kz)/k$ have been used. These are the solutions of Eq. (5.3.13) with $\lambda = 0$, or in the absence of electrolyte, (i.e. $\kappa(z) = 0$). The factor Y is cancelled by the numerator, and the factor ke^{kh} must be incorporated with $\mathcal{D}_1(k)/Y$ in the final expression. Now Ω^{Lif} is the usual Lifshitz interaction, at zero frequency, between two dielectric half-spaces[10]. The free energy Eq. (5.3.20) therefore contains a spurious power law repulsion and for consistency one must add the Lifshitz term back on via H_0

(the permanent dipole fluctuations of the dielectric media in the absence of ions are not included in the above). This point has been made earlier (parts I and II) and is a missing and misleading feature of previous primitive model analyses. In the present analysis in which the Lifshitz term appears explicitly, it is quite clear that it must be cancelled. Clearly too the Lifshitz theory and the double layer theory are now treated at the same level of approximation. This can also be seen from the representation Eq. (5.3.4), which is equivalent to a generalised ring diagram approach. It can be shown that Lifshitz theory can also be derived by that method, and both approximate theories are at the same level, at least for the classical zero frequency term. The high frequency Lifshitz (quantum mechanical) terms (which are approximately independent of the electrolyte), remain in the H_0 and must also be added when describing real physical data. These higher frequency terms are not treated in this monograph. But the zero frequency Lifshitz contribution is added, and so is eliminated the artificial repulsion in Eq. (5.3.20).

Chapter 6 One component double layer

These approximations are now illustrated with an application of to a specific system: two identical charged planar surfaces interacting across an aqueous phase which includes *only* the dissociated counterions. The analysis is here more transparent than for the general double layer problem since the elliptic functions which arise there reduce now to trigonometric functions. The principal qualitative features detailed below are also present in the more general problem.

To calculate the correlation interaction free energy, it is necessary to choose a profile, i.e. specify $\kappa(z)$. The mean field profile given by the Boltzmann form Eq. (5.2.4) is chosen. In principle, one could take the higher order approximation that uses the free energy $\mathcal{F}^{mf} + \mathcal{F}^{corr}$ (rather than $\mathcal{F}^{mf}$ alone), and determine the profile from Eq. (5.1.9). However, the accuracy so gained is more than offset by analytic obscurity. Since the formalism is variational, use of the mean field approximation for the profile should be adequate. Hereafter the results so obtained are referred to as the extended Poisson-Boltzmann (EPB) approximation.

6.1 Poisson-Boltzmann theory

For a single species of counterions of charge q, the PB profile which satisfies Eq. (5.2.6) is given by[24]

$$\kappa^2(z) = 2\alpha^2 \sec^2(\alpha z) \tag{6.1.1}$$

where $\kappa^2(z) = 4\pi\beta q^2 \rho(z) / \varepsilon_1$. The separation dependent parameter α satisfies the transcendental equation

$$\alpha \tan(\alpha h/2) = \frac{-2\pi\beta q\sigma}{\varepsilon_1} \equiv \frac{s}{2} \tag{6.1.2}$$

where σ is the surface charge density ($q\sigma < 0$) and h is defined as in fig. 5.1.

The perpendicular component of the pressure is uniform throughout the system and is given by

$$P^{PB} = k_B T \rho(z) - \frac{\varepsilon_1}{8\pi}\left[\frac{d\psi(z)}{dz}\right]^2 \qquad (6.1.3)$$

Since the electric field vanishes at the midplane (from the symmetry of this system), the mean field pressure can also be written as

$$P^{PB} = k_B T \rho(0) = \frac{\varepsilon_1}{2\pi}\left[\frac{k_B T}{q}\right]^2 \alpha^2 \qquad (6.1.4)$$

The corresponding free energy can be obtained from Eq. (5.2.8) which in the case of the symmetric planar geometry can be rewritten

$$\Omega^{PB}/A = h P^{PB} - 2 k_B T \sum_{\alpha} \Gamma_{\alpha} + 2 \sigma \psi(h/2) \qquad (6.1.5)$$

where Γ_α is the total number of ions per unit area of species α. In the limit of counterions only the thermodynamic potential diverges, so one works with F rather than Ω. Taking $\Gamma = -2\sigma/q$ to be the total number of counterions per unit area and using the profile expression Eq. (5.2.2) to eliminate the chemical potential, it follows that

$$F^{PB}/A = h P^{PB} - 2\Gamma k_B T + \Gamma k_B T \ln[\lambda^3 \rho(h/2)] \qquad (6.1.6)$$

Only the interaction (separation dependent) part of the free energy is here required. The surface charge and Γ are here constant. Equation (6.1.6) can be rearranged using the equations for the profile Eqs (6.1.1), (6.1.2), and (6.1.4) to obtain

$$F_{int}^{PB}/A = \frac{\varepsilon_1}{2\pi}\left[\frac{k_B T}{q}\right]^2 \left\{ \alpha^2 h + s \ln\left[1 + \frac{4\alpha^2}{s^2}\right] \right\} \qquad (6.1.7)$$

This is the interaction free energy per unit area. Differentiation of this with respect to separation followed by some manipulation, yields the pressure Eq. (6.1.4). It is of interest to explore the asymptotic behaviour for large separation. Iterative solution of Eq. (6.1.2) yields the form

$$\alpha \sim \frac{\pi}{h}\left\{ 1 - \frac{2}{sh} + \frac{8}{(sh)^2} + O(sh)^{-3} \right\} \qquad (6.1.8)$$

Note that this is also the expansion for large surface charge, although the PB theory is not expected to be valid there. Using this expansion, one finds for the interaction free energy

$$F_{int}^{PB}/A \sim \frac{\varepsilon_1}{2\pi}\left[\frac{k_B T}{q}\right]^2 \frac{\pi^2}{h}\left\{ 1 - \frac{2}{sh} + \frac{20}{3(sh)^2} + O(sh)^{-3} \right\} \qquad (6.1.9)$$

Asymptotically, the PB interaction free energy behaves as a power law, decaying inversly with separation. What is particularly interesting is that, to leading order, this expression (and hence the pressure) is independent of surface charge. The power law of the one component double layer contrasts with the exponential decay of the pressure for the full double layer.

6.2 Extended Poisson-Boltzmann (EPB) theory

The correlation free energy depends on the secular determinant evaluated at $\lambda=1$. Accordingly, choosing the PB profile Eq. (6.1.1), one must solve the differential equation (5.3.13). With $\lambda=1$ this is

$$f''(z) - [k^2 + 2\alpha^2 \sec^2(\alpha z)]\, f(z) = 0 \qquad (6.2.1)$$

The even and odd solutions that satisfy the initial conditions (5.3.14) can be shown to be

$$C_1(z) = \frac{\alpha}{k}\sinh(kz)\tan(\alpha z) + \cosh(kz) \qquad (6.2.2a)$$

$$S_1(z) = \frac{k}{k^2+\alpha^2}\sinh(kz) + \frac{\alpha}{k^2+\alpha^2}\cosh(kz)\tan(\alpha z) \qquad (6.2.2b)$$

The algebra required to evaluate the secular determinant (5.3.16) is tedious but straightforward. The result, for the interaction part, is

$$\mathcal{D}_1^{int}(k) = \frac{1}{1+(\alpha/k)^2}\left[\left\{1+\frac{\alpha^2}{2kX}\left(1+\Delta_{12}e^{-2kw}\right)\right\}^2 - \left\{\left(\frac{\alpha^2}{2k}+\frac{s^2}{8k}\right)\left(1+\Delta_{12}e^{-2kw}\right) - \left(\frac{s}{2}-k\right)\Delta_{12}e^{-2kw}\right\}^2 \frac{e^{-2kh}}{X^2}\right] \qquad (6.2.3)$$

where $X \equiv k + s/2 + (1+\Delta_{12}e^{-2kw})\, s^2/8k$. In deriving this result a surface term X^2/k^2 has been discarded, and the term Yke^{kh} has been cancelled with the corresponding factor in $\mathcal{D}_0(k)$.

The formal expression for $\mathcal{F}^{corr}$ has the self-interaction term cancelling a divergent contribution in the logarithm of $\mathcal{D}_1(k)$ in Eq. (5.3.20). This self-interaction term splits into the direct Coulomb self interaction and a self image term. Now for the counterion only case, the number of ions Γ is constant (independent of the separation), and hence the direct Coulomb self-potential does not contribute to the interaction free energy. The self-image term is separation dependent. But in converting from $\mathcal{F}$ to the Helmholtz free energy F, this same self image term must be added via the contribution of the external potential (cf. Eq. 5.1.6). It then cancels

identically and does not appear explicitly in F (cf. Eq. 5.3.21). Again, the artificial repulsion represented by $\mathfrak{D}_0(k)$ Eq. (5.3.22) is cancelled identically by the zero frequency Lifshitz contribution in the effective Hamiltonian H_0. This leaves the final expression for the interaction free energy per unit area in the one component double layer,

$$F_{int}/A = F_{int}^{PB}/A + \frac{k_B T}{8\pi^2}\int \ln[\,\mathfrak{D}_1^{int}(k)\,]\,dk \qquad (6.2.4)$$

The EPB result includes the effects of correlations (of both the ions and the dielectric media) and all effects due to images.

In general asymptotic expansions for the correlation contribution are complicated, and are not instructive. However, for the case without images (Δ_{12}=0) the asymptotic form is tractable. It is

$$F_{int}/A \sim F_{int}^{PB}/A + \frac{k_B T}{4\pi}\left\{\alpha^2 \ln\{\frac{2\alpha}{s}\} - \alpha^2(\frac{\pi}{4}+\frac{1}{2}) - \frac{\zeta(3)}{4h^2}\right\} + O(h^{-3}) \qquad (6.2.5)$$

Here $\zeta(3)$=1.202... is a Riemann zeta function. (This term is precisely the classical Lifshitz interaction between conducting surfaces, see part I). Since α decays as h^{-1} Eq. (6.1.8), one sees that the correlation contribution decays more rapidly than the PB expression Eq. (6.1.9) and the usual Poisson-Boltzmann form eventually dominates. If one uses the correct α given by Eq. (6.1.2) (rather than the asymptotic expansion), the above form is surprisingly accurate. For example, for monovalent counterions it already agrees to within 1% of the complete integral of Eq. (6.2.3) at 10Å separation (at 100Å^2 per surface charge). The dependence on surface charge is here also rather weak, at least to this order. Images still contribute to the asymptotics to the same order as the image free case above. Their inclusion requires evaluation of the full integral of $\mathfrak{D}_1^{int}(k)$.

6.3 Numerical results

The results of explicit numerical calculations for the counterion only case are now presented. In order to assess the validity of the EPB approximation, the results are compared with accurate numerical calculations for the same primitive model. The effects of image charges on the predicted pressures are then elucidated. Finally, the regimes in which this analysis, and primitive model analyses generally, may be applied to experiments are demarked.

Figure 6.1 compares the pressure between flat charged surfaces (71.4Å^2 per unit surface charge, or σ=0.224 Cm^{-2}) for the one component double layer. As there are no dielectric discontinuities (ε_2= ε_1=80), in this special case there are no image charge effects. The benchmark for comparison is the numerical solution to the hypernetted chain (HNC) equation[25] for point ions, since those results agree well with the Monte Carlo (MC) simulations[15]. The agreement between HNC and MC is good, particularly when the difficulties presented in simulating this system with long range Coulomb interactions are considered. The errors in the MC at large separations may be due to the size of the box, their results being dominated by their PB correction. In addition, the Swedes introduced a hard wall into their simulations[15]. This precluded fluctuations in ionic numbers across the midplane and therefore some legitimate correlations were neglected.

Within the HNC, one can evaluate the pressure directly (as has been done for the results presented here) or via the free energy[16]. The discrepancy between the two methods (a useful check on the consistency of the HNC) is less than that between the HNC and EPB, and here the former is taken to be exact. One sees that the PB theory Eq. (6.1.4) overestimates the repulsion, being too large by some 30% at 50Å separation. Ionic correlations substantially lower the repulsion, and this means that fitting the PB theory to measured force data underestimates the surface charge (ie predicts more ion binding than occurs in reality). The EPB pressure, obtained by numerical

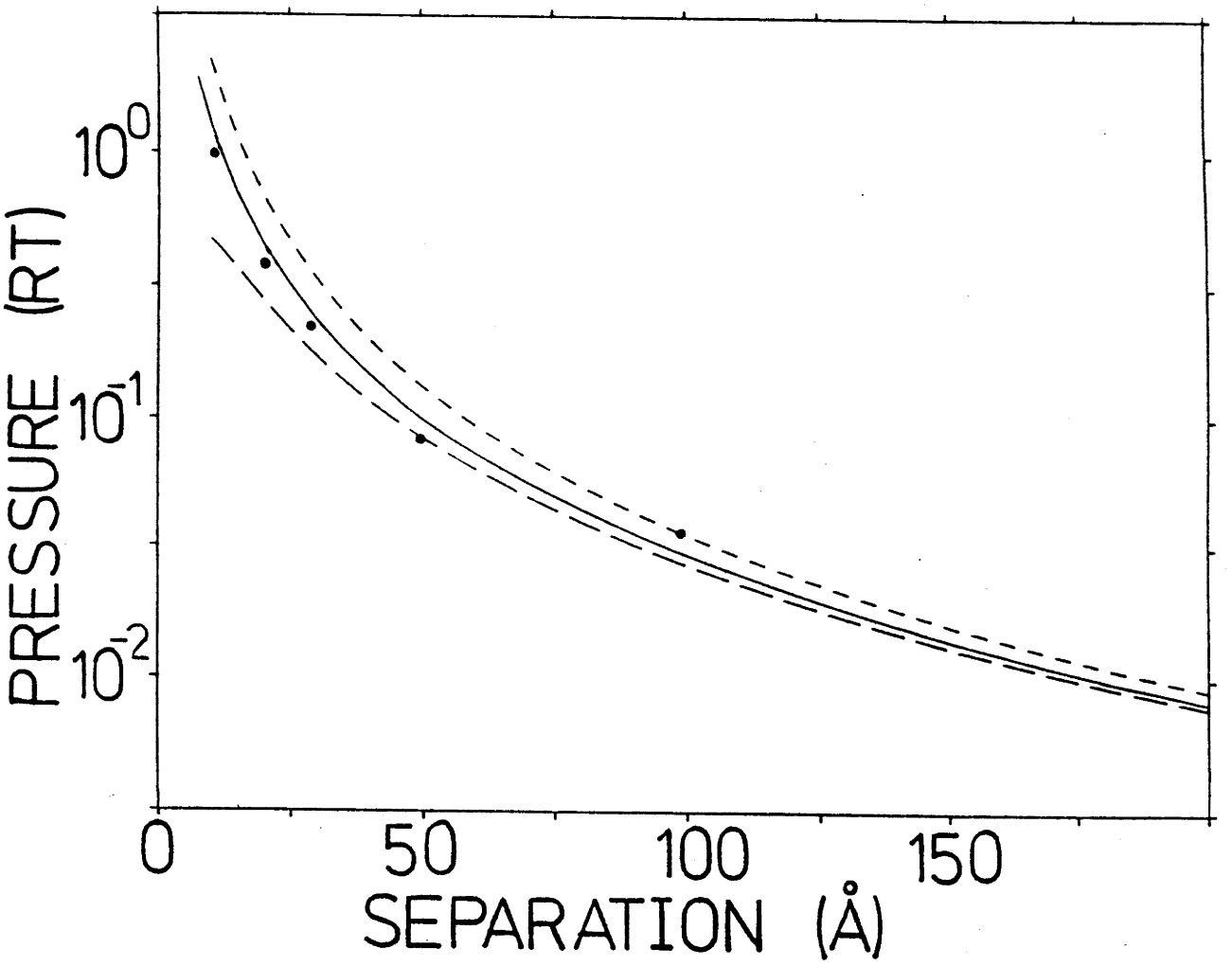

Figure 6.1 Pressure (log scale) for the one component double layer (monovalent counterions) as a function of the separation h. The area per unit surface charge is 71.4Å^2 (σ=0.224Cm^{-2}) and there are no images (ε_1= ε_2=80). The HNC calculations for point ions (———) are from ref. 25 and the MC results (●) from ref. 15. It can be seen that the PB (- - - - -) predicts too high a repulsion whereas the EPB (— — — —) which includes correlations underestimates the repulsion. Both are increasingly accurate at larger separations. To convert from P[RT] to P[Nm^{-2}], multiply by 1000 N_A k_BT. The temperature is here (and for the remaining figures) T= 300K.

differentiation of the total interaction free energy Eq. (6.2.4), is 16% below the HNC result at h=50Å. This qualitative behavior appears to be generally true: accurate solutions of the primitive model (with zero hard core radius) lie between the PB prediction and the EPB result which does include correlations. Indeed, the discrepancy between the latter two may be taken as a guide to the accuracy of the Gouy-Chapman theory. That is a useful result without recourse to involved calculations. Previously there was no easy way of assessing the validity of the PB theory. However since the EPB theory is trivial to implement, it is now possible to estimate the error of the PB theory in any experimental regime.

For large separations, both approximate theories (PB and EPB) become more accurate. At 100Å, the repulsive pressure predicted by EPB is too small by 7%, and by 4% at 200Å. Compare this with the PB theory which is too large by 20% and by 12% respectively. It appears that the EPB approximation predicts the pressure accurately in precisely those large separation regions where HNC (or MC) calculations become difficult.

The EPB results can be expected to be valid in the low surface charge regime where the counterion density is low and the interaction free energy is therefore dominated by the long range tail of the Coulomb potential (cf the Debye-Hückel limiting law for bulk electrolyte). This is illustrated in fig. 6.2, for an area per surface charge of 200Å^2. It can be seen that at 50Å separation, the predictions are 8% lower than the HNC result (cf. Gouy-Chapman which is too large by 20% here).

In the opposite limit of high coupling, short range effects become important and calculated EPB pressures are not quite so accurate. As an example, because the correlations are overestimated attractive pressures are predicted at lower couplings than found by MC [15] or by HNC [16] calculations. (Clearly these attractions also occur for monovalents at close separations and large surface charges, even with a reasonable dielectric constant.) The spurious divergence of the EPB correlation free energy at small separations

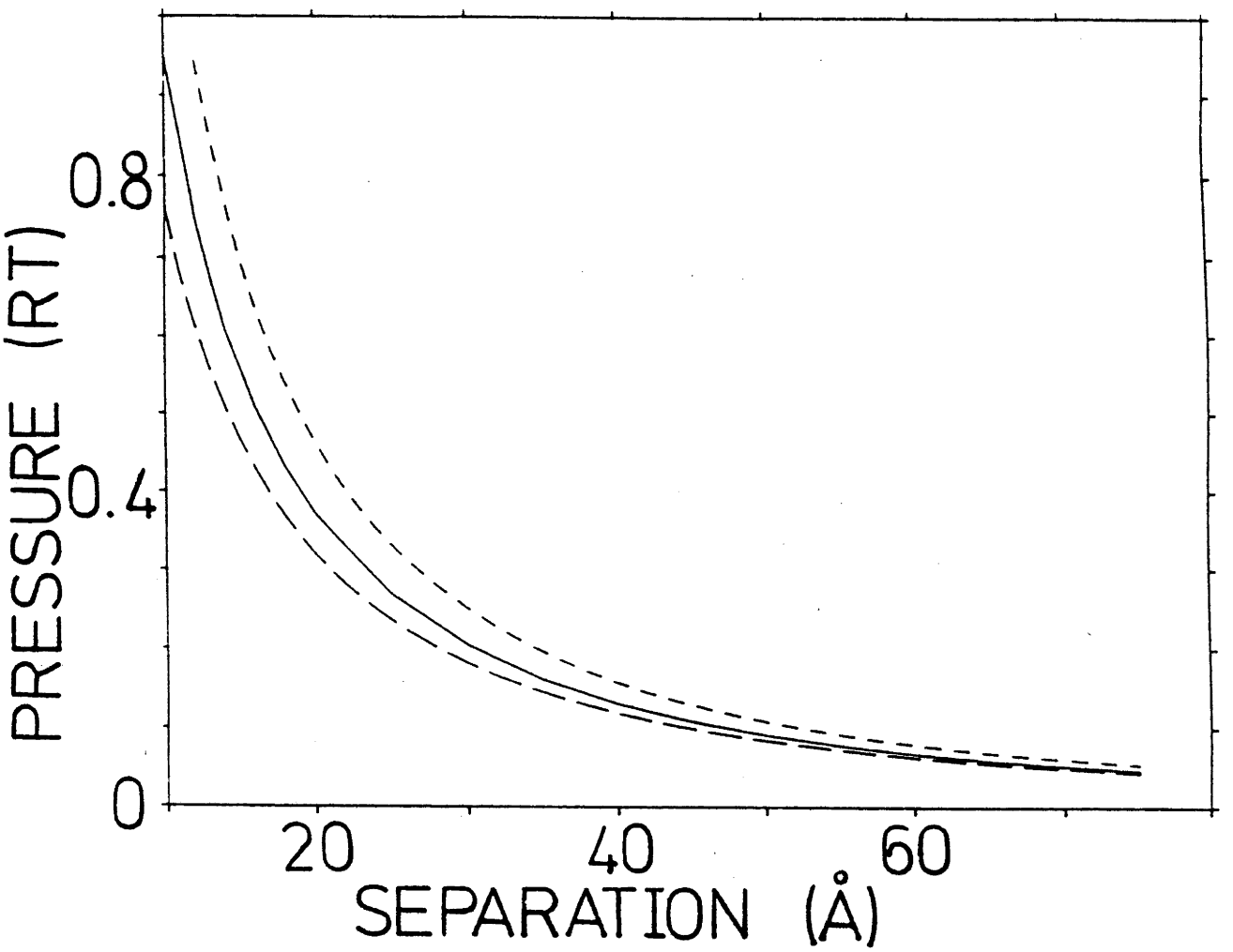

Figure 6.2 The pressure for monovalent counterions at a lower surface charge density (200Å^2 per unit charge) without images ($\varepsilon_1 = \varepsilon_2 = 80$). The various curves are as in fig. 6.1. The pressure is only slightly less repulsive than in the preceding figure, illustrating the weak dependence on surface charge at larger separations. The HNC calculations (and those in the remaining figures) were performed with the computer program of Kjellander and Marčelja.

will be discussed in §7.2. In denser systems the effect of hard cores[18] (e.g. monovalent ions with radius 2.3Å, for σ=0.224Cm^{-2} below about 50Å) conspire to make the pressure more repulsive. These short range effects become less important at larger separations[25].

Figure 6.3 shows the predicted pressures in the presence of dielectric discontinuities. The low dielectric region is placed behind the charged surfaces, as commonly occurs experimentally. Comparing those with fig. 6.2 one sees that the repulsion has now increased, a characteristic of image effects. A consequence of this is that the HNC pressure will lie closer to the PB prediction (which ignores both images and correlations). However, this is coincidental and for larger separations the EPB approximation does better. Note that the zero frequency Lifshitz attraction has been added to the HNC primitive model results. Figure 6.4 shows the effects of varying the dielectric parameters, and gives an indication of the sensitivity of experimental systems to image charge effects. The curves at the lower surface charge density indicate that as the images are turned off ($\Delta_{12}\rightarrow 0$) or as the Stern layer thickness increases, the predicted pressure decreases as it approaches the case without images. The effects of images are obviously relatively more important at low surface charges and close separations. Indeed, at 1000Å^2 per surface charge (σ=0.0160 Cm^{-2}), one sees that EPB predicts a larger repulsion than the PB theory. In an attractive regime, although the present theory is not then quantitatively accurate, the images can enhance the correlations, as has been found by HNC calculations[16].

The PB theory will be valid in experimental systems which are not too highly coupled. To be more precise, note that, for point ions in the one component double layer without images, one can characterise the system by the dimensionless parameters[24]

$$\chi = \frac{4\pi q^2}{k_B T \varepsilon_1}\,\frac{2}{h} \qquad \xi = \frac{-16\pi q^3}{(k_B T \varepsilon_1)^2}\,\sigma \qquad (6.3.1)$$

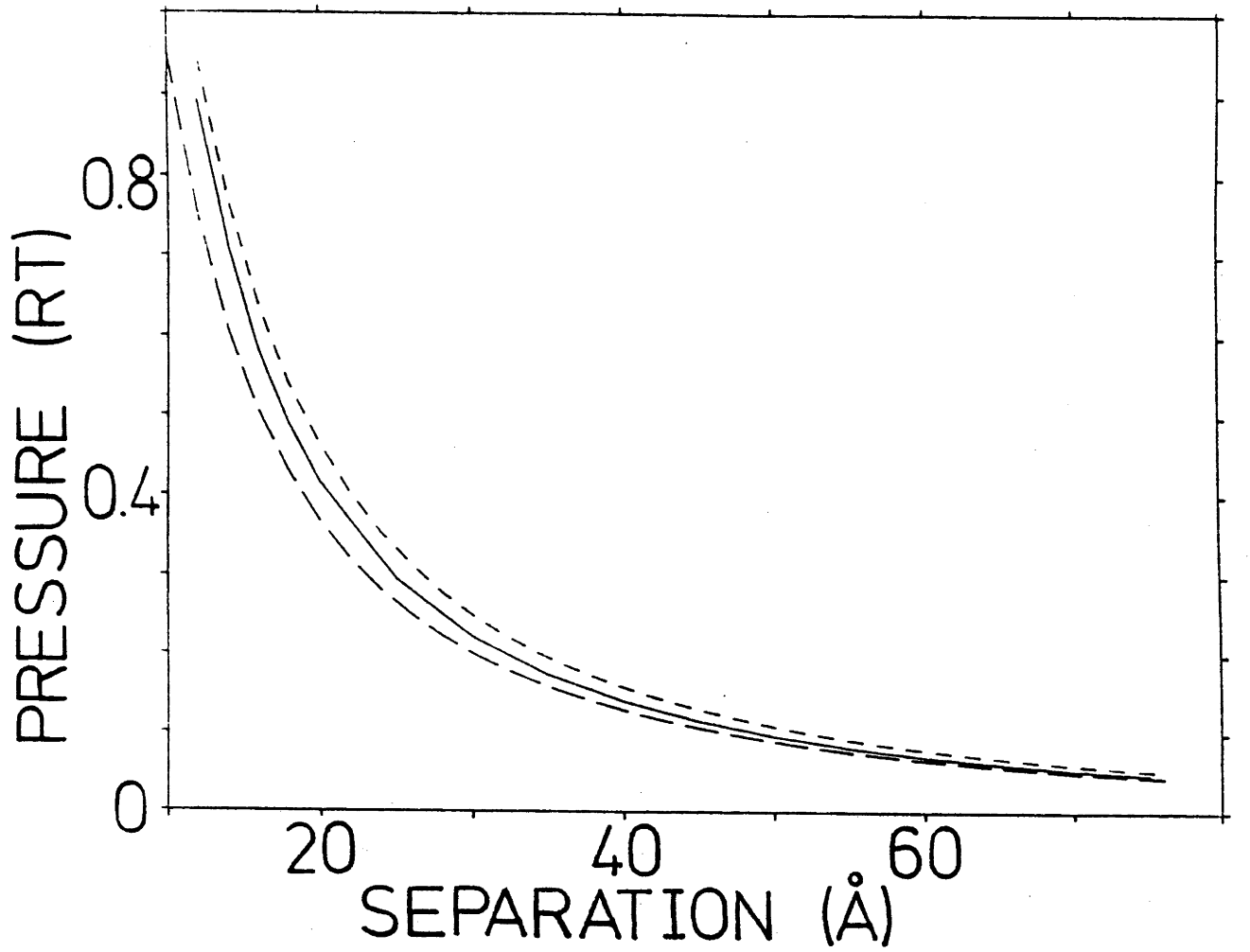

Figure 6.3 Images (ε_1=80, ε_2=2, w=1Å) here increase the repulsion, pushing the HNC (———) and the present theory (— — — —) closer to the mean field Poisson-Boltzmann (- - - -) which ignores images and correlations. The width of the intervening dielectric ε_1 is d=h+2w, 2Å greater than indicated by the ordinate. The area per surface charge is again 200Å^2 .

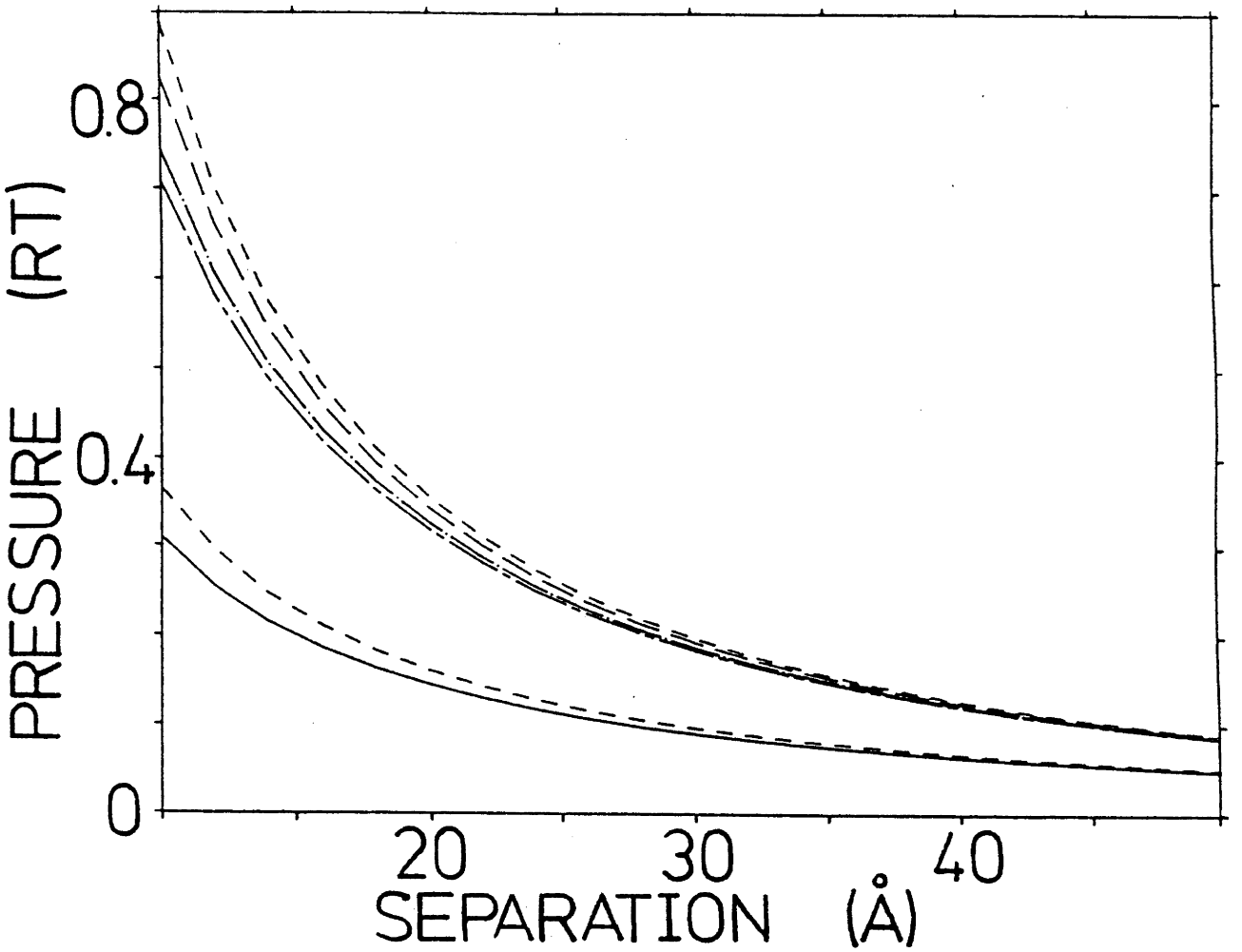

Figure 6.4 The effects of images on the pressure predicted by EPB. The upper curves are for an area per charge of 100Å^2, with ε_1=80, ε_2=2 and w=1Å (- - - - -) showing the largest image charge effects. Turning down the images (ε_1=80, ε_2=20, w=1Å; — — — —) or making the Stern layer larger (ε_1=80, ε_2=2, w=3Å; — · — · — · —) causes the curves to approach that for the system without images (ε_1= ε_2=80; — - — - — - —). At a lower surface charge density (1000Å^2), images become relatively more important (ε_1=80, ε_2=2, w=1Å; - - - - -) , and the predicted repulsion is now larger than the mean field Poisson-Boltzmann (———).

Apart from a trivial factor, the partition function is completely specified by a coordinate in the χ–ξ plane. Higher values of these parameters correspond to increased coupling in the system and it is here that one expects the PB and EPB approximations to break down. This is borne out by fig. 6.5 where the the accuracy EPB expressions is given, as obtained by comparison with HNC calculations. Points lying beyond the outer hyperbola are accurate to better than 10%. The inner curve indicates the limit within which the EPB results are less than half those calculated by the HNC method. Note that for high surface charges there is always a separation beyond which EPB is a good approximation. Similarly, one can find separations and surface charges where the theory will describe the divalent ion situation quite accurately.

For given parameters which specify an experiment, fig. 6.5 allows a quantitative estimate of the accuracy of the theory one fits to the data. Depending on the error one is willing to tolerate, the conclusions drawn from the fitted theory (eg the degree of ion binding or dissociation) may now be treated with a known confidence. The error predictions that result by considering the discrepancy between PB and EPB may be useful more generally. In a practical situation one often wishes to establish the acceptability of the simple PB theory. To do so via the HNC or MC methods requires inordinately lengthy computation for each and every case. By contrast the EPB results are easy to obtain. Since they overestimate deviations from PB due to correlation effects, EPB provides immediate strong bounds on the error.

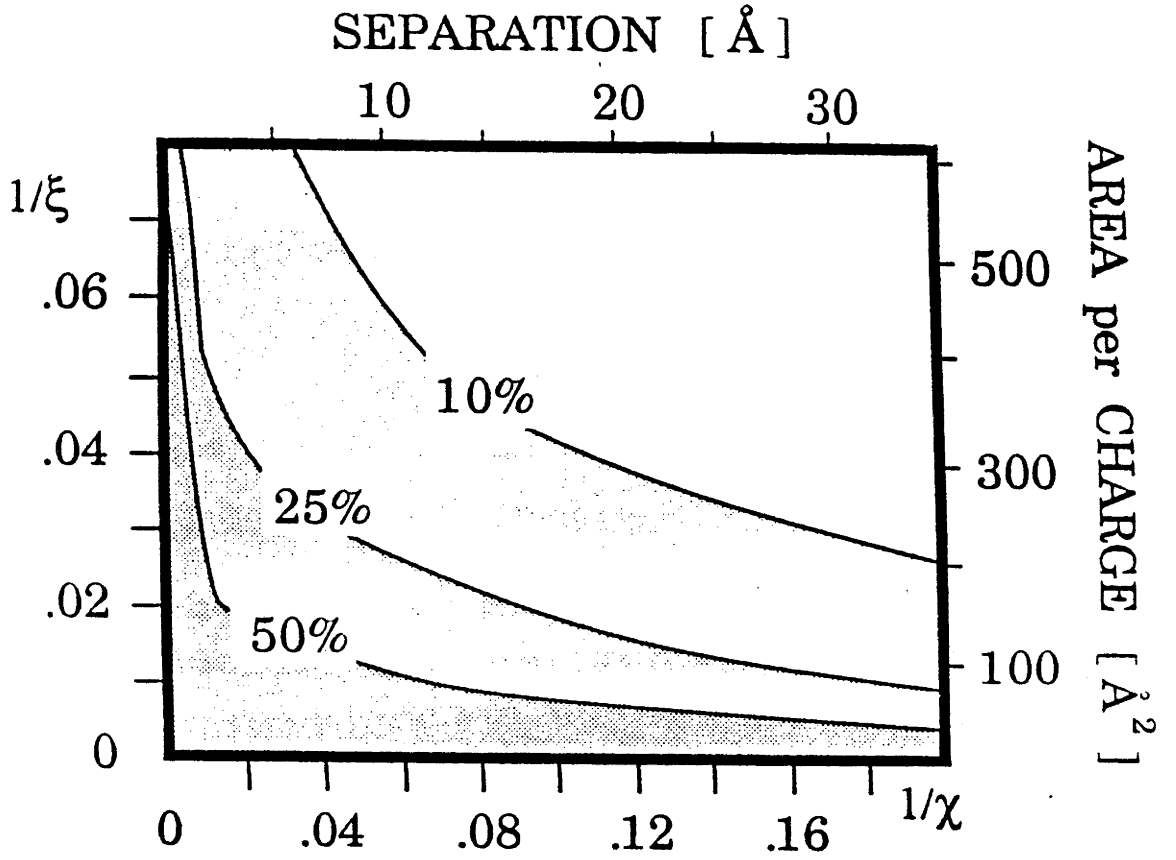

Figure 6.5 The region of validity of EPB approximation as a description of the primitive model for the one component double layer without images. The major axes are the reciprocal of the two dimensionless parameters $\chi=8\pi q^2/(k_B T \varepsilon_1 h)$ and $\zeta=-16\pi q^3\sigma/(\varepsilon_1 k_B T)^2$ which characterise the system. Lower values of these parameters correspond to lower coupling and this is where EPB is valid. Beyond the outer hyperbola the theory is accurate to better than 10%. The inner hyperbola delimits the region within which predicted pressure is less than half the actual pressure in the primitive model. The minor axes (included only for convenience) show the equivalent separation and area per surface charge for monovalent counterions at T=300K and $\varepsilon_1=80$.

Chapter 7 Symmetric electrolyte

7.1 Poisson-Boltzmann theory

7.1A Electrolyte profile

The Poisson-Boltzmann (PB) equation for the mean potential between two charged planar surfaces for the case of a symmetric electrolyte (ions with charge ±q) in equilibrium with a bulk of concentration ρ_∞ is[1,26]

$$\frac{d^2\psi(z)}{dz^2} = \frac{-4\pi q\rho_\infty}{\varepsilon} \left(\exp(-\beta q\psi(z)) - \exp(\beta q\psi(z)) \right) \qquad (7.1.1)$$

Defining the bulk Debye screening length through

$$\kappa_\infty^2 \equiv \frac{8\pi\beta q^2\rho_\infty}{\varepsilon} \qquad (7.1.2)$$

and introducing a non-dimensional length and potential

$$\xi \equiv \kappa_\infty z, \quad y(\xi) \equiv \beta q\psi(z) \qquad (7.1.3)$$

the PB equation becomes

$$\frac{d^2y}{d\xi^2} = \sinh(y) \qquad (7.1.4)$$

Here $\beta=1/k_BT$ is the inverse temperature and q is the coion charge (ie $y\geq 0$).

Let y_0 be the midpoint potential. The first quadrature then yields

$$\frac{dy}{d\xi} = 2\sqrt{\sinh^2(y/2) - \sinh^2(y_0/2)} \qquad (7.1.5)$$

The further change of variables

$$u(\xi) \equiv \sinh(y(\xi)/2) \qquad (7.1.6)$$

allows Eq. (7.1.5) to be rewritten

$$\frac{du}{d\xi} = \sqrt{(u^2-u_0^2)(1+u^2)} \qquad (7.1.7)$$

with solution[27] (AS17.4.49) (equations from ref. 27 are denoted by 'AS')

$$\xi = \int_{u_0}^{u} \frac{dt}{\sqrt{(t^2-u_0^2)(1+t^2)}} = \frac{1}{\sqrt{1+u_0^2}}\, nc^{-1}\left(\frac{u}{u_0}\middle|\frac{1}{1+u_0^2}\right) \qquad (7.1.8)$$

or

$$u \equiv \sinh(y/2) = \sinh(y_0/2)\, nc\left(\frac{\kappa_\infty z}{m^{1/2}}\middle| m\right) \qquad (7.1.9)$$

where the parameter m of the Jacobian elliptic function is

$$m = 1/\cosh^2(y_0/2) \qquad (7.1.10)$$

The midpoint potential y_0 and the parameter m are determined by the Gaussian boundary condition. With σ the surface charge and h the separation, this is

$$\frac{4\pi\beta q\sigma}{\varepsilon\kappa_\infty} \equiv s = 2\sqrt{\frac{m_1}{m}}\; sc\left(\frac{\kappa_\infty h}{2m^{1/2}}\middle| m\right) \qquad (7.1.11)$$

where m_1=1-m is the complementary parameter. The relevant solution to this transcendental equation is chosen through the requirement that the argument be positive and less than the quarter period.

The expression for the mean-field PB profile, which will later be required, is

$$\kappa^2(z) \equiv \kappa_\infty^2 \cosh(y) = \kappa_\infty^2 \left\{1 + 2\frac{m_1}{m}\, nc^2\left(\frac{\kappa_\infty z}{m^{1/2}}\middle| m\right)\right\} \qquad (7.1.12)$$

These equations, (7.1.9 - 11), represent the solution to the Poisson-Boltzmann equation for a symmetric electrolyte. Although equivalent to the usual solutions[1,26], the above forms are more convenient for the present purpose.

7.1B Free Energy and Pressure

Within the PB theory, the net pressure between the surfaces is given by the midpoint concentration less the bulk ($P^{PB}_{net} = P^{PB}_{tot} - P^{id}_{bulk}$) and this is

$$P^{PB}_{net} = k_B T (\rho_+(0) + \rho_-(0) - 2\rho_\infty) = 4 k_B T \rho_\infty m_1 / m \qquad (7.1.13)$$

The free energy per unit area for a planar system symmetric about the midplane is given by Eq. (6.1.5), or

$$\Omega^{PB} = h P^{PB}_{tot} - 2k_B T (\Gamma_+ + \Gamma_-) + 2 \sigma \psi(h/2) \qquad (7.1.14)$$

where $\psi(h/2)$ follows from Eq. (7.1.9). Note that this expression includes the chemical potential (which in this mean field theory is just that of an ideal gas) and the direct interaction between the charged planes (a zero body term). The total number of ions (per unit area) in the double layer is

$$\Gamma_+ + \Gamma_- = (\rho_\infty/\kappa_\infty^2) \int_{-h/2}^{h/2} \kappa^2(z)\, dz = 2\rho_\infty h + \frac{8 \rho_\infty m_1}{\kappa_\infty m^{1/2}} Nc\left(\frac{\kappa_\infty h}{2m^{1/2}} \middle| m \right)$$

$$= \frac{4\rho_\infty h E_1}{m K_1} - 2\rho_\infty h - \frac{8 \rho_\infty}{\kappa_\infty m^{1/2}} i Z\left(\frac{i\kappa_\infty h}{2m^{1/2}} \middle| m_1 \right) \qquad (7.1.15)$$

as follows from Eqs (AS16.25.1, AS16.26.8, AS17.4.28, AS17.4.36, and AS17.3.13). Here $K_1=K(m_1)$, $E_1=E(K_1)$ are the complete elliptic integrals of the first and second kinds (defined in AS§17.3; iK_1 is also called the imaginary quarter period) and the Jacobi Zeta function (defined in AS§16.34) has an imaginary argument and complementary parameter.

One method of measuring double layer forces accurately is with a surface forces balance[28-30] in which the measured force between two crossed cylinders is related to the interaction free energy per unit area between two planes (via the Derjaguin approximation). The analytic expression for the PB free energy, Eq. (7.1.14), with the bulk and surface contributions subtracted (cf Eqs (7.1.19) below) is more convenient for comparison of experiment with theory than the cumbersome method of numerically integrating the pressure from infinite separation[31].

7.1C Asymptotic results

As the separation h between the charged surfaces goes to infinity, the midpoint potential goes to zero. Using the Gaussian boundary condition Eq. (7.1.11), explicit calculation (relegated to the Appendix), yields the expansion

$$y_0 \sim A e^{-\gamma/2} + B e^{-3\gamma/2} + O(e^{-5\gamma/2}) \qquad (7.1.16)$$

where $\gamma \equiv \kappa_\infty h \to \infty$ and the coefficients are given by

$$A = \frac{16}{s}\left(-1+\sqrt{1+s^2/4}\right) \sim 2s, \; s\to 0 \qquad (7.1.17a)$$

$$B = A\left[1-\frac{\gamma A^2}{32}-\frac{A^2}{4096}\right] - \frac{A^3}{48}\left[\frac{5-sA/16}{1+sA/16}\right] \qquad (7.1.17b)$$

with s defined in Eq. (7.1.11). Hence the net pressure has the form

$$P_{nett}^{PB} \sim 2\rho_\infty k_B T\left(\frac{A^2}{2}e^{-\gamma} + (AB+A^4/16)\,e^{-2\gamma} + O(e^{-3\gamma})\right) \qquad (7.1.18)$$

In the asymptotic regime the pressure decays exponentially, with a decay length given by the Debye screening parameter, κ_∞. Note that the leading term can be derived by the usual overlapping double layer approximation in non-linear Poisson-Boltzmann theory. In the limit of small surface charge ($s\to 0$, cf. Eq. (7.1.17a)), this first term reduces to that given by the linear PB theory.

The successive terms in the large separation expansion for the free energy yield the bulk, surface and interaction free energies (per unit area). These are

$$\Omega_{bulk}^{id} = -2k_B T \rho_\infty h \qquad (7.1.19a)$$

$$2\Omega_{surface}^{PB} = 2\sigma\Psi_s(\infty) - k_B T sA\rho_\infty/\kappa_\infty \qquad (7.1.19b)$$

$$\Omega_{int}^{PB} \sim \frac{\rho_\infty k_B T}{\kappa_\infty}\left[A^2 e^{-\gamma} + (AB+A^4/16)\,e^{-2\gamma} + O(e^{-3\gamma})\right] \qquad (7.1.19c)$$

where the surface potential at infinite separation is

$$\beta q \psi_s(\infty) = 2\ln\left[s/2+\sqrt{1+s^2/4}\right] \qquad (7.1.20)$$

Thus for large separations the PB interaction free energy also shows

exponential decay, with decay length κ_{∞} , and with a coefficient which depends on the surface charge.

7.2 Extended Poisson Boltzmann

7.2A The Lamé equation

The extended Poisson-Boltzmann (EPB) theory applies the Debye-Hückel theory of a bulk electrolyte to the electric double layer. By solving the inhomogeneous Ornstein-Zernike equation with Debye-Hückel closure, EPB expresses the correlation free energy (which includes effects due to dielectric images and ionic fluctuations) as an integral over Fourier space of a secular determinant giving the allowed electrostatic modes which satisfy the boundary conditions of the planar geometry (fig. 5.1). What is required is the solution of a second order differential equation (5.3.13, λ=1):

$$f''(z) - (k^2 + \kappa^2(z)) f(z) = 0 \qquad (7.2.1)$$

Since the expression for the free energy is optimised with respect to the profile, an approximate form for the profile is sufficient; it is not neccessary to determine this quantity self-consistently. The extended Poisson-Boltzmann theory consists in taking the profile to be given by the mean field PB equation. This choice allows explicit solution of the differential equation and an analytic form for the free energy. Thus EPB is really a perturbation about, or a correction to mean field Poisson-Boltzmann theory.

For the problem of the symmetric electrolyte between two planar surfaces, here one uses the PB profile given by Eq. (7.1.12) and proceeds as follows. Invoke the Jacobi imaginary transformation, and so rewrite the differential equation (7.2.1) as

$$\frac{d^2 f(\alpha)}{d\alpha^2} = \{ 2m_1 \, sn^2(\alpha \,|\, m_1) - m[1 + k^2/\kappa_\infty^2 + 2m_1/m] \} f(\alpha) \qquad (7.2.2)$$

where $\alpha = i\xi/m^{1/2} = i\kappa_\infty z/m^{1/2}$. Now this is the Lamé equation of order 1. The solution of Hermite (see §23.71 of ref. 32 and also ref. 13) is

$$f(\alpha) = \frac{H(\alpha+\alpha_1|m_1)}{\Theta(\alpha|m_1)} \exp\{-\alpha Z(\alpha_1|m_1)\} \qquad (7.2.3)$$

where α_1 is given by $sn^2(\alpha_1 \,|\, m_1) = -mk^2/(m_1 \kappa_\infty^2)$ or, using Eq. (AS17.4.44),

$$\alpha_1 = i\int_0^{km^{1/2}/\kappa_\infty} \frac{dt}{\sqrt{(1+t^2)(m_1+t^2)}} \qquad (7.2.4)$$

The arguments of the Jacobi Eta (H), Theta (Θ) and Zeta (Z) functions are pure imaginary (see AS§§16.31, 16.34 for their definitions). In Chapter 5 the secular determinant was given in terms of the even and odd solutions to the differential equation, normalised at z=0. It turns out to be simpler to rewrite the secular determinant in terms of the general solution (provided this is neither even nor odd). The determinant then becomes

$$\mathfrak{D}_1(k) = \frac{1}{4f(0)f'(0)}\left\{ [\delta_+ f'(h/2) + k\delta_- f(h/2)]^2 - [\delta_+ f'(-h/2) - k\delta_- f(-h/2)]^2 \right\} \qquad (7.2.5)$$

where

$$\delta_\pm \equiv 1 \pm \Delta_{12} e^{-2kw} \qquad (7.2.6)$$

The dielectric disparity is given by $\Delta_{12} = (\varepsilon_1 - \varepsilon_2)/(\varepsilon_1 + \varepsilon_2)$ and w is the width of the zeroth order Stern layer (cf. fig. 5.1). The primes above denote differentiation with respect to z. Explicitly, from Eq. (7.2.3), one has

$$f(\pm h/2) = \frac{\pm H(\alpha \pm \alpha_1 | m_1)}{\Theta(\alpha|m_1)} \exp\{\mp \alpha\, Z(\alpha_1|m_1)\} \qquad (7.2.7a)$$

$$f'(\pm h/2) = \frac{\pm i\kappa_\infty f(\pm h/2)}{m^{1/2}}\left\{ \frac{H'(\alpha \pm \alpha_1|m_1)}{H(\alpha \pm \alpha_1|m_1)} - Z(\alpha|m_1) \mp Z(\alpha_1|m_1) \right\} \qquad (7.2.7b)$$

$$f(0) = \frac{H(\alpha_1|m_1)}{\Theta(0|m_1)}, \quad f'(0) = \frac{i\kappa_\infty f(0)}{m^{1/2}}\left\{ \frac{H'(\alpha_1|m_1)}{H(\alpha_1|m_1)} - Z(\alpha_1|m_1) \right\} \qquad (7.2.7c)$$

On the right hand side of Eqs (7.2.7b,c) where the logarithmic derivative of the Eta function occurs, the prime denotes differentiation with respect to the argument α_1. Here now $\alpha = i\kappa_\infty h/(2m^{1/2})$ and α_1 is given by Eq. (7.2.4).

The secular determinant is now fully defined and hence the correlation free energy (cf Eq. 5.3.20) per unit area is

$$\mathfrak{F}^{corr} = \frac{k_B T}{8\pi^2}\int dk \left\{ \ln[e^{-kh}\mathfrak{D}_1(k)/k] - \frac{2\pi\beta q^2}{\varepsilon_1 k}(\Gamma_+ + \Gamma_-) \right\} \qquad (7.2.8)$$

with $d\mathbf{k}\equiv 2\pi k dk$. Note that here has been added on the Lifshitz zero frequency interaction term andhence the artificial repulsion (which always appears in primitive model analyses) has been cancelled. The factor e^{-kh}/k comes from the remaining part of $\mathfrak{D}_0(k)$, the secular determinant for $\lambda=0$. The self-image interaction is included in $\mathfrak{D}_1(k)$ and gives a finite contribution to the free energy so long as the width of the Stern layer, w, remains non-zero. The last term in Eq. (7.2.8) is the direct Coulombic self-interaction which cancels a divergent contribution in the logarithm of $\mathfrak{D}_1(k)$.

One of the causes of the divergence in the work of Barouch, Perram, and Smith[13] is that these authors had no Stern layer, and hence the self-image potential of the ions at the surface is infinite. The other reason for the divergence in their theory is that the (spurious) direct Coulombic self-interaction remains in their expressions, since they have not subtracted it explicitly as is done automatically in the present theory. Since the number of ions in the double layer (and also the contact density) changes with separation, these infinite terms give divergences in the pressure. On the other hand, while Ninham and Parsegian[9,10] have also neglected these points, the infinities there only contribute to the surface and bulk free energies (because they use a constant bulk profile for their uncharged surface problem). Hence the pressure found by these authors can be shown to agree with the pressure predicted by EPB for the same problem, when the width of the Stern layer is set to zero in the EPB theory.

Now the free energy per unit area of the double layer is

$$\Omega^{EPB} = \Omega^{PB} + \mathfrak{F}^{corr} - (\Gamma_+ + \Gamma_-)\mu_{ni}^{DH} \qquad (7.2.9)$$

Note that the PB free energy, Eq. (7.1.14), contains the ideal part of the chemical potential and the direct interaction between the charged surfaces. The rest of the zero body interaction term (the zero-frequency Lifshitz term) has been included in $\mathfrak{F}^{corr}$ and there remains the non-ideal part of the chemical potential. In the Debye-Hückel theory this is given by

$$\mu_{hi}^{DH} = \frac{-k_B T \kappa_\infty^3}{16\pi\rho_\infty} \qquad (7.2.10)$$

The final answer is given by Eq. (7.2.9). The total pressure follows by numerical differentiation; to obtain the net pressure, subtract the bulk pressure as given by Debye-Hückel theory.

7.2B Computational techniques

Before discussing explicit results, it seems appropriate to make some remarks on numerical methods. The most convenient way to evaluate the Eta, Theta and Zeta functions which occur implicitly in the integrand of Eq. (7.2.8) is by their theta function expressions (AS§§16.31, 16.34). This method is also suitable for determining the midpoint potential y_0 and the parameter m of the PB theory, Eq. (7.1.11). The theta functions can be computed via the rapidly convergent expansions in the nome q (AS§16.27). In practice one usually requires at most five terms in the rapid q expansions. The value of the nome q is determined from the parameter via the expansion (see §21.8 of ref. 32)

$$q = \varepsilon + 2\varepsilon^5 + 13\varepsilon^9 + 150\varepsilon^{13} + O(\varepsilon^{17}) \quad , \quad \varepsilon \equiv \frac{1}{2}\frac{1-m_1^{1/4}}{1+m_1^{1/4}} \qquad (7.2.11)$$

It is the complementary nome, $\ln q_1 = \pi^2 / \ln q$, which is required for the evaluation of the elliptic functions (7.2.7). The series may be differentiated term by term as required (this is actually a better way of evaluating the Zeta function than Eq. (AS17.4.38)).

It can be shown that the integrand in Eq. (7.2.8) behaves as $k^{-3}dk$ for large k, and hence the integral converges. However, this analytic result follows after cancellation of the first several terms of the large k asymptotic expansion of the individual functions. This creates special difficulties in the evaluation of the integral since roundoff can mask the requisite exact

cancellation; library quadrature routines perceive the integral as divergent. A solution is to choose a large but finite cutoff for the integral, using the exact analytic forms for the elliptic functions of the integrand. The asymptotic tail can then be integrated (either analytically or numerically). The leading non-zero term in the integrand of Eq. (7.2.8) is

$$\frac{dk\,\kappa_\infty^3}{m^{3/2}k^3}\left[\left(\frac{\Theta''(\alpha)}{2\Theta(\alpha)}+\frac{1+m_1}{3}\right)i\,Z(\alpha)-\frac{i}{3}Z^3(\alpha)-\frac{i\Theta'''(\alpha)}{6\Theta(\alpha)}\right.$$

$$\left.+\frac{\kappa_\infty h}{m^{1/2}}\left(\frac{1+2m_1-3m_1^2}{24}-\frac{1+m_1}{6}\frac{E_1}{K_1}\right)\right]\ ,\quad k\to\infty \qquad (7.2.12)$$

where the argument of the elliptic functions is still $\alpha=i\kappa_\infty h/(2m^{1/2})$. Their parameter is m_1, and the primes denote differentiation by α. The value of the integral is insensitive to the choice for the cutoff.

The complementary parameter has been used above, since this is the one which goes to zero for large separations. For small separations it is preferable to work with the conjugate of Eq. (7.2.3) and, apart from immaterial constants, this is

$$f(z) = \frac{H(\beta+\beta_1|m)}{H_1(\beta|m)}\exp\left\{-\beta\frac{H_1'(\beta_1|m)}{H_1(\beta_1|m)}\right\} \qquad (7.2.13)$$

Here the arguments are real ($i\beta\equiv\alpha$, $i\beta_1\equiv\alpha_1$), the new Eta function H_1 is given by Eq. (AS16.31.4), and the prime denotes differentiation by β. The analogues of Eqs (7.2.7) follow. In practice the regimes of validity of the two solutions overlap, and it is not really necessary to implement Eq. (7.2.13).

In some cases the pressure will be of more interest than the free energy. Numerical differentiation of the free energy is quite stable and a suitable formula is

$$g'(x) \approx \frac{g(x-2\Delta)-8g(x-\Delta)+8g(x+\Delta)-g(x+2\Delta)}{12\Delta} \qquad (7.2.14)$$

with $\Delta/x \approx 0.01$.

7.2C Surface free energy

The extended Poisson-Boltzmann expression for the grand potential (7.2.9) contains bulk and surface as well as interaction terms. For comparison with some experimental data, it is the latter which is of most interest; in this case the expressions given here allow the two other contributions to be subtracted, leaving only the interaction free energy. In this Debye-Hückel level of theory the bulk free energy per unit area is well known, namely,

$$\Omega_{bulk}^{DH} = -2k_B T \rho_\infty h + \frac{k_B T h}{24\pi} \kappa_\infty^3 \qquad (7.2.15)$$

The ideal part of this would normally be associated with the PB expressions (7.1.14, 7.1.19); the remainder should be subtracted from the correlation free energy (7.2.8).

The surface free energy per unit area may be derived from the asymptotic expansion (see the appendix). The result (for two surfaces) is

$$2\Omega_{surface}^{EPB} = 2\Omega_{surface}^{PB} - 4(z-1)\rho_\infty \mu_{ni}^{DH} / \kappa_\infty +$$

$$\frac{k_B T \kappa_\infty^2}{4\pi} \int_0^\infty \left\{ \ln\left[\frac{x(y+z)^2}{y(y+1)^2}\right] + 2\frac{1-z}{x} + 2\ln\left[1 + \frac{\delta_+}{2x}\left(y - x + \frac{z^2-1}{y+z}\right)\right] \right\} x\, dx \qquad (7.2.16)$$

where

$$x \equiv k/\kappa_\infty \;,\quad y \equiv \sqrt{1+x^2} \;,\quad z \equiv \sqrt{1+s^2/4} \qquad (7.2.17)$$

and the surface parameter s is defined in Eq. (7.1.11). Note that if one requires the interfacial tension, one should subtract from this a bulk free energy term corresponding to the negative adsorption excess of ions from the Stern layers (e.g. Eq. (7.2.15) with h replaced by 2w). For the case of zero surface charge (s=0, z=1), the surface free energy per unit area corresponds directly to the interfacial tension. In order to obtain this quantity in the more general case of non-zero charge, one should differentiate the above taking into account the area dependence of the surface charge.

Equation (7.2.16) represents more than just a generalisation of the

Onsager-Samaras result[33] to the case of a charged interface.In the small κ_∞ limit of Eq. (7.2.16) one obtains

$$\Omega_{surface}^{EPB} \sim \frac{k_B T (1-2z^2) \Delta_{12}}{8\pi} \kappa_\infty^2 \ln \kappa_\infty a + O(\kappa_\infty^2) \qquad (7.2.18)$$

where a has the dimensions of length (in fact, a=2w here) and does not contribute to the leading order. Now for zero surface charge (s=0, z=1) this is the Onsager-Samaras result, which gives the change in free energy (or surface tension increment) of an uncharged interface upon addition of electrolyte. It arises from the repulsion of the ions from the interface by their dielectric images, is valid in the limit of infinite dilution, and behaves as $\rho_\infty \ln \rho_\infty$. However, in the opposite large κ_∞ limit, one finds that the images are screened, and the leading order is given by the image free case ($\Delta_{12}=0$, $\delta_+=1$). Then the integral in Eq. (7.2.16) may be done giving

$$I = \frac{1+2\ln 2}{4} - \frac{z^3-z^2+1/2}{2z^2-1} - \frac{z^2(z^2-1)}{1+4z^2(z^2-1)} \left\{ 4z\sqrt{z^2-1}\, \tan^{-1}\sqrt{\frac{z-1}{z+1}} - \ln(2z+2z^2) \right\} \qquad (7.2.19)$$

In this image free case, which is also the large κ_∞ limit, one obtains twice the surface free energy by multiplying this by $k_B T \kappa_\infty^2/(4\pi)$ and adding to it the PB and chemical potential terms from Eq. (7.2.16) (and also subtracting 2w/h times the bulk free energy (7.2.15)). The interesting point about the large κ_∞ limit is that the surface free energy now scales linearly with concentration. Thus this Debye-Hückel theory, even in the absence of surface charge, predicts behaviour beyond the Onsager-Samaras limiting law. While caution should be exercised in applying the EPB for large couplings, one notes that experimental data[34-36] does become linear in ρ_∞ at higher concentrations.

7.2D Asymptotic interaction free energy

The EPB interaction free energy follows from Eq. (7.2.9) by subtracting the bulk (7.2.15) and surface (7.2.16) terms. The method of deriving the asymptotic expansion ($\gamma \equiv \kappa_\infty h \to \infty$) for the interaction free energy per unit

area is discussed in the Appendix. The result is

$$\Omega_{int}^{EPB} \sim \Omega_{int}^{PB} + \frac{2 k_B T \kappa_\infty^2 q_1}{\pi} \{ \ln 2 + \int_0^\infty \left(\frac{2 \delta_+ (1+2yz)}{y z [\delta_-(y+z) + \delta_+(y^2+yz+z^2-1)]} - \frac{2}{y^2} \right) x \, dx \} + O(e^{-2\gamma}) \quad (7.2.20)$$

where the complementary nome has the form Eq. (7.A.6)

$$q_1 \sim \frac{z-1}{z+1} e^{-\gamma} + O(e^{-2\gamma}) \quad (7.2.21)$$

The most important feature of this result is that images and correlations affect the free energy even in the asymptotic limit. That is, they decay with the same screening length (κ_∞) as does the elementary Poisson-Boltzmann prediction. One important consequence of this is that an experimental determination of the force between surfaces at large separations will have the PB form, but with a *different* coefficient. The measured coefficient does not correspond to the real surface charge but to an effective surface charge. This interpretation of measured PB parameters has been made previously[25] in HNC studies of the one component double layer. However, for that problem the pressure is independent of surface charge in the full asymptotic limit (see chapter 6). In contrast, for the pressure in the symmetric electrolyte double layer, one finds that the coefficient of the leading asymptotic term has a different dependence on surface charge than that given by simple PB theory.

This point deserves emphasis. For the symmetric electrolyte the EPB theory predicts that, in the asymptotic limit, the pressure shows PB-like behaviour but with a uniquely defined *effective* surface charge different to the actual surface charge. Physically the effect can be interpreted as due to a shift in the PB profile (note that even though the PB profile is input into the theory, a different profile is implied by the calculated free energy). For example correlations may allow more ions to crowd near the surface until, at some distance from the surface, the charge is sufficiently screened. From

then on the profile shows PB-like behaviour (ie an effective surface charge) as has been previously suggested for the one component double layer[25]. The relationship between the real surface charge (as given by EPB theory) and the fitted PB effective surface charge is discussed in §7.3.

For the special case without images ($\Delta_{12}=0$, $\delta_{\pm}=1$) the integral (7.2.20) may be done. Writing this as the ratio of the total net pressure ($P^{PB}+P^{corr}$) to the PB net pressure (P^{PB}, the leading term in Eq.(7.1.18)), one has

$$\frac{P^{PB}+P^{corr}}{P^{PB}} = 1 + \frac{\beta q^2 \kappa_\infty}{4\varepsilon}(\ln 2 + 2I) + O(e^{-\gamma}) \qquad (7.2.22)$$

where

$$I = \frac{1}{2}\left(1+\frac{2z^2-3}{(2z^2-1)^3}\right)\ln 2 + \frac{2-2z^3+z}{2z(2z^2-1)^2} - \frac{1}{2}\left(1-\frac{2z^2-3}{(2z^2-1)^3}\right)\ln(z+z^2)$$
$$- \frac{\sqrt{z^2-1}}{z}\left(1+\frac{2z^2+1}{(2z^2-1)^3}\right)\tan^{-1}\sqrt{\frac{z-1}{z+1}} \qquad (7.2.23)$$

Usually this ratio is less than unity, and can even be negative for large enough concentrations (κ_∞) and surface charge (s), although the EPB has only limited validity in this latter regime. A truly interesting limit is that of low surface charge ($s\to 0$, $z\to 1$), and then

$$I = 1/2 - \ln 2 \qquad (7.2.24)$$

Here the EPB predicts a pressure slightly larger than that given by PB, in a limit where one expects both theories to be valid. Including correlations can actually give a larger repulsion than the mean field theory alone, a counterintuitive result! This may be rationalised by considering an uncharged surface with bulk uniform profile. Since there is electrolyte on only one side of an ion at the surface, it sees its cloud of counterions and experiences a potential of mean force which repels it from the interface. Thus there is a depletion of the (bulk) profile near the surface. (This, in fact, causes the positive surface tension increment at high concentrations, cf Eq. (7.2.19), z=1 above). Now if a small charge is put on the interface, the double

layer is less able to screen the surface charge, at least in the vicinity of the surface, and a larger repulsion than that given by PB theory results. This effect would be further enhanced by images. Note that for the case of neutral surfaces with constant bulk profile[9-12] this same repulsion of the ions from between the surfaces leads to an attractive pressure. The HNC double layer calculations have not as yet been performed in regimes with low enough surface charge to see this predicted effect.

7.3 Numerical results

Accuracy tests of the extended Poisson-Boltzmann theory have already been given for the one component double layer (Chapter 6). The theory seems to work well in the large separation / low surface charge regime. The benchmark for the comparison was the anisotropic hypernetted chain (HNC) calculations of Kjellander and Marcelja. The HNC method is known to work well for bulk Coulomb systems[37-39]. The anisotropic version has also been favourably compared[16,18] to the limited simulation data for the one component[15] and symmetric electrolyte[40] double layers. For the present purpose one can take the HNC results to be the exact pressure for the primitive model, inhomogeneous double layer problem.

In fig. 7.1 is compared the pressures predicted by HNC, PB, and EPB for a 1:1, 2mM electrolyte at the fixed separation of 150Å (1.5 Debye lengths) as the area per surface charge is varied. It is clear that the EPB theory does substantially better than PB over the range exhibited, although at higher surface charges the theory will predict attractions rather sooner than HNC does (if at all). This deficiency will be addressed further below. As in the one component double layer, EPB here overestimates the correlation correction to PB, although this is no longer a general rule when electrolyte is present.

Figure 7.2 shows a similar comparison of the pressure at varying separations but at a fixed area per surface charge of 60Å^2 (0.267 Cm^{-2}). At smaller separations the EPB theory begins to noticably overestimate the correlation correction, and will turn attractive, whereas the HNC will continue toward the PB (from above or below, depending on the hard core radius). A non-linear closure, and/or one that includes a short range core repulsion (such as the HNC) gives finite correlation contributions to the pressure as the separation goes to zero. Hence the pressure (then, and it is believed, in reality) will be dominated by the kinetic (PB) repulsion which is diverging as h^{-1}. The unphysical behaviour of the EPB (which uses a linear closure) at high coupling is similar to that of the Debye-Hückel limiting law

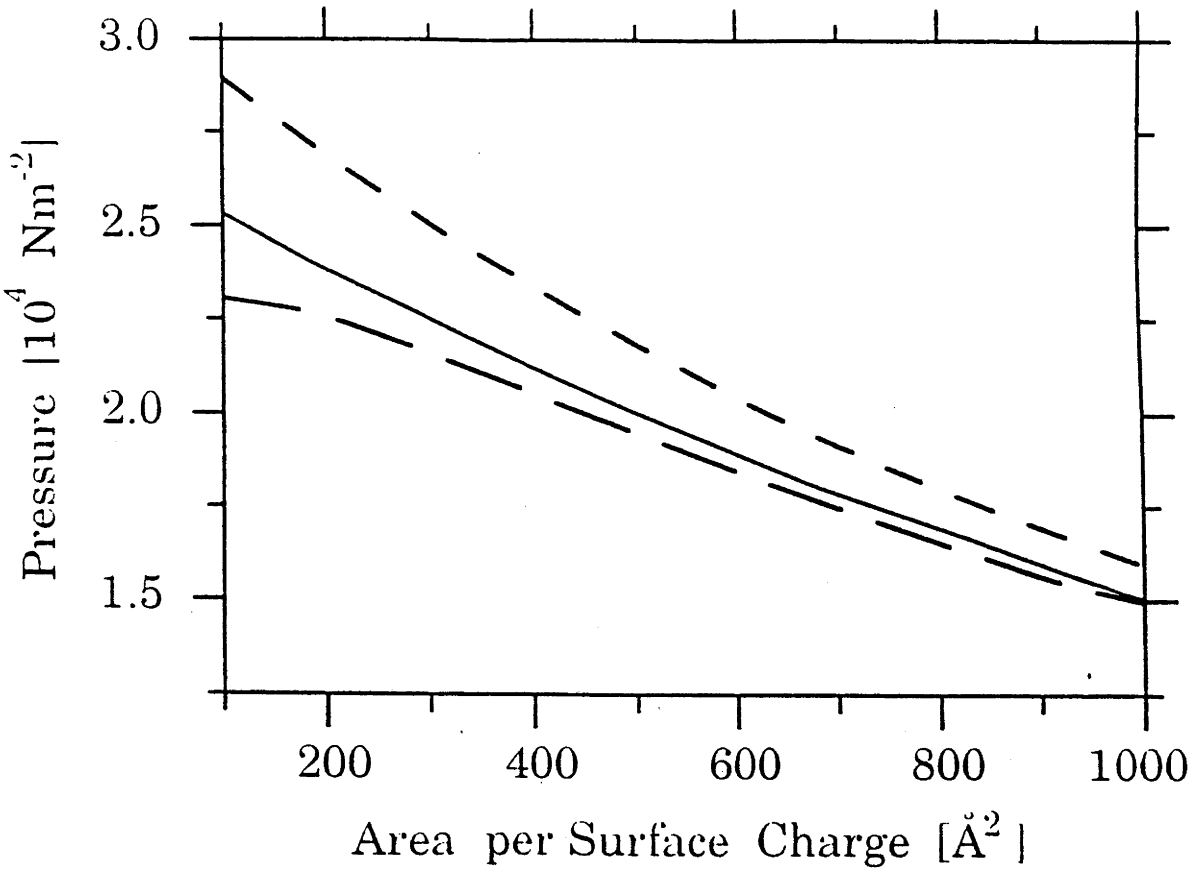

Figure 7.1 The double layer pressure for various areas per surface charge in a 2mM, 1:1 electrolyte at a separation of 150Å. The HNC (———) calculations (here and in fig. 7.2) are unpublished data of Kjellander and Marčelja. The EPB theory (— — — —) underestimates the repulsion but generally does better than the PB (– – – – –) result. The temperature is 298.15K, $\varepsilon_1=\varepsilon_2=78.358$, and the hard core diameter used in the HNC calculations is 4.25Å.

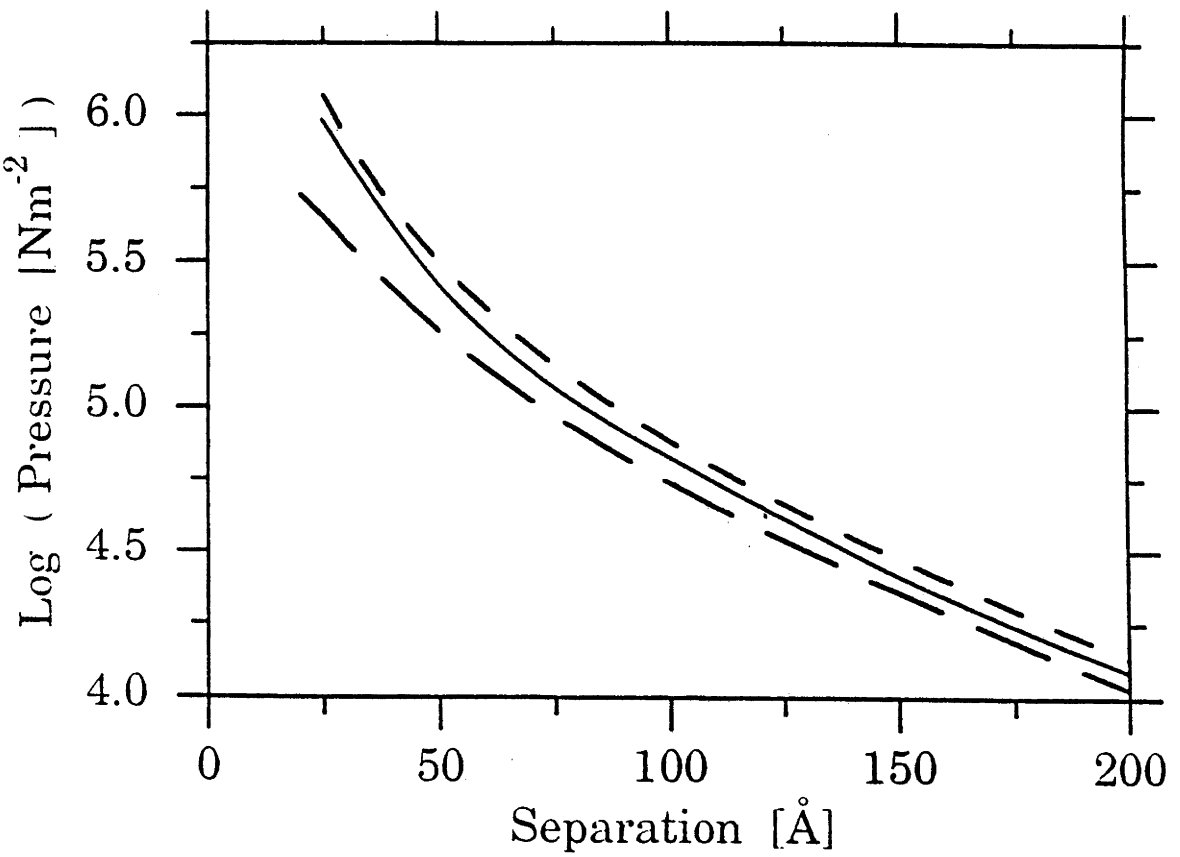

Figure 7.2 Pressure as a function of separation for the same case as in the preceding figure, but at a fixed area per surface charge of 60Å^2. HNC, EPB and PB curves are denoted as above.

for strong electrolytes which also becomes unphysical at high concentrations (predicting e.g. negative osmotic coefficients). Nevertheless just as the DHLL remains useful for the description of dilute bulk electrolytes, so does the EPB in describing double layers with low coupling.

One procedure for softening the artificial divergence in the Debye - Hückel correlations at small separations follows from recognizing its source. One can calculate the correlation part of the EPB free energy at a slightly larger (of the order of the molecular diameter) separation than one uses for the mean field terms. This non-zero separation increment then guarrantees the correct behaviour of the pressure at small separations and, in fact, also gives a potential minimum seen in experimental data[41].

From the comparison with HNC in fig. 7.2, one can see that the EPB does slightly better than PB at larger separations, but, unlike the one component double layer, the agreement no longer improves as the separation increases. For the symmetric electrolyte, EPB is not quantitatively exact asymptotically because of its inadequate treatment of near surface ionic correlations. The *form* for the interaction free energy (7.2.20) is correct. It shows that the double layer interaction appears PB-like but with a different surface charge. It is the correlations which alter the double layer profile near the surface and give a different coefficient to the asymptotic force law. EPB does not get the effects of the correlations precisely (nor the effects of hard cores) and so it cannot be an exact asymptotic theory. (In any case it is known that the Debye length is not the exact screening length of an electrolyte[42]). However for low enough coupling near the surface it appears an excellent approximation.

The above comparisons were made for a 2mM electrolyte, dilute enough so that Debye-Hückel type of theory should work. For higher concentrations the theory becomes less reliable, but ought still to do better than PB. An example is 0.1M 1:1 electrolyte, at 500Å^2 per surface charge and 50Å separation. Here the HNC predicts a pressure of 0.96, the EPB 1.09, and the

PB 1.20 (10^4 Nm^{-2}). Note that here the EPB lies above the HNC prediction, and, in fact, will eventually lie above the PB for low enough surface charge. Since this is a limit in which one expects EPB to be valid, it is plausable that this latter behaviour is indeed correct. Very recent HNC calculations (just on the limit of their accuracy) also show this qualitative behaviour.

Figures 7.3 and 7.4 may prove useful in analyzing experimental data which have previously been fitted to PB theory. They show (with and without the absence of images) the real surface charge which corresponds to the effective charge required to fit measured force data with the non-linear PB theory in the asymptotic regime. If the PB equation were exact, the curves would be a single straight line from the origin. While EPB (used to estimate the real surface charge) is not exact, one expects it to lie much closer to reality than the simple PB estimate of the surface charge. The figures may at first appear counterintuitive since the PB appears to work better at higher concentrations. However in both PB and EPB theory the surface is characterised by the parameter s Eq. (7.1.11) which depends on σ/κ_∞ . Hence for fixed surface charge, this parameter decreases as the electrolyte concentration is increased (the surface is more screened). This is reminiscent of the increasing validity of the linear PB (cf the non-linear theory) at high concentrations.

As an example of the use of the figures, consider the results of Israelachvili and Pashley[29] who measured the forces between mica surfaces in 0.1mM NaCl. They estimated the surface area per charge as 10 nm^2 by fitting to the non-linear Poisson-Boltzmann at large separations. However the real area given by EPB is about 7.5 nm^2. Including images in the model (ε_2=2,w=2Å) gives an area of 8 nm^2 which is still substantially more highly charged than estimated by those authors. It would appear that any binding constants estimated by force measurement fitted to PB must be treated with extreme caution.

One can also use figs 7.3 and 7.4 to work out the real surface charge if

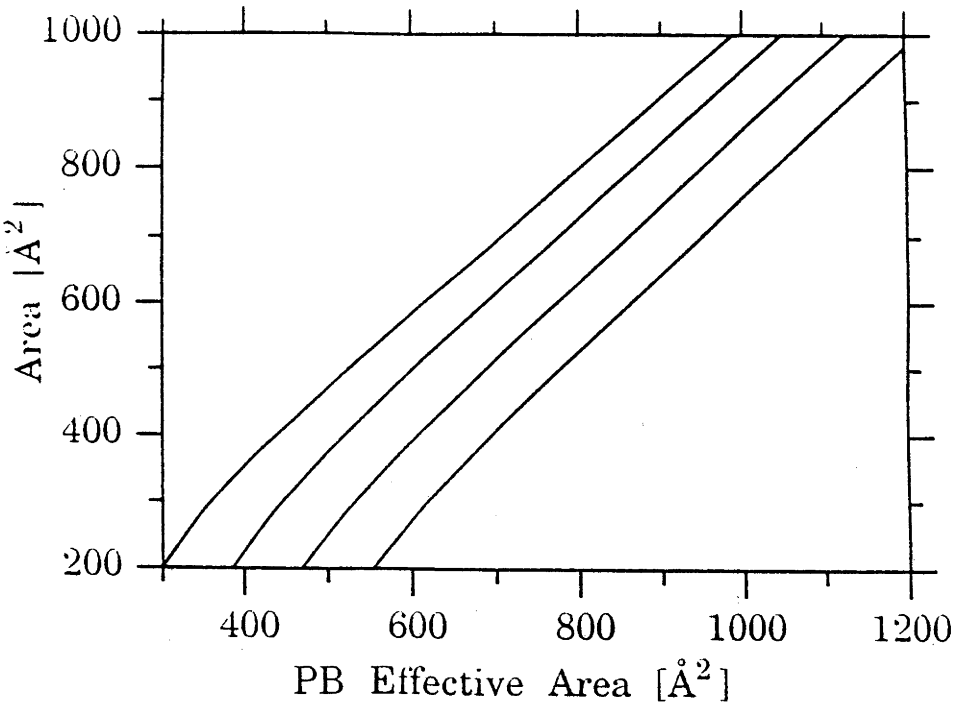

Figure 7.3 The actual areas per surface charge (given by the EPB theory) which correspond to the efffective area fitted to the non-linear PB equation for measured force data in the asymptotic regime. The curves are for monovalent electrolyte at concentrations of, from left to right, 100, 10, 1, and 0.1 mM. The temperature is 300K and $\varepsilon_1=\varepsilon_2=80$.

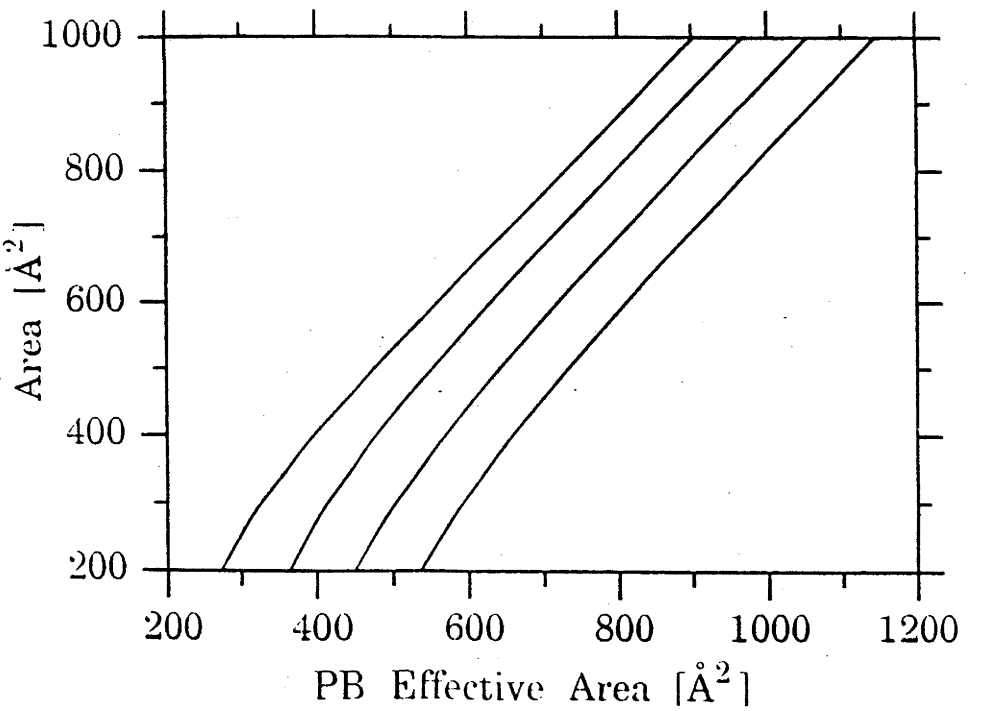

Figure 7.4 Same as the preceding figure but including the effects of images, with $\varepsilon_1=80$, $\varepsilon_2=2$ and w=2Å.

the experimental data have been fitted with the linear PB theory. Call the effective (linear) area A_L, and, in terms of the s_L from Eq. (7.1.11), the equivalent non-linear PB surface parameter is

$$s_{NL} = \frac{s_L}{1 - s_L^2/16} \quad , \quad s_L \equiv \frac{4\pi\beta q^2}{\varepsilon \kappa_\infty A_L} \tag{7.3.1}$$

From this s_{NL} one can work out the effective area per surface charge given by non-linear PB theory (inverting Eq. (7.1.11) or Eq. (7.3.1) to obtain A_{NL}) and this is just a point on the ordinate of figs 7.3 or 7.4. The real area per surface may then be read from the curves.

To estimate the actual area per surface charge A from an effective A_{NL} obtained at a value of the bulk concentration ρ not given in the figures, the following interpolation appproximation may prove useful. Suppose ρ_1 and ρ_2 are two concentrations accessable from the figures, and suppose that A_1 and A_2 are the actual areas which correspond to A_{NL}, as given by the curves at these two concentrations. Then the actual area per surface charge at the density ρ is approximately given by

$$A \approx A_1 - (A_1 - A_2)\frac{\ln(\rho/\rho_1)}{\ln(\rho_2/\rho_1)} \tag{7.3.2}$$

Alternatively, one could implement Eq. (7.2.20) or Eq. (7.2.22) and calculate the correspondance directly.

Appendix

7.A Asympototic expansions

Here is briefly discussed the large separation asymptotic expansions given in the body of the paper. Since not everyone shares our "pathological fascination for the manipulation of elliptic functions"[22], only an outline of the steps in the derivation will be given. Both PB and EPB theories require the parameter m (or m_1=1-m) for the various elliptic functions. While this is determined by the boundary condition (7.1.11), it is not convenient to begin the asymptotic analysis directly from there because the argument of the elliptic function diverges to infinity. However one can define a new argument

$$\zeta \equiv \frac{i\kappa_\infty h}{2m^{1/2}} - iK(m) \tag{7.A.1}$$

which remains finite as $\gamma \equiv \kappa_\infty h \to \infty$. Now with this change of argument (AS§16.8), and performing a Jacobi imaginary transformation (AS §16.20), the boundary condition (7.1.11) becomes

$$m^{1/2}\, sn(\zeta \mid m_1) = -2i/s \tag{7.A.2}$$

One may solve this equation by expanding everything in terms of the nome q_1. Using the theta function definitions (AS §§16.27,16.36) one has

$$(1-m_1)^{1/2} \frac{\vartheta_3(0)}{\vartheta_2(0)} \frac{\vartheta_1\left(\frac{\pi\zeta}{2K_1}\right)}{\vartheta_4\left(\frac{\pi\zeta}{2K_1}\right)} = -2i/s \tag{7.A.3}$$

where the theta functions have nome q_1, the quarter period K_1=K(m_1) is given by (AS16.38.6)

$$(2K_1/\pi)^{1/2} = \vartheta_3(0, q_1) = 1 + 2q_1 + 2q_1^4 + \ldots \tag{7.A.4}$$

and the complementary parameter is (AS16.38.7)

$$m_1^{1/4} = \frac{\vartheta_2(0, q_1)}{\vartheta_3(0, q_1)} = 2q_1^{1/4} \frac{1 + q_1^2 + q_1^6 + \ldots}{1 + 2q_1 + 2q_1^4 + \ldots} \tag{7.A.5}$$

Note that $K(m) = - \ln(q_1) K(m_1) / \pi$. To leading order one obtains the solution to Eq. (7.A.3):

$$q_1 \sim \frac{e^{-\gamma}}{(2/s + \sqrt{1 + 4/s^2})^2} + O(e^{-2\gamma}) \qquad (7.A.6)$$

From the nome one can immediately obtain the parameter (7.A.5) and hence the leading part of the asymptotic forms for the midpoint potential (7.1.16) and the pressure (7.1.18), within the mean field Poisson-Boltzmann theory. Continuing the process gives successive terms in the expansion.

To obtain the results for $\mathfrak{F}^{corr}$, one requires an expression for α_1 from Eq. (7.2.4) which, by analogy with Eq. (7.A.2) may be written

$$m^{1/2} \, sn(\zeta_1 | m_1) = -i \kappa_\infty / k \qquad (7.A.7)$$

with $\zeta_1 = \alpha_1 - iK(m)$. Again using the rapid q expansions for the theta functions it follows

$$\frac{\pi i \zeta_1}{2 K_1} \sim \ln(\kappa_\infty /k + \sqrt{1 + \kappa_\infty^2/k^2}) + \frac{4 q_1 (1-\kappa_\infty^2/k^2)}{\sqrt{1 + k^2/\kappa_\infty^2}} + O(e^{-2\gamma}) \qquad (7.A.8)$$

An analogous expression holds for ζ with 2/s replacing κ_∞/k in the above.

The leading asymptotic terms (bulk, surface and leading interaction) for the free energy come from the first part of the secular determinant (7.2.5), which may be written in terms of the (normalised) Lamé function, $E(\alpha) \equiv f(\alpha)/f(0)$

$$e^{-kh} \mathfrak{D}_1(k) / k \sim \frac{e^{-kh} E^2(\alpha)}{4 k (i\kappa_\infty /m^{1/2}) E'(0)} \left[k\delta_- + \delta_+ \frac{(i\kappa_\infty /m^{1/2}) E'(\alpha)}{E(\alpha)} \right]^2 + O(e^{-2\gamma}) \qquad (7.A.9)$$

where the prime denotes differentiation with respect to argument $\alpha = i\kappa_\infty h/(2m^{1/2})$. This normalised solution to Lamé's equation (7.2.2) may be written in terms of the shifted arguments (7.A.1) (cf AS§16.33)

$$E(\alpha) = \exp\{ \frac{-\pi i \zeta_1}{2K_1} \} \frac{H(\zeta+\zeta_1) \Theta(0)}{H(\zeta) \Theta(\zeta_1)} \exp\{ -\alpha \frac{H'(\zeta_1)}{H(\zeta_1)} \} \qquad (7.A.10)$$

and the parameter remains m_1. It follows

$$\frac{E'(\alpha)}{E(\alpha)} = \frac{H'(\zeta+\zeta_1)}{H(\zeta+\zeta_1)} - \frac{H'(\zeta)}{H(\zeta)} - \frac{H'(\zeta_1)}{H(\zeta_1)} \qquad (7.A.11)$$

$$E'(0) = \frac{\Theta'(\zeta_1)}{\Theta(\zeta_1)} - \frac{H'(\zeta_1)}{H(\zeta_1)} \qquad (7.A.12)$$

Now expand Eqs (7.A.10), (7.A.11) and (7.A.12) in powers of the nome q_1, using Eq. (7.A.8) for ζ and ζ_1 , to give ln $E(\alpha)$, $E'(\alpha)/E(\alpha)$, and $E'(0)$. This involves some fascinating algebraic manipulation and gives $\ln \mathcal{D}_1(k)$ to linear order in q_1. It yields the bulk (7.2.15) and surface (7.2.16) as well as the leading interaction free energy (7.2.20) given in the text.

The asymptotic expansion for the total number of ions (per unit area) in the double layer, Eq. (7.1.15), also follows from the theta function expansions. It is

$$\Gamma_+ + \Gamma_- = 2\rho_\infty h + \frac{s A \rho_\infty}{2\kappa_\infty} + \left\{ \frac{\rho_\infty h A^2}{2} - \frac{\rho_\infty A^2}{2\kappa_\infty} \frac{3A^2 - 64}{A^2 + 64} \right\} e^{-\gamma} + O(e^{-2\gamma}) \qquad (7.A.12)$$

with A defined in Eq. (7.1.17a). Here the bulk, surface and leading interaction terms are quite clear explicitely. It is remarked that the asymptotic analyses have been done completely independently in two different ways. The results are in full numerical agreement with each other and with that given by the computation of the full solution in the large separation regime.

Appendix

7.B Self - consistent profiles

The extended Poisson-Boltzmann approach consisted of using a first approximation for the density profile -the mean field form. This was justified by stating that, since the grand potential functional was optimal with respect to the profile, it was unnecessary to consider a self-consistent profile in any regime where the application of the theory could be expected to be valid. Here a bulk electrolyte is investigated, and it is shown that an approximate relationship between the density and chemical potential actually gives better results than the self-consistent formulation, at least in going beyond the regime of vanishing density. The reason is related to the fact that the Debye-Hückel (DH) approximation, a linear closure with no hard cores, overestimates the correlations, and so neglecting these effects on the profile to some extent compensates their exaggerated contribution to the free energy.

The mean potential can be chosen to vanish in the bulk, and one has from eqs (5.2.1) and (5.1.14)

$$\mathcal{F}^{mf} = \mathcal{F}^{id} = 2\, k_B T\, V \rho_\infty [\, \ln(\lambda^3 \rho_\infty) - 1\,] \qquad (7.B.1)$$

for a symmetric electrolyte of concentration $\rho_\infty = \rho_+ = \rho_-$ in a volume V. Applying eq. (5.3.6) to a bulk, one has

$$\mathcal{F}^{corr} = \frac{k_B T V}{2(2\pi)^3} \int d\mathbf{k}\, [\, \ln((1-\Lambda(k)) + \Lambda(k)\,] \qquad (7.B.2)$$

with the element of three dimensional Fourier space being $d\mathbf{k} = 4\pi k^2\, dk$. Using the eigenvalue determined from eq. (5.3.8) in Fourier space

$$\Lambda(k) = -\kappa_\infty^2 / k^2 \qquad (7.B.3)$$

one obtains for the correlation contribution to the free energy

$$\mathcal{F}^{corr} = \frac{-k_B T V}{12\pi} \kappa_\infty^3 \qquad (7.B.4)$$

Since there are no mean or external fields in the bulk, this is just the non-ideal part of the Helmholtz free energy (*cf* eq. (5.1.6)) given by

Debye-Hückel theory[43]. The grand potential functional (5.1.6) is

$$\Omega = \mathfrak{F}^{id} + \mathfrak{F}^{corr} - V(\rho_+ \mu_+ + \rho_- \mu_-) \qquad (7.B.5)$$

This is a function of the densities ρ_+, ρ_- and the chemical potentials μ_+, μ_-. Differentiating

$$\frac{1}{V}\frac{\partial \Omega}{\partial \rho_+} = k_B T \ln(\lambda_+^3 \rho_+) - \mu_+ - \frac{k_B T \ \kappa_\infty^3}{8\pi(\rho_+ + \rho_-)} \qquad (7.B.6)$$

To optimise the functional, one requires this derivative to vanish, and this occurs when

$$\mu_+ = k_B T \ln(\lambda_+^3 \rho_+) - \frac{k_B T \ \kappa_\infty^3}{8\pi(\rho_+ + \rho_-)} \qquad (7.B.7)$$

This is just the DH form for the chemical potential, and with this choice the grand potential (7.B.5) is

$$\Omega^{DH} = -2 V k_B T \rho_\infty + \frac{V k_B T}{24\pi} \kappa_\infty^3 \qquad (7.B.8)$$

When the DH closure is used for the direct correlation function (5.3.1), the DH relationship between the chemical potential and the density is the one that optimises the grand potential functional; that choice is self-consistent.

Now consider an approximation similar to the extended Poisson - Boltzmann method used in the text. Make the fugacity approximation for the chemical potential:

$$\mu_1 = k_B T \ln(\lambda_1^3 \rho_1) \qquad (7.B.9)$$

Anticipating the results to follow, ρ_1 is not identified with the bulk concentration; it is the density profile specified in this approximation. The grand potential, a function of ρ_1 and ρ_2 becomes

$$\Omega^{PA} = -k_B T V(\rho_1 + \rho_2) - \frac{k_B T V}{12\pi} \kappa_1^3 \qquad (7.B.10)$$

where PA stands for 'Profile Approximation', and does not relate to any eponymous aspirations of the author. Differentiate Ω to obtain the implied concentration

$$\rho_+ = \frac{-1}{V}\frac{\partial\Omega}{\partial\mu_1} = \frac{-\rho_1}{Vk_BT}\frac{\partial\Omega}{\partial\rho_1} = \rho_1 + \frac{1}{8\pi}\kappa_1^3 \qquad (7.B.11)$$

Therefore in order to describe a bulk electrolyte of concentration ρ_∞ ($= \rho_+ = \rho_-$), solve this transcendental equation for ρ_1 ($= \rho_2$) and obtain the grand potential from eq. (7.B.10).

Figure 7.5 compares the osmotic coefficient $\phi = P/2k_BT\rho_\infty$ in the DH, PA, and MSM (mean spherical model[44]) approximations, with MC simulation data[37]. All the approximate theories agree at lower concentrations, and give the primary departure from ideality correctly. The agreement between PA and DH here results from the variational nature of the formalism. However at higher concentrations, beyond the regime where one has any right to expect either the present approximation or DH to work, one sees that it actually does better than DH theory.

To see this explicitly, do a low density expansion. Then since

$$\rho_1 \sim \rho_+ - \frac{\kappa_\infty^3}{16\pi} + \frac{3\,\kappa_\infty^6}{2^9\pi^2\rho_+} + \ldots \qquad (7.B.12)$$

one has

$$\Omega^{PA} \sim k_BT\,V\left[-2\rho_+ + \frac{\kappa_\infty^3}{24\pi} - \frac{\kappa_\infty^6}{2^8\pi^2\rho_+} + \ldots\right] \qquad (7.B.13)$$

which to leading order agrees with the DH result (7.B.8), as it should. Now consider the MSM which is known to work well for bulk electrolytes up to ~1M. The (energy) osmotic coefficient is there (*cf* ref. 45, p.356)

$$\phi_E^{MSM} = \phi_{HS}^{PY} + \frac{1}{8\pi d^3\rho_+}\left[\frac{2}{3} + \kappa_\infty d + \kappa_\infty d(1+2\kappa_\infty d)^{1/2} - \frac{2}{3}(1+2\kappa_\infty d)^{3/2}\right] \qquad (7.B.14)$$

where d is the hard core diameter and ϕ_{HS}^{PY} is the Percus-Yevick osmotic coefficient for the hard sphere fluid without electrostatic interactions. Defining

$$y = 2\pi\rho_+ d^3/6 \qquad (7.B.15)$$

and using the low density expansion of the Carnahan-Starling equation of

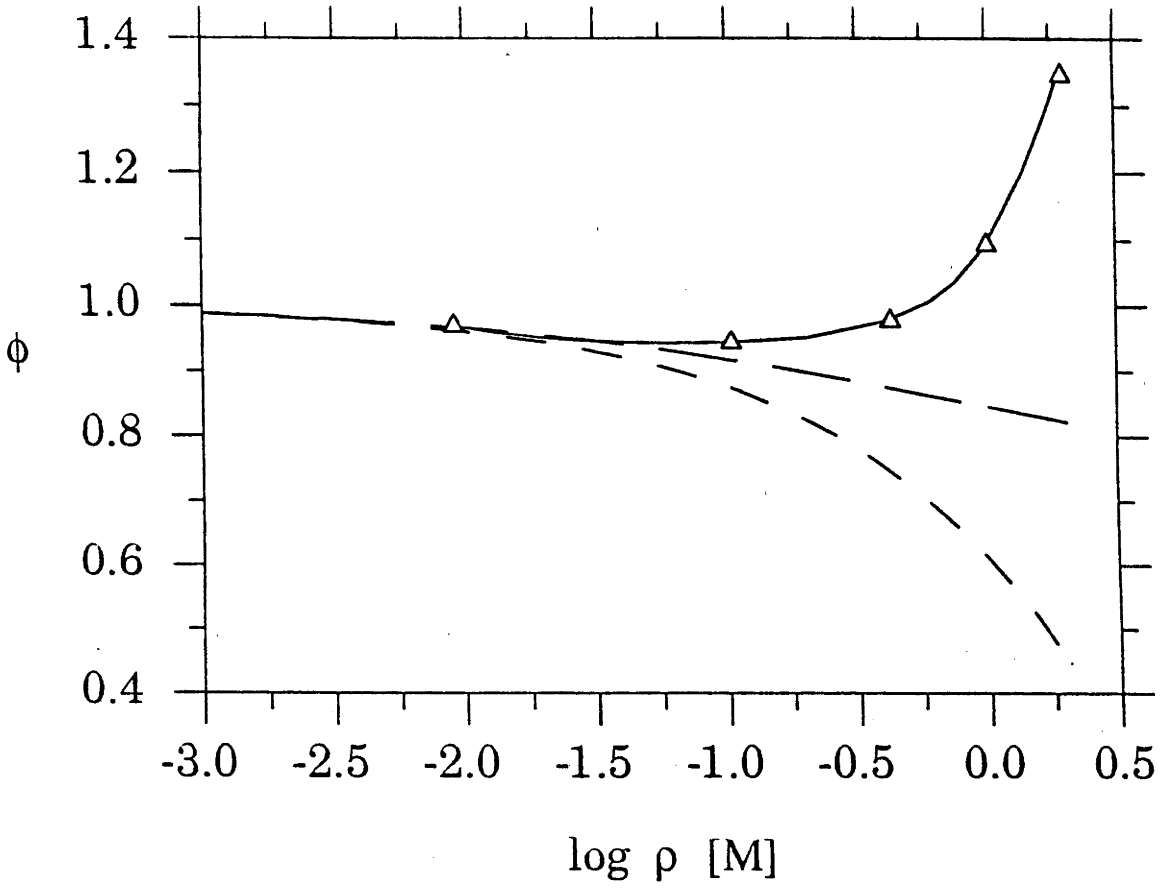

Figure 7.5 The osmotic coefficient versus concentration (log scale) for a 1:1 symmetric electrolyte as given by MC (Δ), MSM (———), DH (– – – –) and PA (— — —) approximations. The temperature is 298K, ε=78.5, d=4.25Å.

state[46]

$$\phi_{HS}^{CS} = \frac{1+y+y^2-y^3}{(1-y)^3} \sim 1 + 4y + \ldots \qquad (7.B.16)$$

one can show

$$\Omega^{MSM} \sim k_B T V \left[-2\rho_+ + \frac{\kappa_\infty^3}{24\pi} - \frac{8\pi d^3 \rho_+^2}{3} - \frac{d\,\kappa_\infty^4}{16\pi} + \ldots \right] \qquad (7.B.17)$$

When does the first departure of PA (7.B.13) from DH agree with the analagous MSM correction? The answer is when $D(3+2D^2)=3/2$ ($D \equiv \varepsilon d/\beta q^2 = d/7.7\text{Å}$ for a monovalent electrolyte) or $d \approx 3.4$Å. By some serendipity, the traditional hard core diamter used in simulations is 4.25Å and so PA gets the first departure of the MC data nearly correct, as is apparent from the figure.

The approximation considered in this appendix consisted in taking the relationship between the profile and the chemical potential to be ideal. The density which then appears in the grand potential functional is the fugacity, and the value of this (or equivelently μ) was determined such that Ω^{PA} implied the correct density. This procedure agrees with Debye-Hückel theory at low concentrations (because the grand potential functional is optimised with respect to the density profile) and actually does better in more highly coupled systems. When considering the EPB as applied to the electrical double layer, one has to be cautious in drawing conclusions based on the present investigation of a bulk electrolyte. Nevertheless, it seems reasonable to say that both the PB profile and a self-consistent profile will give the same answers at low concentrations. Also one suspects that the latter (numerical) profile may in fact overestimate the correlation contribution to the free energy, more so than the present EPB approach.

Conclusion to Part III

The zero size mean spherical model has been solved for inhomogeneous planar Coulomb systems. The analytic result is in terms of the solutions of a second order differential equation and depends on the profile. Since the free energy functional is optimal, the lowest order approximation for the profile was used. Choosing the PB profile allows explicit solution of the differential equation and the free energy reduces to a one dimensional integral. An advantage of the analytic approach is that the relationship between Lifshitz theory and the primitive model is transparent. In particular if ionic correlations are allowed by a theory, one would predict a spurious repulsion unless the effects of fluctuations in the polar media (the Lifshitz zero frequency term) were also added.

The EPB method has been implemented explicitly for the particular limiting case of the one component double layer. The theory gives the primary departure from the PB approximation, and allows the EPB to be used to easily assess the accuracy of the PB theory. In this case the accuracy of the extended Poisson-Boltzmann scheme itself was also shown to be satisfactory in the large separation and/or low surface charge regime. It can be inferred that the theory provides an acceptable approximation to the primitive model of the double layer, a model which might be expected to be a valid description of reality asymptotically, as indeed is Lifshitz theory.

For the symmetric electrolyte, the extended Poisson-Boltzmann theory appears to be accurate for low concentrations. The theory offers an improvement in accuracy while remaining not too much more complicated than the traditional PB treatments. Both the double layer and van der Waals forces are now treated consistently and at the same level of approximation. The distinction so often made between van der Waals and double layer forces is illusory.

In general correlations lower the total pressure. For the case of the one component double layer this means the net pressure is also less repulsive

since here there is no bulk. Hence for this case the results are readily interpreted in terms of two mechanisms[15,16]: correlations mean that the counter-ions feel a higher local potential, and therefore they move closer to the surfaces, depleting the midpoint concentration (it is a canonical ensemble) and lowering the kinetic pressure. In addition, an ion on one side of the system repels ions on the other side (correlations) and sees a less screened oppositely charged surface. This gives an additional attraction across the midplane. For the symmetric electrolyte the situation is less clear since both the bulk and the double layer have lower pressures when the effects of correlations are included. One cannot say *a priori* whether the net pressure will be increased or decreased by including correlations. An example of the difficulty is that one finds an enhanced repulsion for low surface charges which may be rationalised in terms of correlations causing the ions to be repelled from the surface, decreasing the screening by the double layer. Yet for zero surface charge[9-12] this same mechanism gives a net attraction. Similarly images can increase the coupling and hence the effects of correlations, yet they may also increase the repulsion in the double layer.

The asymptotic analysis for the symmetric electrolyte clearly indicates a PB-like decay but with an effective surface charge. This again contrasts with the one component double layer where the PB theory appears exact asymptotically (it is independent of any surface charge) and where EPB appears to give the primary asymptotic correction to that theory. For the symmetric electrolyte, the effective surface charge depends on the behaviour of the ions near the surface, and EPB gets this quantity only approximately correct at low surface couplings. This suggests an alternative way to get accurate asymptotic results for the double layer, without going to the sophistication (and large scale numerical computation) of the anisotropic HNC or simulations. If the isolated double layer could be treated accurately, then the computed effective surface charge could be used in the PB equations.

For the present, the extended Poisson-Boltzmann theory represents an improvement on mean field Poisson-Boltzmann theory, and may be used to calculate the real surface charge from fitted effective surface charges in many situations.

Beyond these conclusions, and despite the clear limitations of the EPB theory, the physical insight gained through this (approximate) analytic treatment of the double layer is of some value. First, the generalisation, to higher concentrations and to charged interfaces, of the Onsager-Samaras result for the surface free energy change, should prove useful. In particular, it can at least explain qualitatively the larger concentration data[34-36]. Second, it is evident that if double layer force measurements are interpreted by the classical PB theory with fitted association constants for the interacting surfaces, those inferred ion binding constants have to be taken with some caution. The degree of real as opposed to effective ion binding must be crucial in extracting and assigning a meaning to the ubiquitous "hydration forces", those forces beyond continuum theories which are currently of some interest.

References for Part III

1 E.J.W. Verwey and J.Th.G. Overbeek, *Theory of the Stability of Lyotropic Colloids* (Elsevier, Amsterdam, 1948).

2 B.V. Derjaguin and L. Landau, Acta Phys.-Chim. USSR **XIV**, 663 (1941).

3 G. Gouy, J. Phys. Radium, **9**, 457 (1910).

4 D.L. Chapman, Phil. Mag. **25**, 475 (1913).

5 H.C. Hamaker, Physica, **4**, 1058 (1937).

6 F. London, Z. f. Physik, **63**, 245 (1930); Z. f. Phys. Chem. B **11**, 222 (1930).

7 E.M. Lifshitz, Sov. Phys. JETP, **2**, 73 (1956); I.E. Dzyaloshinskii, E.M. Lifshitz, and L.P. Pitaevskii, Adv. Phys., **10**, 165 (1961).

8 B.W. Ninham and V.A. Parsegian, J. Chem. Phys. **52**, 4578 (1970).

9 B.W. Ninham and V.A. Parsegian. The original work (1972) is unpublished, but the theory is presented in Chapter 7.4 of ref. 10.

10 J. Mahanty and B.W. Ninham, *Dispersion Forces* (Academic Press, London, 1976).

11 B. Davies and B.W. Ninham, J. Chem. Phys., **56**, 5797 (1972).

12 V.N. Gorelkin and V.P. Smilga, Sov. Phys. JETP, **36**, 761 (1973).

13 E. Barouch, J.W. Perram and E.R. Smith, Proc. Roy. Soc. (London) **334**, 49 (1973).

14 D.J. Mitchell and P. Richmond, J. Coll. Interface Sci. **46**, 118 (1974); *idem.* **46**, 128 (1974).

15 L. Guldbrand, Bo. Jönsson, H. Wennerström and P. Linse, J. Chem. Phys. **80**, 2221 (1984); see also D. Bratko, Bo. Jönsson and H. Wennerström, Chem. Phys. Lett. **128**, 449 (1986).

16 R. Kjellander and S. Marčelja, Chem. Phys. Lett. **112**, 49 (1984).

17 R. Kjellander and S. Marčelja, J. Chem. Phys., **82**, 2122 (1985).

18 R. Kjellander and S. Marčelja, Chem. Phys. Lett. **127**, 402 (1986).

19 N.G. van Kampen, B.R.A. Nijboer and K. Schram, Phys. Lett. **26a**, 307 (1968).

20 C.J. Barnes and B. Davies, J. Chem. Soc. Faraday Trans II **71**, 1667 (1975).

21 C.W. Outhwaite, J. Chem. Soc. Faraday Trans. 2 **74**, 1214 (1978); S. Levine and C.W. Outhwaite, *ibid.* **74**, 1670 (1978); C.W. Outhwaite, L.B. Bhuiyan and S. Levine, *ibid.* **76**, 1388 (1980).

22 S.L. Carnie and D.Y.C. Chan, Mol. Phys., **51**, 1047 (1984).

23 R. Evans, Advances in Physics, **28**, 143 (1979).

24 S. Engström and H. Wennerström, J. Phys. Chem. **82**, 2711 (1978).

25 R. Kjellander and S. Marcelja, J. Phys. Chem. **90**, 1230 (1986).

26 V.A. Parsegian and B.W. Ninham, Biophys. J. **10**, 646 (1970).

27 M. Abramowitz and I.A. Stegun, *Handbook of Mathematical Functions*, (Dover, 1965).

28 J.N. Israelachvili and G.E. Adams, J. Chem. Soc. Faraday Trans. 1 **74**, 975 (1978).

29 J. Israelachvili and R.M. Pashley, J. Col. Interface Sci., **98**, 500 (1984).

30 J.L. Parker, H.K. Christenson, and B.W. Ninham J. Phys. Chem. (in press).

31 D.Y.C Chan, R.M. Pashley, and L.R. White, J. Col. Interface Sci. **77**, 283 (1980).

32 E.T. Whittaker and G.N. Watson, *A Course in Modern Analysis*, 4th Ed., (Cambridge at the University Press, 1969).

33 L. Onsager and N.T. Samaras, J. Chem. Phys., **2**, 528 (1934).

34 K. Johansson and J.C. Eriksson, J. Col. Interface Sci., **49**, 469 (1974).

35 R. Aveyard and S.M. Saleem, J. Chem. Soc. Faraday Trans. 1 **72**, 1609 (1976).

36 J. Ralston and T.W. Healy, J. Col. Interface Sci., **42**, 629 (1973).

37 J.C. Rasaiah, D.N. Card, and J.P. Valleau, J. Chem. Phys., **56**, 248 (1972).

38 J.P. Valleau, L.K. Cohen, and D.N. Card, J. Chem. Phys., **72**, 5942 (1980).

39 F. Lado, Phys. Rev., B **17**, 2827 (1978).

40 G.M. Torrie and J.P. Valleau, J. Chem. Phys., **73**, 5807 (1980).

41 R. Kjellander, S. Marcelja, and J.P. Quirk, J. Col. Interface Sci., (in press); R.M. Pashley, R. Kjellander, S. Marcelja, and J.P. Quirk, (to be published).

42 D.J. Mitchell and B.W. Ninham, Chem. Phys. Lett. **53**, 397 (1978).

43 P. Debye and E. Hückel, Phys. z., **24**, 185 (1923).

44 E. Waisman and J.L. Lebowitz, J. Chem. Phys., **52**, 4307 (1970); **56**, 3086 (1972).

45 D.A. McQuarrie, *Statistical Mechanics*, (Harper & Row, New York 1976).

46 N.F. Carnahan and K.E. Starling, J. Chem. Phys. **51**, 635 (1969); **53**, 600 (1970).

Perspective

It remains for us to put the work presented in this Thesis into a broader scientific context and to attempt to point to future directions for research. Inhomogenous fluids, including electric double layers, are ubiquitous. Their properties are of interest in many fundamental and technological disciplines. The field is not so esoteric as it seems. For example, forces due to ionic correlations are implicated in the anomalous swelling of Calcium clays, a problem of immense practical importance to oil reservoir stability and the design of drilling muds. Further, it is evident that any attempt to unravel "hydration forces", or to assign a meaning to "ion binding" in biological or other systems, has to begin with a proper knowledge of these newly quantified forces.

The research and techniques developed here represent a beginning. The story is by no means complete, yet we believe the investigation to be timely. Only recently have advances in experimental techniques and theory facilitated progress in our understanding of inhomogeneous systems. The particular results we have obtained here for the electric double layer should prove useful in re-interpreting ion binding imputed experimentally. In the immediate future, the present methods can and should be extended to explore self consistent profiles, and to consider discrete surface charges. A particularly interesting notion is that the one component double layer results, obtained here in a low coupling approximation, may in fact embrace the exact asymptotic behaviour of the system. Such a hypothesis could be tested by the methods of Parts I and III. Our present approximate but analytic treatment complements the numerical benchmarks set by Marčelja and Kjellander. Yet it seems that what is required in practice is intermediate between the two. It is in this sense that the formalism of Part III, in the context of some numerical scheme for more general

inhomogeneous fluids, may prove more valuable than the particular results. The world does not consist of planes, and the application of either the present approach or more definitive numerical schemes to different geometries must soon be undertaken.

The present primitive model of the electric double layer focuses on the behaviour of the ions and treats the solvent as a dielectric continuum. Already there are experiments at short surface separations where this approximation is invalid. Lifshitz theory is satisfactorilly established (theoretically, if not experimentally) and is clearly asymptotic. What is needed is to go beyond the continuum macroscopic approximation for the media. Other than a full solution of the ion-solvent fluid, there are two possibilities:- non-uniform density profiles and non-local dielectric response. It is the latter which is likely to yield first to analysis and the results of Part II (which include the non-local response of the two-dimensional dipole system) represent a start. We feel that that functional form for the response is likely to be more appropriate for the planar inhomogeneous system than is the bulk specular reflection approximation currently used by some authors. The techniques used in Part II, in conjunction with the methodology of Part III, suggest a possible route for systematic corrections to Lifshitz theory.

Also beyond the primitive model is the hydration force:- strongly repulsive, monotonic, short ranged and poorly understood. This intriguing phenomenon has motivated much of this Thesis, including Parts I and III where the actual content of the primitive model was explored, and Part II where a proposed electrostatic mechanism was ruled out. While the theoretical results presented here do not rule out non-local electrostatics, the experimental evidence does correlate with the hydrogen bonding ability of the fluid. We suggest that the repulsive hydration force measured between polar surfaces originates from the strongly oriented boundary molecules in

hydrogen bonded liquids. The repulsion is due to the entropy lost (or enthalpy gained) upon the approach of the surfaces, there being fewer configurations which are able to satisfy the boundary conditions without breaking the bond network of the fluid phase. This proposed mechanism seems a very likely candidate, and we have recently derived lattice and mean field approximations which give results comparable to experiment. For the future, the hydration force represents a challenge which demands more realistic treatments.

In summary, we believe the work here presented represents a real contribution, albeit incomplete, to a second generation of problems that confront colloid and surface chemistry. That it is incomplete is a source of both comfort and dismay. If it were complete, the field would be devoid of interest. Progress is measured by successive generations. So too in science.